DEVELOPMENT OF A MODIFIED METHODOLOGY FOR DETERMINATION AND CHARACTERIZATION OF FAULT SYSTEMS WITHIN THE KABUL BLOCK (EASTERN AFGHANISTAN) USING REMOTE SENSING AND GIS TECHNIQUES

Hemayatullah AHMADI

PhD Dissertation

Department of Remote Sensing and Geographic Information Systems

Supervisor: Asst. Prof. Dr. Emrah PEKKAN

(Co-Supervisor: Prof. Dr. Gürol SEYİTOĞLU)

Eskişehir

Eskişehir Technical University

Institute of Graduate Programs

December 2023

FINAL APPROVAL FOR THESIS

This thesis titled DEVELOPMENT OF A MODIFIED METHODOLOGY FOR DETERMINATION AND CHARACTERIZATION OF FAULT SYSTEMS WITHIN THE KABUL BLOCK (EASTERN AFGHANISTAN) USING REMOTE SENSING AND GIS TECHNIQUES has been prepared and submitted by Hemayatullah AHMADI in partial fulfillment of the requirements in "Eskişehir Technical University Directive on Graduate Education and Examination" for the Degree of PhD in Remote Sensing and Geographic Information Systems Department has been examined and approved on 07/12/2023.

Committee Members		Title, Name and Surname	Signature
Member	:	Asst. Prof. Dr. Emrah PEKKAN	
Member	:	Asst. Prof. Dr. Hakan UYGUÇGIL	
Member	:	Prof. Dr. Hakan A. NEFESLİOĞLU	
Member	:	Prof. Dr. Murat UYSAL	
Member	:	Asst. Prof. Dr. Muzaffer ÖZBURAN	

Prof. Dr. Semra KURAMA
Director of the Institute of Graduate Programs

07/12/2023

SUPERVISOR APPROVAL

PhD student Hemayatullah AHMADI, whom I supervise, has completed this thesis titled DEVELOPMENT OF A MODIFIED METHODOLOGY FOR DETERMINATION AND CHARACTERIZATION OF FAULT SYSTEMS WITHIN THE KABUL BLOCK (EASTERN AFGHANISTAN) USING REMOTE SENSING AND GIS TECHNIQUES. According to my inspections, the work is scientifically and ethically appropriate for the student to the thesis defense exam.

Supervisor
Asst. Prof. Dr. Emrah PEKKAN

ABSTRACT

DEVELOPMENT OF A MODIFIED METHODOLOGY FOR DETERMINATION AND CHARACTERIZATION OF FAULT SYSTEMS WITHIN THE KABUL BLOCK (EASTERN AFGHANISTAN) USING REMOTE SENSING AND GIS TECHNIQUES

Hemayatullah AHMADI

Department of Remote Sensing and Geographic Information Systems

Eskişehir Technical University, Institute of Graduate Programs, December 2023

Supervisor: Asst. Prof. Dr. Emrah PEKKAN

(Co-Supervisor: Prof. Dr. Gürol SEYİTOĞLU)

This research focuses on detecting and redefining active fault zones, related segments, and lineaments within the Kabul Block in eastern Afghanistan using manual and automatic remote sensing techniques.

Additionally, the study aims to develop an active tectonics model that considers local and regional active fault zones in the Kabul Block and its surrounding regions. To achieve these objectives, various remote sensing data sets were utilized, including radar data (Digital Elevation Models [DEMs], Sentinel-1B), optical data (Advanced Spaceborne Thermal Emission and Reflection Radiometer [ASTER], Sentinel-2A), and high-resolution imagery from Google Earth Pro.

Manual interpretation of the high-resolution imagery was employed to redefine active fault zones, measure river channel offset, and deflection within the study area. Moreover, automatic algorithms, particularly the LINE module, were utilized to identify geological lineaments, determine their spatial distribution, and assess their correlation with active fault zones. Consequently, an integrated remote sensing approach was established to identify active fault zones and associated structures in any similar geography.

The analysis resulted in the identification of 653 left-lateral, right-lateral, and normal active fault segments within the Kabul Block and surroundings. In addition, DEM-5m data identified 414,069 lineaments ranging from 10 to 948.31 meters in length, while Sentinel-1GRD data detected 86,438 lineaments with lengths between 16.62 and 2469.91 meters. Additionally, Sentinel-2MSI and ASTER data revealed 80,243 lineaments spanning 40 to 2436.47 meters, and 42,443 lineaments ranging from 0.46 to 3722.17 meters across the Kabul Block. Strong correlations were observed between the active fault segments and detected geological lineaments, leading to the proposal of an escaping tectonic model for the Kabul Block.

Keywords: Active faults, Kabul Block, Lineament, Remote sensing, Morphotectonic analysis.

ÖZET

KABİL BLOĞUNDAKİ (DOĞU AFGANİSTAN) FAY SİSTEMLERİNİN UZAKTAN ALGILAMA VE CBS TEKNİKLERI KULLANILARAK BELİRLENMESİ VE KARAKTERİZASYONU İÇİN MODİFİYE BİR METODOLOJİNİN GELIŞTİRİLMESİ

Hemayatullah AHMADI

Uzaktan Algılama ve Coğrafi Bilgi Sistemleri Anabilim Dalı

Eskişehir Teknik Üniversitesi, Lisansüstü Eğitim Enstitüsü, Aralık 2023

Danışman: Dr. Öğr. Üyesi Emrah PEKKAN

İkinci Danışman: Prof. Dr. Gürol SEYİTOĞLU

Bu araştırma, doğu Afganistan'daki Kabil bloğu içindeki aktif fay zonlarının, ilgili segmentlerin ve çizgiselliklerin manuel ve otomatik uzaktan algılama teknikleri kullanılarak tespit edilmesine ve yeniden tanımlanmasına odaklanmaktadır.

Çalışma, Kabil bloğu ve çevresindeki bölgelerdeki yerel ve bölgesel aktif fay zonlarını dikkate alan yeni bir aktif tektonik modeli geliştirmeyi amaçlamaktadır. Bu hedeflere ulaşmak için, radar verileri (Dijital Yükseklik Modelleri [DEM'ler], Sentinel-1B), optik veriler (Gelişmiş Uzay Kaynaklı Termal Emisyon ve Yansıma Radyometresi [ASTER], Sentinel-2A) ve Google Earth Pro'dan yüksek çözünürlüklü görüntüler kullanılmıştır.

Aktif fay bölgelerini yeniden tanımlamak ve çalışma alanı içindeki nehir kanalı ötelemesini ve sapmasını ölçmek için yüksek çözünürlüklü görüntüler klasik tektonik yöntemlerle yorumlanmıştır. Jeolojik çizgiselliklerin ve bu çizgiselliklerin mekansal dağılımlarının belirlenmesi ve aktif fay bölgeleri ile korelasyonlarının değerlendirilmesi amacıyla ise otomatik algoritmalardan (LINE modülü) yararlanılmıştır. Sonuç olarak, benzer coğrafyalardaki aktif fay bölgelerinin ve ilgili jeolojik yapıların tespitine yönelik entegre bir uzaktan algılama yaklaşımı oluşturulmuştur.

Analizler sonunda , Kabil Bloğu ve çevresinde 653 sol yanal, sağ yanal ve normal aktif fay segmentleri tanımlanmıştır. DEM-5m verileri ile uzunlukları 10 ila 948,31 metre arasında değişen 414.069 çizgisellik tespit edilirken, Sentinel-1GRD verileri ile uzunlukları 16,62 ila 2469,91 metre arasında değişen 86.438 çizgisellik tesbit edilmiştir. Bunun yanıda Sentinel-2MSI ve ASTER verileri ile Kabil bloğu boyunca 40 ila 2436,47 metre arasında değişen 80.243 çizgisellik ve 0,46 ila 3722,17 metre arasında değişen 42.443 çizgisellik ortaya çıkarılmıştır. Aktif fay alanları ile tespit edilen jeolojik çizgisellikler arasında güçlü korelasyonlar gözlemlenmiş ve bu da Kabil bloğu için kaçan bloklarla temsil edilen bir tektonik model önerisinde bulunulmuştur.

Anahtar Sözcükler: Aktif faylar, Kabil Bloğu, Çizgisellik, Uzaktan algılama, Morfotektonik analiz.

ACKNOWLEDGEMENTS

I would like to offer my heartfelt prayers to the pure soul of my late father, who was the spiritual wealth of my life. Unfortunately, he passed away during the early stages of my Ph.D. journey. Pursuing my Ph.D. was one of his dreams, and today, I have been able to achieve that dream. However, it saddens me that he is not here to witness it. Therefore, I dedicate the credit of this dissertation to my beloved father.

I am deeply grateful to my esteemed supervisors, Asst. Prof. Dr. Emrah PEKKAN and Prof. Dr. Gürol SEYİTOĞLU, for their tireless contribution and support throughout this academic journey. I am particularly grateful for the invaluable advice and suggestions provided by Prof. Dr. Gürol SEYİTOĞLU, which greatly influenced the development of the active tectonics aspect of this research. Without his contribution, the success achieved in this project would not have been possible. His extensive experience in the field of active tectonics inspired me to delve deeply into this topic within the Kabul Block, eastern Afghanistan, even in challenging circumstances. I am also deeply thankful to Asst. Prof. Dr. Emrah PEKKAN, my primary supervisor, for his unwavering motivation and guidance, which played a crucial role in the success and progress of this thesis, as well as the completion of the accepted papers.

I am also grateful to the members of my thesis committee, Asst Prof. Dr. Hakan UYGUÇGİL and Prof. Dr. Hakan Ahmet NEFESLİOĞLU, for their guidance and persistent assistance on the subject matter of my dissertation. Their constructive suggestions significantly improved the quality of this work.

I would like to express my gratitude to my colleagues and friends at Kabul Polytechnic University in Afghanistan, especially to my supervisor, Prof. Abdul Barqi RAHMANI, and my dear friends, Asst. Prof. Atal YOUSUFI and Asst. Prof. Ahmad Walid AYOOBI, who provided continuous support, motivation, and assistance.

I am sincerely grateful to the Republic of Türkiye for hosting and providing me with a Ph.D. scholarship, enabling me to embark on this academic journey. I am also thankful to the Turkish people for their kindness and warm hospitality during my stay.

I would like to acknowledge the National Aeronautics and Space Administration (NASA), the European Space Agency (ESA), the United States Geological Survey (USGS), and the Afghanistan Ministry of Mines and Petroleum for providing the geological and remote sensing datasets crucial for this research.

Last but certainly not least, my deepest gratitude goes to my family: my beloved mother, my brothers, my sister, my uncles, and my aunt, for their unwavering support, encouragement, and dedication. I express my utmost appreciation and love to my wife and children for their unwavering dedication, support, and endurance during the most challenging times and situations throughout this journey.

I would not have been able to achieve this milestone without the support and guidance of all of the people mentioned above. I am truly grateful for their contributions, and I am honored to have had them on this journey with me.

Hemayatullah AHMADI

07/12/2023

STATEMENT OF COMPLIANCE WITH ETHICAL PRINCIPLES AND RULES

I hereby truthfully declare that this thesis is an original work prepared by me; that I have behaved in accordance with the scientific ethical principles and rules throughout the stages of preparation, data collection, analysis and presentation of my work; that I have cited the sources of all the data and information that could be obtained within the scope of this study, and included these sources in the references section; and that this study has been scanned for plagiarism with “scientific plagiarism detection program” used by Eskişehir Technical University, and that “it does not have any plagiarism” whatsoever. I also declare that, if a case contrary to my declaration is detected in my work at any time, I hereby express my consent to all the ethical and legal consequences that are involved.

Hemayatullah AHMADI

CONTENTS

Page

LIST OF TABLES

Page

LIST OF FIGURES

Page

GLOSSARY OF SYMBOLS AND ABBREVIATIONS

USSR	:	United of Soviet Socialist Republic
USGS	:	United States Geological Survey
AGS	:	Afghanistan Geological Survey
GIS	:	Geographic Information Systems
DEM	:	Digital Elevation Model
Mm	:	Millimeter
Yr	:	Year
AD	:	Anno Domini
GPs	:	Global Positioning System
InSAR	:	Interferometric Synthetic Aperture Radar
SRTM	:	Shuttle Radar Topography Mission
Be	:	Beryllium
ALOS	:	Advanced Land Observing Satellite
PRISM	:	Panchromatic Remote-sensing Instrument for Stereo Mapping
RS	:	Remote Sensing
USA	:	United States of America
SAR	:	Synthetic Aperture Radar
PCA	:	Principal Component Analysis
TM	:	Thematic Mapper
JERS	:	Japanese Earth Resources Satellite
ASTER	:	Advanced Spaceborne Thermal Emission and Reflection Radiometer
ETM	:	Enhanced Thematic Mapper
PALSAR	:	Phased Array type L-band Synthetic Aperture Radar
OLI	:	Operational Land Imager
TIRS	:	Thermal Infrared Sensor
SPOT	:	Satellite Pour 1'Observation de la Terre (Satellite for Observation of Earth
MNF	:	Minimum Noise Fraction
AM	:	Alburz Mormul
BB	:	Bande Bayan
BT	:	Bande Turkestan

CH	:	Chaman
DS	:	Darafshan
DV	:	Darvaz
DM	:	Dosi Mirz-Valan
GA	:	Gardiz
HA	:	Henjan
HR	:	Herat
HM	:	Helman
KR	:	Kaj Rod
KO	:	Konar
MO	:	Mokur
ON	:	Onay
PM	:	Paghman
PJ	:	Panjsher
QA	:	Qarghandaw
SA	:	Sarobi
SP	:	Spin Ghar
TPB	:	Transpressional Plate Boundary
AT	:	Accreted Terranes
SZ	:	Shear Zone
NP	:	North Platform
N	:	North
S	:	South
E	:	East
W	:	West
MSI	:	Multi-Spectral Instrument
ISC	:	International Seismological Centre
2D	:	Two Dimension
3D	:	Three Dimension
ESRI	:	Environmental Systems Research Institute
DTM	:	Digital Terrain Model
RADAR	:	Radio Detection and Ranging
GRD	:	Ground Range Detection

GHz	:	Gigahertz
IW	:	Wide Swath
WV	:	Wave Mode
SM	:	Strip Map
VV	:	Vertical-Vertical
HH	:	Horizontal-Horizontal
VH	:	Vertical-Horizontal
HV	:	Horizontal-Vertical
SLC	:	Single Look Complex
GEE	:	Google Earth Engine
VNIR	:	Visible and Near-Infrared
SWIR	:	Shortwave Infrared
CFZ	:	Chaman Fault Zone
SFZ	:	Sarobi Fault Zone
CKFZ	:	Charikar Fault Zone
KFZ	:	Konar Fault Zone
HFZ	:	Herat Fault Zone
Af	:	Basin Asymmetry Factor Index
MSS	:	Multispectral Scanner
GDEM	:	Global Digital Elevation Model
STA	:	Segment Tracing Algorithm
LESSA	:	Lineament Extraction and Strip Statistical Analysis
LINDA	:	Lineament Detection and Analysis
GTHR	:	Filter Radius
LTHR	:	Edge Gradient Threshold
FTHR	:	Line Fitting Error Threshold
ATHR	:	Angular Difference Threshold
DTHR	:	Linking Distance Threshold
LFF/LPF	:	Low-pass Filter
SE	:	Southeast
SW	:	Southwest
NW	:	Northwest
FCC	:	False Color Composite

BR	:	Band Ratio
OIF	:	Optimum Index Factor
BV	:	Brightness Value
ENVI	:	Environment for Visualizing Images
IBM	:	International Business Machines
SPSS	:	Statistical Package for Social Sciences
TCN	:	Terrestrial Cosmogenic Nuclide
NNE	:	North Northeast
σ_1	:	Sigma One
σ3	:	Sigma Thress
SSW	:	South Southwest
ENE	:	East Northeast
WSW	:	West Southwest
ESE	:	East Southeast
WNW	:	West Northwest
NEIC	:	National Earthquake Information Center
GCMTP	:	Global Centroid Moment Tensor Project

1. INTRODUCTION

Afghanistan, located in Central and South Asia, is a region of significant geological interest due to its tectonic setting. The region is located in a continental collision zone, where the Indian, Arabian, and Eurasian plates are converging. This convergence has led to the formation of complex geological features, such as structures, mountains, valleys, and landforms throughout the country.

The collision between these tectonic plates has given rise to the development of high peak ranges, particularly in the northeastern regions of Afghanistan. These mountain ranges have been sculpted through the forces of compression and uplift, as the plates continue to interact and exert pressure on each other. The collision zone acts as a geological laboratory, allowing scientists to study the processes of mountain building and structural deformation.

To further understand the geological features and tectonic subdivisions within Afghanistan, researchers have identified exotic terranes and defined tectonic boundaries based on the complex structures observed. These boundaries are often marked by active faults and suture zones, which delineate distinct tectonic blocks within the country. Active faults are geological fractures along which significant movement has occurred or is anticipated to occur in the future. Suture zones, on the other hand, represent regions where two or more tectonic plates have collided and fused.

In order to investigate the active faults of Afghanistan, collaborative efforts have been made by geoscientists from France, the USSR, Germany, and the United States Geological Survey (USGS) in conjunction with the Afghanistan Geological Survey (AGS). Through their joint research endeavors, these teams have conducted primary investigations to characterize the active faults, determine their level of activity, and assess the resulting land deformation.

The majority of these studies have followed traditional scientific approaches, employing field surveys, geological mapping, and geophysical measurements to analyze the active faults and associated geological features. However, researchers have also recognized the value of satellite imagery in studying fault traces and have utilized basic satellite observations to supplement their conventional methods. This combination of techniques has allowed for a more comprehensive understanding of the active faults and their behavior in Afghanistan.

The collective findings from these scientific investigations have highlighted the presence of 22 seismically active faults within the country. These faults represent areas of increased seismic activity, where tectonic stress is released through periodic earthquakes. The identification and characterization of these faults are crucial for seismic hazard assessments, as they provide valuable information for understanding the potential for future earthquake events in Afghanistan.

The Kabul Block, a collection of fault-bounded fragments located in eastern continuing to southeastern Afghanistan, is recognized as one of the intricate tectonic subdivisions within the country and has garnered significant attention from geoscientists. This Block is delimited by several prominent faults: to the west, the Chaman, to the southeast, Gardiz (an eastern splay of the Chaman fault zone), and to the northeast, the Sarobi fault. Considering the complex geology and tectonic framework of the Kabul Block, it is plausible that numerous additional small and large faults exist within its boundaries. The identification and characterization of these structures are not only essential for assessing seismic activity but also hold implications for exploring mineralization zones associated with metallic and non-metallic deposits.

To address these objectives, a comprehensive investigation of the regional tectonic framework of the Kabul Block, including its bounding faults and surrounding areas, is required. Such an investigation aims to develop a neotectonic model that conceptualizes the Block's geological evolution and subsequently enables the assessment of structures consistent with the proposed model. By understanding the tectonic history of the Kabul Block and its associated fault systems, researchers can gain insights into the dynamic processes that have influenced the formation of mineral deposits within the region.

This comprehensive investigation entails studying the geometry, kinematics, and displacement patterns of the bounding faults as well as their interactions with subsidiary faults within the Kabul Block. The neotectonic model should integrate data from geological mapping, geophysical surveys, and remote sensing techniques, allowing for a multidisciplinary approach to better understand the structural complexities within the Block.

By establishing a robust neotectonic model, researchers can delineate fault systems and identify potential areas of heightened seismic activity within the Kabul Block. Furthermore, the model can aid in the identification of structural controls on mineralization, contributing to the exploration and exploitation of metallic and non-metallic mineral resources in the region. The geological framework and tectonic settings and evolution of the Kabul Block is paramount for both seismic hazard and mineral resource assessments.

Conducting a comprehensive investigation on-site using conventional approaches in the Kabul Block and surrounding regions presents significant challenges and consumes a considerable amount of time. It requires several years, the hiring of numerous professionals and staff, a substantial budget, and the implementation of special protective measures. However, accomplishing all of these requirements in the current situation is practically impossible. Additionally, the rugged topography of the site makes fieldwork on the ground daunting. To effectively address this challenge and achieve the desired objectives, alternative approaches such as Remote Sensing and Geographic Information Systems (GIS) are recommended.

In recent years, the rapid advancement of technology has made it possible to utilize remote sensing and GIS in geological studies, particularly for lithological mapping, mineral exploration, and structural analysis, including fault detection. The use of remote sensing in fault detection offers various advantages from different perspectives, including time-saving, cost-effectiveness, accessibility, effectiveness, and reliability.

Quaternary faults are predominantly marked by linear features on the Earth's surface and are influenced by land deformations such as slip or dip, morphotectonic evidence, or seismic distribution. Aerial and satellite imagery, along with distinct techniques, can be employed to detect fault traces and their diagnostic indicators. Active faults, their associated segments, and deformations are manually identified using high spatial resolution imagery. Since the early 20th century, linear structures on the Earth's surface have been referred to as lineaments. The term was first introduced by Hobbs (1904) to describe valleys, visible fracture or fault zones, ridge crests, boundaries of elevated terrains, drainage channels, coastlines, and contact of rock formations. Lineaments are linear features on the Earth's surface that can be mapped. They can be simple, meaning they are composed of a single line, or composite, meaning they are composed of multiple lines. (O'leary, D. W., Friedman, J. D., & Pohn, 1976).

To a whole extent, the lineaments are used in different disciplines of geology e.g. lithological mapping, hydrothermal alteration zone mapping, morphotectonic and active fault detections, ore deposits and mineral prospecting and exploration, hydrogeology and groundwater exploration, hydrocarbon prospecting and exploration, geothermal potential assessment, landslide and rock fall mapping, and construction projects. The lineaments are detected using optic and radar remote sensing data and deployment of various techniques and algorithms of automated or manual approaches. The lineaments can be geologic, geomorphological, or topographic, and pseudo. In which the lineaments corresponding to faults, fractures, joints, dykes, and shear zones are considered geological lineaments.

The main problem addressed in this research is the lack of comprehensive methodology in determining active fault zones and related structures and also lack of significant and comprehensive investigation into the active faults, their associated structures, and the tectonic architecture of the Kabul Block using remote sensing approaches. The findings of this study aim to provide insights in geological remote sensing and the first results on the neotectonics and faulting structure in the study area.

1.1. Objectives and Scope

To achieve the goals of this research, the main objectives were set as follow:

1. To assess and propose a model for the neotectonics of the Kabul Block and its surroundings and manually detect fault traces with the associated segments using remote sensing approach.
2. To assess displacement, including drainage offsets and morphotectonic structures, inferred from active fault activity by using high-resolution imagery from Google Earth Pro and digital elevation models (DEMs).
3. To detect geological lineaments, analyze their density and tempo-spatial distribution, and investigate their relationship with active fault zones using optical and radar data.
4. To develop a modified methodology for identifying and characterizing fault zones using remote sensing and geographic information systems (GIS).
5. To validate the identified faults, fault segments, and geological lineaments by comparing them with previous geological and tectonic data.

This investigation aims to address the following research questions regarding the Kabul Block in southeastern Afghanistan, utilizing remote sensing approaches:

1. Do the current active fault lines in the Kabul Block align with the regional neotectonic activity?

2. What are the potential fault systems and associated segments present in the Kabul Block?
3. How can we characterize the newly proposed faults and segments?
4. What type of tectonic regime is prevalent in the Kabul Block?
5. What are the tectonic implications of the identified geological lineaments?
6. How can we assess the reliability of remote sensing data and approaches for neotectonic studies, specifically in the context of the Kabul Block?

1.2. Thesis Structure

The thesis is structured into seven distinct chapters which are brief as follow:

1.2.1. Introduction

This chapter aims to provide a comprehensive understanding of the research background, problem statement, novelty, and core objectives of the study. By delving into these aspects, we can gain valuable insights into the context and significance of the research conducted.

In the beginning, the chapter sheds light on the research background, offering a thorough exploration of the existing knowledge and studies related to the subject matter. This background analysis sets the stage for identifying the research gap that the current study aims to address.

Next, the problem statement is clearly articulated, highlighting the specific issue or challenge that the research seeks to tackle. By clearly defining the problem, the study establishes a solid foundation for subsequent investigations and analyses.

In terms of novelty, the chapter underscores any innovative or groundbreaking aspects of the research. This can include novel methodologies, approaches, or theoretical frameworks that differentiate the study from previous work in the field. By highlighting the novelty, the chapter emphasizes the potential contributions and advancements the research can make.

Furthermore, the chapter examines the limitations of conventional studies in the field of active fault mapping. It outlines the challenges and shortcomings associated with traditional methods and techniques used in this area of study. This critical assessment serves as a rationale for exploring alternative approaches, specifically remote sensing techniques and data. These innovative methods offer promising possibilities for more accurate and comprehensive fault mapping.

By introducing remote sensing techniques and data as an alternative approach, the chapter lays the groundwork for the subsequent discussions. It outlines the key characteristics and advantages of remote sensing in the context of fault mapping, emphasizing its potential to overcome the limitations of conventional methods.

Consequently, the chapter concludes by highlighting the specific objectives and contributions of the current study. These objectives serve as a roadmap for the research, guiding the subsequent investigations, data collection, and analysis. Additionally, the chapter emphasizes the potential contributions that the study can make to the field, such as advancing the understanding of fault mapping and potentially improving hazard assessments.

1.2.2. Literature review

This chapter serves as a dedicated section for a comprehensive systematic literature review on the topic of this thesis. The aim is to delve into the subject matter by dissecting it into two distinct parts, each offering valuable insights.

In the first part, meticulous attention is given to the reviewed literature surrounding the active faults of Afghanistan, with a specific focus on the Kabul Block. This entails an in-depth exploration of their characteristics, encompassing detailed descriptions and other essential tectonic features. The scope of this investigation spans the entire timeline of geological studies in Afghanistan, providing a historical context that sheds light on the development of our understanding of these active faults.

Moving forward, the second part of this chapter delves into the reviewed literature pertaining to the methodology used for determining active faults and geological lineaments that express geological faults using remote sensing and geographic information systems. With the advent of remote sensing technologies and the launch of earth observational satellites in 1970, a wealth of data and algorithms have become available for scientific exploration. This section offers an insightful analysis of the various remote sensing algorithms employed for the identification and characterization of lineaments associated with geological faults. Additionally, it examines the usage of diverse remote sensing data sources, highlighting the advancements made in this field over the years.

By structuring the literature review in this manner, the chapter provides a comprehensive and thorough examination of the topic at hand. It ensures that both the geological characteristics of the active faults in Afghanistan and the methodologies employed to study them are adequately explored, allowing for a comprehensive understanding of the subject matter.

1.2.3. Geographic and geologic settings

This chapter serves as a comprehensive framework encompassing a range of vital aspects. Firstly, it provides a succinct yet informative account of the geographic location of the Kabul Block, accompanied by a detailed exploration of the prevailing environmental conditions. By delving into these factors, the chapter aims to establish a solid foundation for subsequent discussions.

Another pivotal focus of this chapter is the thorough examination of the geologic settings within the Kabul Block and its surrounding regions. Considerable attention is dedicated to elucidating the distribution patterns of various formations, meticulously analyzing their age and compositional attributes. By undertaking this comprehensive exploration, valuable insights are gained into the intricate geological framework that underpins the Kabul Block.

Furthermore, a diverse array of tectonic studies to shed light on the tectonic subdivision and its associated ramifications within the Kabul Block is highlighted in this chapter. Also, direct attention is paid to the major active fault zones that exert a significant influence on the region. These fault zones, renowned for their seismic activity and propensity to generate earthquakes, are thoroughly expounded upon within this chapter.

1.2.4. Materials and methods

This chapter is structured into two distinct sections to facilitate a comprehensive examination of the subject matter. The primary objective of the first section is to provide readers with a comprehensive understanding of the essential materials required for this study. These materials encompass a range of crucial data, including remote sensing, geologic, tectonic, and seismic data. In addition, this section aims to shed light on the authorized sources from which each of these data sets has been obtained, ensuring transparency and accountability in the research process.

Moving on to the second section, the primary focus is centered around presenting the proposed methodology employed for the determination and characterization of active faults within the Kabul Block, as well as the subsequent exploration of their neotectonic implications. The intricacies of this methodology are explored in detail, with particular emphasis placed on the automated, manual, and semi-automated detection of geological lineaments. These methods, selected for their efficacy and relevance, serve as invaluable tools in analyzing and interpreting the data collected.

Moreover, this section delves into the specific filters that are crucial for preprocessing the data before initiating the analysis. By elucidating the rationale behind their usage and elucidating their function, readers gain a thorough understanding of their significance in optimizing the accuracy and reliability of the subsequent findings. Furthermore, the morphotectonic analysis applied in this research is meticulously explained, providing insights into the techniques employed to study the geological features and their dynamic nature.

1.2.5. Results and data analysis

Within this chapter, the acquired results obtained through the implementation of the proposed methodology are meticulously presented and comprehensively explained. As this research endeavor encompassed a wide array of remote sensing data and employed various methodologies, it becomes imperative to assess the efficacy and reliability of each dataset and algorithm utilized. Consequently, this chapter delves into a thorough examination of the effectiveness and dependability of the employed data sources and algorithms, while simultaneously addressing the limitations inherent in their application.

Furthermore, in recognition of the challenges and limitations faced during the research process, this chapter offers valuable suggestions and recommendations aimed at mitigating these obstacles. By proposing insightful strategies and approaches, the intention is to enhance the overall robustness and validity of the findings, ensuring a more comprehensive and accurate interpretation of the results obtained.

Moreover, a vital aspect of this chapter involves the meticulous interpretation and analysis of the statistical data derived from the results. By scrutinizing and extracting meaningful insights from the statistical findings, the research aims to provide a deeper understanding of the observed patterns and trends, contributing to a more comprehensive evaluation of the research outcomes.

1.2.6. Discussion

This chapter places a strong emphasis on the geologic and tectonic implications stemming from the identified segments and geological lineaments. It delves into a comprehensive exploration of the detected fault lines and geological lineaments, shedding light on their significance within the broader geological context. Furthermore, this chapter delves into a thorough examination of the seismic activity relevant to the study, providing valuable insights into its relationship with the identified features. By considering all aspects, this chapter presents a new tectonic model for the Kabul Block and surroundings.

Additionally, the chapter delves into the correlation and validation of the results obtained through both automatic and manual detection methods employed to identify active faults. By scrutinizing the outcomes of these detection techniques, this chapter seeks to establish a robust foundation for the findings, ensuring their accuracy and reliability. Ultimately, the chapter concludes by engaging in a comprehensive discussion and analysis of these correlations and validations, consolidating the understanding of the detected active faults and their implications.

1.2.7. Conclusions and recommendations

The concluding chapter serves as a culmination of this research, offering a comprehensive overview of the key findings and future contributions. It begins by highlighting the hypothesized tectonic model of the Kabul Block and the associated structures, emphasizing the role played by both remote sensing and conventional data in their development. Furthermore, this chapter explores the broader implications of the tectonic model, discussing its potential contributions to other disciplines within the fields of geology and neotectonics.

Concluding on a forward-looking note, the chapter concludes with essential recommendations that stem from the limitations encountered during the study. These recommendations serve as valuable insights for future research endeavors, guiding the exploration of avenues for further advancement and refinement in the field.

In essence, this final chapter provides a comprehensive summary of the research, highlighting its significant findings, discussing the potential contributions to related disciplines, and concluding with essential recommendations derived from the study's limitations.

2. LITERATURE REVIEW

2.1. Active Faults of the Kabul Block and Surroundings

The Afghan Block, situated at the junction of the Indian, Arabian, and Eurasian plates, has been the subject of interest for local and foreign geoscientists due to its diverse geologic and tectonic features. The country's spectacular geological structures have also attracted the attention of geologists.

Official geological studies in Afghanistan began in 1955 with the establishment of the National Geological Survey. The department has since collaborated with geologic groups from France, Italy, Germany, and Russia (the former Soviet Union) to conduct further studies. Kabul Block and Hindu Kush–Pamir Syntax are among the tectonic blocks in Afghanistan that have been studied extensively. However, due to limited research, several questions and problems related to active faults, tectonic models, and architecture remain unresolved.

The earlier description of the Chaman fault zone with left-lateral motion to the west of the Kabul Block, was reported by Griesbach, (1893) and McMahon, (1897) after an earthquake in 1892 along the borders of Kandahar and Chaman. Wellman, (1966) conducted earlier regional studies of active faults throughout Iran, Afghanistan, and Pakistan, using aerial photographs to detect the fault traces of the Chaman fault zone along the west margin of the Kabul crustal Block based on their apparent displacement.

A comprehensive geological framework of Afghanistan was compiled in two volumes on the geology and mineral resources of Afghanistan on a scale of 1:500,000 by Abdullah & Chmyriov, (2008), as a result of cooperative works between the Afghan Geological Survey and the former Soviet Union (Russia) geoscientists. In this report, the authors described the major active faults and other geo-structural features in a general context. They also focused on the overall description of the slip rates, geological environment, and Quaternary displacement of the Paghman–Chaman, Sarobi, and Gardiz (Altimur) faults. Another regional fault-based study was carried out by Trifonov, (1978) over central and western Asia, in which the author only focused on the Chaman fault zone at a regional scale based on previous studies.

In 1979, Quittmeyer & Jacob, (1979) examined the seismicity of Pakistan, Afghanistan, India, and Iran based on recorded earthquake data between 1914 and 1965 to characterize the active faults in the region. Within the territory of Afghanistan, the authors highlighted the Chaman and Herat faults as seismically active faults.

At the same time, Yeats et al., (1979) assessed the surface impact of the 1979 earthquake along the borders between Afghanistan and Pakistan and consequently determined the motion and slip rate of the active fault in the region. A study on shallow earthquakes and active tectonics of eastern Afghanistan was conducted by Prevot et al., (1980). The authors installed several temporary seismic stations in four separate areas to characterize the nearby faults, particularly the Chaman and Sarobi faults, and also calculated some fault plane solutions. Shareq, (1981) summarized all the geological and geophysical investigations conducted between 1972 and 1979, compiling the geologic and tectonic maps of Afghanistan. The author characterized the overall tectonic structure framework of the country and highlighted the focal mechanisms of the recorded earthquakes based on seismic observations.

In collaboration with a French geoscientist group, Tapponnier et al., (1981) investigated the Mesozoic ophiolites and associated suture zones, and large-scale tectonic movements along the Chaman and Gardiz (Altimur) faults in Afghanistan. The authors focused on the distribution of ophiolitic complexes along the faults and associated overthrusting blocks. Lawrence et al. (1992) reported that the Chaman fault zone has a slip rate of 19-24 millimeters per year (mm/yr) over the past 20-25 million years.

Ambraseys & Bilham (2003) summarized the historical record of earthquakes in Afghanistan from 734 to 2002 AD, including both instrumental and narrative records. This was after a period of time when there were no geological investigations in Afghanistan. The investigation focused on the deformed regions of the Chaman fault zone inside Afghanistan and the damage caused by high-magnitude earthquakes in Afghanistan.

After the initiation of USGS cooperation in Afghanistan, Wheeler et al., (2005) compiled a seismotectonic map of Afghanistan based on the major active faults determined by past studies and the earthquakes that had occurred. Considering factors such as surface rupture, landform offset, and clustering of earthquake epicenters, the authors identified 22 significant active faults in Afghanistan, including the Paghman–Chaman, Sarobi, and Gardiz faults within the Kabul Block. The authors noted that the Chaman fault zone is a major and active geological fault in Afghanistan, and that it is capable of producing large earthquakes. They also highlighted the importance of seismotectonic mapping in Afghanistan, as it can help to identify areas that are at risk of earthquakes and to mitigate the damage caused by these events.

In a recent report by Ruleman et al., (2007), the probable and possible Quaternary faults of Afghanistan were mapped. Based on tectonic, geomorphic, and physiographic analysis and interpretation, all the existing faults in the country were subdivided into eight different tectonic domains:

- The Chaman Fault System
- The Sulaiman Fold and Thrust Belt and Associated Contractional Zones
- The Hindu Kush–Pamir Intermontane Region
- The Hari Rud–Northern Afghan Platform System
- The Tajik Basin and Alburz–Marmul Fault System
- The Western Hari Rud Fault System
- Central Afghanistan Accreted Terranes
- The Helmand Basin–Makran System

Remote sensing interpretation using Landsat imagery and previous related studies were used in this report.

In 2010, Mohadjer et al., (2010) conducted GPS measurements by installing temporary stations in Kabul and Peshawar to investigate the slip rate of the Chaman and Gardiz left-lateral strike-slip faults over limited regions of the Kabul Block. Afterward, Szeliga et al., (2012) used GPS and InSAR data to measure the slip rate of the Chaman fault zone at different scales. They reported a geodetic slip rate of 16.8 ± 2.7 mm/yr near Qalat city in Zabul province, and 16.8 ± 0.51 mm/yr near Kabul province. In another study, Barnhart, (2017) used InSAR data to measure the fault creep rate of the Chaman fault zone. The findings showed that the peak creep rates on the fault are between 9 and 12 mm/yr, and that 25–33% of the total motion is accommodated by the Indian and Eurasian plates.

A recent fault-based investigation on the mapping of active and presumed active faults in Afghanistan was carried out by Shnizai, (2020). In this study, the author mapped all the possible active faults in the country by manually interpreting 1-arcsecond SRTM anaglyph images. This resulted in the identification of three dominant types of faults: left-lateral, right-lateral, and thrust. The author then combined the fault map with earthquake data to interpret the seismic hazard and define earthquake sources. Four zones in terms of seismicity were demarcated: E-NE, Afghanistan-North Pamir, Northern Afghanistan platform, and middle and SW Afghanistan. The east and northeastern regions of Afghanistan were considered with high risk of seismicity in the country.

In another study, Shnizai et al., (2020) defined the Pleistocene left-lateral slip rate of the northern extension of the Chaman fault zone in the Kabul Block using 10Be dating of offset alluvial fan surfaces at two displaced alluvial fans over the Ghat Bandakul and Azadkhail areas of Wardak province. In this investigation, the authors used remote sensing data from CORONA and ALOS PRISM images, followed by fieldwork.

A review of the literature on active faults in Afghanistan, particularly in the Kabul Block, reveals that limited studies have been conducted. These studies have characterized individual faults by highlighting their general description, relative slip rates, seismic activity, and landform offset. The methodologies used in these studies have been conventional, visual interpretation of aerial images, and limited studies with InSAR data.

However, these studies have some limitations. First, they have only characterized individual faults, and not the tectonic architecture of the entire Kabul Block. Second, they have not considered all possible faults in the Kabul Block, and have only focused on the Paghman–Chaman, Sarobi, and Gardiz faults. Third, they have not used the most advanced remote sensing techniques and high-resolution image data, to map active faults.

To address these limitations, a comprehensive investigation of the neotectonics of the Kabul Block is needed. This investigation used advanced remote sensing techniques to map all possible active geological faults in the Kabul Block. It also characterized the tectonic architecture of the Kabul crustal Block and identify the associated segments of the active faults. Such a comprehensive investigation would provide a valuable dataset for understanding the seismic hazard in the Kabul Block. It would also help to identify areas that are at risk of earthquakes, and to mitigate the damage caused by these events.

2.2. Remote Sensing-Based Active Fault and Geological Lineaments Detection

Remote Sensing (RS) and Geographic Information Systems (GIS) have been widely used for various geologic and neotectonics applications, such as lithological mapping, structural analysis, active fault, and seismic hazard assessment, since the discovery of satellite imageries. A diversity of automated, semi-automated, and manual interpretation approaches and algorithms have been examined for geological-based lineaments and fault mapping. In addition, interpretations of satellite imageries are employed for the characterization of tectonic regimes and models of regions surrounded by the faults and their associated land deformation.

A systematic literature review on the determination of geological lineaments, methods, and data was carried out in the framework of a review article within the scope of this dissertation, which has been published in Geosciences. More details on the state of the art in lineaments extraction using remote sensing and GIS are described in (Ahmadi & Pekkan, 2021). The most significant and influential literature on the geological lineaments detection is briefly summarized here.

The initial detection of lineaments dates back to 1974, when Kowalik & Gold, (1974) used Landsat 1 to map lineaments in Pennsylvania. This study demonstrated the capabilities of this sensor in its early stages. The authors used a basic methodology of color composite to differentiate drainage networks and faults. A year later, Podwysocki et al., (1975) used analog analysis after directional filtering of Landsat 1 to delineate geological lineaments in the Anadarku basin of the Colorado Plateau. In 1980, Burdick & Speirer, (1980) developed a computer-aided approach to detect geological lineaments and other linear features from Landsat images. They verified their results with ground truth, which showed a high correlation between the results.

Abrams et al., (1985) applied several digital image processing techniques, including false color composite, supervised classification, bright color gradient, and filtering, to distinct satellite imageries to accomplish geological mapping, automatic lineament extraction, and textural measurement in Wyoming, USA. Joshi, (1989) applied several other methods, including image enhancement, binary image conversion, and structure analysis, for automatic lineament detection on Landsat data over the Tamil Nadu, India.

The early use of radar data, particularly Synthetic Aperture Radar (SAR) interferometry, was examined by Gabriel et al., (1990) to measure very small (1 cm or less) surface deformation. The authors also confirmed the capability of radar data for vertical and lateral displacement generated by seismic activities. The generation of a synthetic stereo pair of Landsat images for geologic and morphotectonic interpretation was first tested by Salvi, (1995) in the Abruzzo region of central Italy. The authors cross-checked their results with field geology and structural surveys.

Different filtering algorithms, such as histogram equalization and stretching for single bands, principal component analysis (PCA) for multiple bands, and Prewitt and Sobel filters for spatial domains on satellite imageries, were employed by Suzen & Toprak, (1998) to analyze the geological lineaments in the center of Turkey throughout a fault zone. Lee & Moon, (2002) examined diverse remote sensing data, such as DEM, JERS-1, and Landsat TM for automated and manual extraction of lineaments expressing geological fault lines in Kyungasang, Korea. The authors used Hough Transform techniques and claimed the successful extraction of lineaments. Mavrantza & Argialas, (2003) employed spatial filtering and automatic edge detection techniques to automatically delineate lineaments over the Alevrada in Central Greece.

After the promotion of satellite industries and the emergence of ASTER data, Hung et al., (2005) used two distinct remote sensing data, Landsat ETM, and ASTER, to compare their capabilities in lineaments extraction. They tested these data over the tropical region of Suoi Moi karst catchments in Vietnam. In addition, in this study, the authors deployed visual interpretation and digital image processing approaches and claimed that ASTER data had a higher capability due to its higher spatial resolution.

Despite the promotion of remote sensing data, algorithms for different purposes have also been developed. In this regard, Gloaguen et al., (2007) applied object-based classification of remote sensing data on DEM and radar imageries to extract geologic faults within Lake Magandi in southern Kenya. Moreover, Elliott et al., (2008) measured the slip rate of a strike-slip fault in northern Tibet using remote sensing techniques on InSAR imageries. Based on their results, lateral strike-slip motion with no relative vertical motion was revealed.

Integration of remote sensing with geophysical data has also proven the capability of effective fault system determination. A. A. Masoud & Koike, (2011) combined SRTM DEM and gravity and magnetic data to detect major faults with their tectonic implications over Egypt. In this investigation, the authors examined various techniques, such as adaptive shading of grid data and B-spline smoothing for lineament segmentation and grouping. Finally, they attempted to classify the fault system based on their orientations.

In another location, in 2013, Thannoun demonstrated that the Landsat ETM+ satellite sensor can be used to automate the mapping and analysis of lineaments and their importance in the tectonics of northern Iraq. This was done by applying Sobel-Kernel directional filters to the satellite imagery. In a tropical region, Pour & Hashim, (2015) used PALSAR data to map the geological structures in Peninsular Malaysia. In this study, the authors applied an automatic lineaments extraction approach, including preprocessing and processing, such as local sigma filter and directional filtering, to highlight geological lineaments. They then carried out a correlational analysis to find out their correlations with tectonic activities and features. Radar and optical data, including Landsat-8

OLI/TIRS, SPOT-5, and DEM, were utilized by Benaafi et al., (2017) to analyze lineaments and their tectonic implications over southern Saudi Arabia by examining spatial and radiometric enhancement. Finally, the authors conducted statistical analysis to define the lineament trends and their possible stress regime.

Recently, Farahbakhsh et al., (2020) conceptualized the capability of optical remote sensing data, particularly Landsat 8 OLI/TIRS, for the delineation of tectonic lineaments in Gascoyne Province, southern Australia. The authors achieved their objectives by applying the Minimum Noise Fraction (MNF) transformation, Laplacian filter, and directional filter techniques. A recent work by Andongma Wanduku Tende et al., (2022) highlights the effectiveness of hybrid extraction of tectonic lineaments using DEM. The authors applied filtering algorithms, an automatic extraction approach, Euclidean distance analysis, binary discretization, spatial integration, and manual digitization over the Mandara Mountain, the northern extension of the Cameroon basement complex. They also conducted spatial and statistical analysis to evaluate the tectonic and geologic configurations. Lastly, the authors characterized the case study as having poor mineral resources potential and poly-deformational tectonic episodes due to a relatively low fractal dimension.

The reviewed literature reveals that there is not a unique framework for the delineation of lineaments expressing geological faults. The different studies reviewed in this paper have utilized a variety of methods, including manual digitization, image processing, and integration with geophysical data. The choice of method depends on the specific objectives of the study, the availability of data, and the expertise of the researcher. Despite the lack of a single framework, the reviewed studies suggest that a comprehensive and integrated approach is the most effective way to delineate lineaments. This approach should include the use of multiple methods, as well as the integration of geological, geomorphological, and geophysical data. By taking this approach, researchers can better understand the tectonic significance of lineaments and their implications for the distribution of mineral resources, morphotectonic deformations, and stress regimes.

3. GEOGRAPHICAL AND GEOLOGICAL SETTINGS

3.1. Geographical Position

Afghanistan is a landlocked country in the heart of Asia. It is bordered by Pakistan to the east, Iran to the west, Tajikistan, Uzbekistan, and Turkmenistan to the north, and China to the northeast. The country is mountainous, with the Hindu Kush Mountain range running through the center. The Kabul Block is located in the eastern part of Afghanistan, extending between 69°15'59.07"E and 68°28'37.65"E and 35°09'50.54"N and 33°28'53"N, with an average elevation of 2,678 meters. It starts in the southeastern part of Parwan and the northwestern part of Kapisa provinces, crosses the southern Hindu Kush ranges, and passes through the central parts of Kabul and Logar provinces. It terminates in a region that covers southeastern Wardak, southwestern Paktya, and eastern Ghazni province (Figure 3.1).

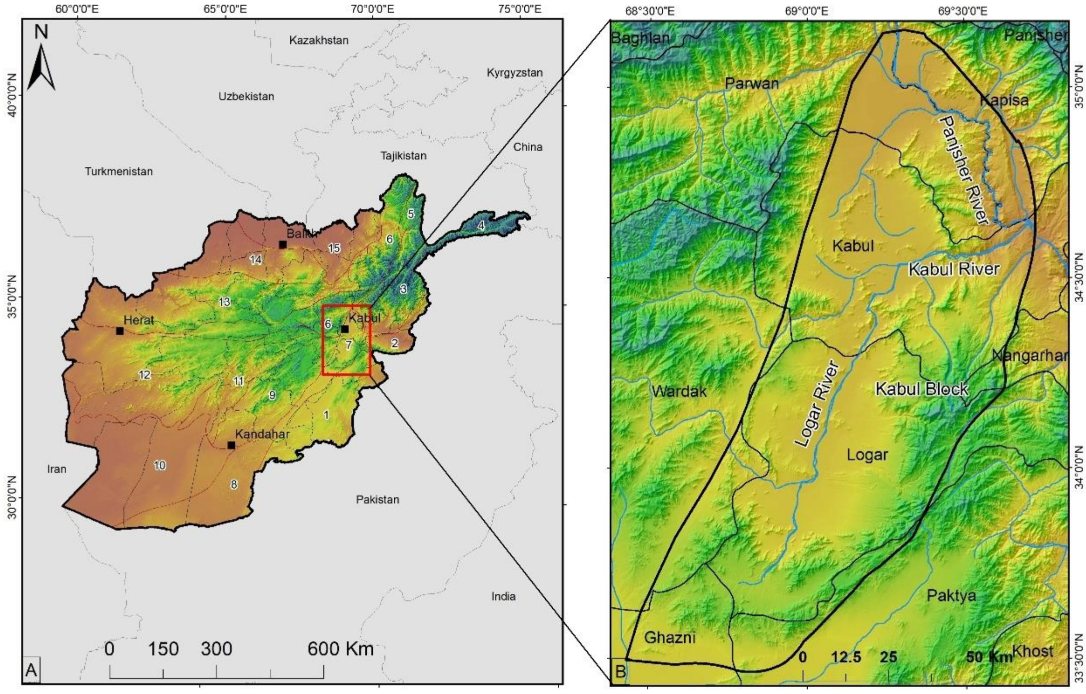

Figure 3.1. *The geographic location of study area and its surroundings. A) The location of Afghanistan in the region, B) The location of the Kabul Block and its geomorphological settings*

Two major rivers flow through the area, draining the predominant sedimentary basin system (Figure 3.1B). The northern and eastern margins of the basin are bounded by the Hindu Kush ranges, while the Paghman ranges form the western margin. The Kabul Block is characterized by a semi-arid climate, with precipitation that is primarily rainfall in the spring and snow in the winter. The temperature in winter can drop as low as -10 °C, while it can reach 30–40 °C during the summer, especially in Kabul city (Ahmadi & Uygucgil, 2021; Ayoobi et al., 2021).

3.2. Geological Settings

3.2.1. Stratigraphy

The Kabul Block is a fault-block region that is separated from adjacent blocks by faults. It has a length of approximately 200 kilometers and a width of approximately 70 kilometers, and it has an elongate or oblong shape. The Kabul Block is made up of old, deformed rocks that formed from the Archean to Cenozoic eras. These rocks are covered by younger Paleozoic and Cenozoic sediments (Ahmadi & Uygucgil, 2021; Faryad et al., 2016; Yousufi et al., 2023) (Figure 3.2A).

3.2.1.1. Precambrian

Four distinct formations have been identified in the Kabul Block, all of which are related to Precambrian basements. Bohannon, (2010) divided the Kabul Block into two formations, (Abdullah & Chmyriov, 2008) separated three formations, and Karapetov et al., (1981) defined four different formations in the area. The formations are Khair Khana, Sherdarwaza, Kharog, and Welayati, in order from oldest to youngest.

The Khair Khana Formation is a geological unit first identified by Karapetov et al. in 1981. It is made up of xenoliths, or fragments of rock, that have been altered to granulite facies, a type of high-grade metamorphic rock. The age of the xenoliths is uncertain, but they may be Archean, meaning they are over 2.5 billion years old, and it is found in the Khair Khana hills, which are located in the northwest of Kabul. Karapetov et al. (1981) classified the rocks of the Khair Khana formation as orthogneiss, which are foliated metamorphic rocks that were originally granitic in composition. They also noted that the formation does not contain marble or calc-silicates. Abdullah et al. (2008) did not identify any formations or lithologies in the Kabul Block, while Bohannon (2010) hypothesized that the Khair Khana formation is part of the Sherdarwaza formation.

The Sherdarwaza formation contains distinct rocks of migmatites, gneiss, marble, amphibolite, and quartzite. These rocks are exposed in the hills surrounding the Kabul city, Koh-i-Safi to the east of the city, and in limited areas in the south of the Kabul Block (Abdullah & Chmyriov, 2008; Karapetov et al., 1981) (Figure 3.2B). According to

Bohannon (2010), the northern localities are characterized by gneiss and migmatite, while the southern areas are characterized by schist. Marble is found in the form of single beds or lenses within schist, gneiss, and migmatites. Amphibolite bodies, on the other hand, are distributed throughout the Sherdarwaza formation. (Abdullah & Chmyriov, 2008).

The Kharog formation is a stratigraphic unit that is separated from the Sherdarwaza formation by an apparent disconformity. The Kharog formation is composed of basal conglomerate, quartzite, crystalline schist, gneiss, amphibolite, and marble. The extent of the Kharog formation is contradictory. Karapetov et al. (1981) determined that the extent of the formation in the south and west of Kabul is older than the Sherdarwaza formation, while Bohannon (2010) observed that these areas are part of the Sherdarwaza formation and cannot be distinguished from the Welayati formations.

Abdullah et al. (2008) stated that the Welayati formation lies conformably on top of the Kharog formation. The Welayati formation is made up of three layers: a base layer of crystalline schist, a middle layer of amphibolite, and a top layer that is a mixture of crystalline schist and amphibolite.The Welayati formation crops out in the south of Kabul city, around the Koh-i-Safi, and Sarobi fault, northeast of the Kabul Block.

3.2.1.2. Vendian – Cambrian

Around the Aynak copper mine in the southeast of the Kabul Block, the Vendian-Cambrian Loy Khwar and Gulhamid meta-sediment formations unconformably overlay the Welayati formation (Abdullah & Chmyriov, 2008; Ahmadi & Uygucgil, 2021; Bohannon, 2010) (Figure 3.2B). According to Bohannon (2010), the Loy Khwar formation, which is composed of dolomite marble, carbonaceous quartz-schist, quartz-biotite-schist, and quartzite, hosts copper mineralization at the Aynak copper mine. The Gulhamid formation is composed of intermediate volcanic rocks, including conglomerate, meta-sandstone, schistose tuff, breccias, and tuffaceous sandstones of andesitic to dacitic composition (Bohannon, 2010).

3.2.1.3. Carboniferous - Permian

Volcanic and sedimentary rocks that formed from the Carboniferous to Lower Permian eras are exposed in the southern part of the Kabul Block. These rocks are made up of low-grade phyllite and slate, limestone, dolomite, sandstone, conglomerate, and basalt (Abdullah & Chmyriov, 2008) (Figure 3.2B). The ages of these rocks have been determined based on the indicator fossils.

3.2.1.4. Permian – Jurassic (Khengil Series)

Based on Abdullah et al. (2008) and Bohannon (2010), the Permian to Jurassic rocks along the eastern edge of the Kabul Block are made up of carbonates, and they are characterized by the Khengil Series (Figure 3.2B). (Fischer Jochen, 1971) reported seven distinct units over the Khengil Series:

1. Guadalupian basal conglomerate
2. Reef limestone of late Permian age
3. Ceratiten-bearing limestone of Lower Triassic
4. Limestone, dolomite, and tuff related to Middle to Upper Triassic
5. Ammonite-bearing limestone of Jurassic age
6. Belemnite-bearing limestone of Jurassic age
7. Mostly Jurassic undifferentiated limestone

3.2.1.5. Undifferentiated – Eocene (?) (Kotagai Melange)

The Khengil Series is unconformably overlain by the volcano-sedimentary rocks of the Kotagai Melange (Abdullah et al., 2008). The Kotagai Melange is a strongly deformed mixture of rocks, including limestone, meta-sandstone, shale, basaltic schist, andesite, and serpentinized basalt. The age of the mélange is unknown because no fossils or radiometric dating techniques have been able to accurately date it. However, Abdullah et al. (2008) suggested that the Kotagai Melange formed from the Cretaceous to Eocene eras, while Mennessier (1977) proposed that some parts of the mélange may be as old as the Paleozoic era. Bohannon (2010) argued that the Kotagai Melange in the southern Koh-i-Safi is overlain by the Sherdarwaza gneiss.

3.2.1.6. Neogene – Holocene

The Lataband Series, a set of Neogene-Holocene covering sediments, is widely distributed throughout the Kabul Block. In addition, Pleistocene and Holocene alluvial deposits are found in the floodplains of the Kabul and Panjsher rivers (Abdullah & Chmyriov, 2008). (Figure 3.2B).

3.2.2. Magmatism

3.2.2.1. Ultramafic rocks

Ultramafic bodies are reported along the eastern (Koh-i-Safi) and southwestern (Logar Ophiolite Complex) margins of the Kabul Block (Ahmadi & Kalkan, 2021; Tapponnier et al., 1981; Yousufi et al., 2023). Bohannon (2010) suggests that these rocks have been thrusted onto the Kotagi Melange in the east, which is described as the Khost Ophiolite Complex, and onto the Carboniferous-Permian metasedimentary rocks in the west and southwest, which are indicated as the Logar Ophiolite Complex. These rock complexes are made up of mostly peridotite, dunite, harzburgite, and serpentinite. (Ahmadi & Kalkan, 2021; Benham et al., 2009) (Figure 3.2B).

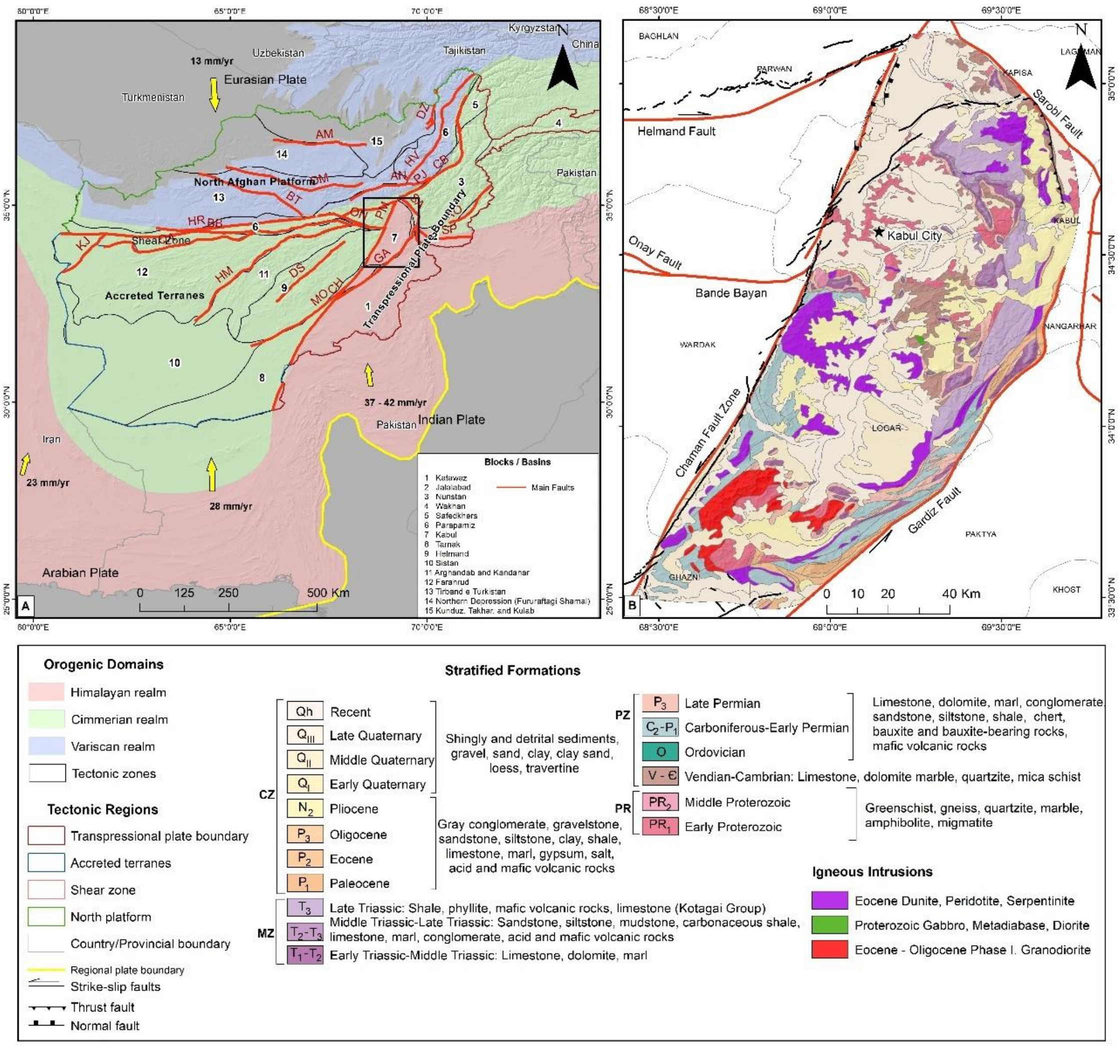

Figure 3.2. *Regional tectonic and geologic evolution of Kabul Block. A) Tectonic sketch, regions and zone of Afghanistan after* (Abdullah et al., 2008; Wheeler et al., 2005), *yellow arrows represents the plate movement velocity from* (Ambraseys & Bilham, 2003; Mohadjer et al., 2010; Revel Sella A, 2002; Ruleman et al., 2007), *B) Geologic map of Kabul Block modified from* (Abdullah & Chmyriov, 2008; Bohannon, 2010; Karapetov et al., 1981), *Red line represents previously*

major faults from (Abdullah et al., 2008; Ruleman et al., 2007)*, black lines indicate the predefined fault segments by (Ahmadi et al. 2022). The local name of faults: AM, Alburz Mormul; AN, Andarab; BB, Bande Bayan; BT, Bande Turkestan; CH, Chaman; CB, Central Badakhshan, DS, Darafshan; DV, Darvaz; DM, Dosi Mirz-Valang; GA, Gardez; HA, Henjvan; HR, Herat; HM, Helmand; KR, Kaj Rod; KO, Konar; MO, Mokur; ON, Onay; PM, Paghman; PJ, Panjsher; QA, Qarghandaw; SA, Sarobi; SP, Spin Ghar*

3.2.2.2. Granitoid complexes (Eocene – Oligocene)

A body of igneous rock known as granitoid, which formed in the Eocene-Oligocene era, has been found in the southern part of the Kabul Block. This granitoid intrudes, or cuts through, the Precambrian basement rocks and the Carboniferous-Permian metasediments (Abdullah & Chmyriov, 2008) (Figure 3.2B). Debon et al. (1987) hypothesize that the granitic intrusions are linked to a continental collision that happened after the Indian and Eurasian plates subducted or slid beneath each other.

3.2.3. Tectonic settings and active faults

Afghanistan is located in a collision zone between the Eurasian, Arabian, and Indian plates, as part of the active orogenic belt of the Alpine-Himalayan range. In the northern regions, the Eurasian plate is subducting beneath the Indian plate, which is causing the uplift of the Hindu Kush mountains. The Afghan territory is influenced by the southward movement of the Eurasian plate at a velocity of about 12 mm/yr., while in the south, the regions between the southeast of Iran and southwest of Pakistan, the Arabian plate is moving northward at a velocity of between 23–28 mm/yr. in a zone known as the Makran subduction zone (Ahmadi & Uygucgil, 2021; Ambraseys & Bilham, 2003; Aslam & Naseer, 2020; Seyitoğlu et al., 2019; Shroder et al., 2021) (Figure 3.2A). In the southeastern part of Afghanistan, there is another tectonic structure called the Chaman Fault Zone. It is a left-lateral fault that lies between the Eurasian plate and the northward-moving Indian plate. The relative velocity between the two plates is 37–42 mm/yr. (Ruleman et al., 2007; Wheeler et al., 2005). Further, in the northeastern parts of the country, the Hindu Kush-Pamir ranges mark the contact of the Eurasian and Indian plates, which is responsible for the major seismic activity (Figure 3.2A). This collision has caused the major active faults and shaped the complex structure of Afghanistan.

Based on the literature (Abdullah & Chmyriov, 2008; Shroder et al., 2021; Siehl, 2017; Treloar & Izatt, 1993; Wheeler et al., 2005), three orogenic segments have been identified in Afghanistan:

- The Variscan (Hercynian)-Late Paleozoic (Devonian–Permian) segment in northern Afghanistan
- The Cimmerian–Mesozoic (Late Triassic–Early Cretaceous) segment in the Central Afghan Block
- The Himalayan (Alpine)–Cenozoic (Late Cretaceous–Quaternary) segment in the eastern regions, along the transpressive boundary of the Indian plate

Magmatic activity and ophiolitic nappes are the indicators of these orogenic domains in the country. Wheeler et al. (2005) further separated Afghanistan territory into four tectonic subdivisions:

- The Transpressional Plate Boundary (TPB), which covers eastern Afghanistan
- The Accreted Terranes (AT), which limits the central parts of the country
- The Shear Zone (SZ), in the middle of Afghanistan
- The North Platform (NP), to the north of the country

(Abdullah & Chmyriov, 2008; Leven, 1997) carried out a minor tectonic subdivision of Afghanistan, dividing it into 15–26 tectonic zones. All of these orogenic realms, tectonic regions, and zones are separated by abundant local and regional suture and fault zones, which produce seismic activity. Twenty-two significant seismically active faults have been reported in the northern, northeastern, eastern, southeastern, central, and western regions of Afghanistan (Abdullah et al., 2008; Ruleman et al., 2007; Shroder et al., 2021) (Figure 3.2A).

According to the above classifications, the Kabul Block is located at the edge of the Himalayan-Alpine domain and is affected by the Transpressional Plate Boundary Tectonic Region. This region was created by the collision of the Indian plate with the Afghan promontory of the Eurasian plate, which started around 55 million years ago in the southeastern corner of Afghanistan (Figure 3.2A) (I. H. Khan & Clyde, 2013; Siehl, 2017).

According to Ahmadi & Uygucgil (2021) and Collett & Faryad (2015), the Kabul Block, along with the other Farah and Helmand (Afghan central blocks), are connected to the plates of Indian and Eurasian by suture zones, which are geological structures that mark the boundaries between tectonic plates. The Kabul Block is separated from other adjacent blocks by active fault systems. The Herat–Panjsher faults to the north, the

Chaman fault zone to the west, the Sarobi fault to the east, and the Gardiz fault to the southeast act as borders between the Kabul Block and the Hindu Kush and Parapamiz blocks, the Helmand Block, the Nuristan Block, and the Katawaz basin, respectively (Ahmadi & Uygucgil, 2021; Wheeler et al., 2005) (Figure 3.2A).

The Chaman fault zone, trending from N10°E to N35°E, is a major left-lateral strike-slip fault zone with an oblique motion and a total length of 860 km, of which 650 km is located in Afghanistan (Lawrence et al., 1992). The fault detaches the Indian plate from the southward-moving Eurasian plate to the west, and in a local scale, it separates the Kabul Block from the Helmand Block (Ahmadi et al., 2022; Ruleman et al., 2007; Wellman, 1966) (Figure 3.2A).

Based on Ambraseys & Bilham (2003), the fault zone has caused extremely high deformation in the region between 150–300 km throughout Afghanistan and Pakistan. The term for the fault has been reported differently in the literature, e.g., Chaman fault, Chaman–Makur or Mokur fault, and even recently, Ruleman et al. (2007) subdivided it into four segments from south to north: Chaman, Mokur, Gardiz, and Paghman (Figure 3.2A). In this research, updated local names were selected for the fault segments, which are discussed in further chapters.

Distinct geologic and geodetic slip rates have been reported along the Chaman fault zone by employing conventional and remote sensing data. Most of the slip rates were calculated over the southern sections. Based on the literature, the geologic slip rate ranges between 2–40 mm/yr., while the geodetic slip rate varies between 5.4–16.8 mm/yr. (Beun et al., 1979; Jay et al., 2017; Mohadjer et al., 2010; Shnizai et al., 2020; Szeliga et al., 2012; Ul-Hadi et al., 2013; Wellman, 1966; Yeats et al., 1979).

The Gardiz fault, an eastern splay of the Chaman fault zone, bounds the southeastern edge of the Kabul Block and separates it from the adjacent Katawaz basin (Figure 3.2A). It trends in an E–NE direction with a length of about 300 km. The fault is also called the Altimur fault by Abdullah et al. (2008). The Chaman fault zone, which includes the Gardiz fault, is characterized by a number of morphotectonic features, including linear, discontinuous scarps on piedmont alluvium and river channel displacement. Other features include offset and beheaded stream channels, offset alluvial fans, shutter ridges, and tilted alluvial fans (Ruleman et al., 2007; Shnizai, 2020).

The northern extension of the Chaman fault zone, with a length of about 80 km, starts in the Paghman district and terminates in the Shutul and Unaba districts of the

Panjsher province. The fault system that trends from N16°E to N35°E along the northern edge of the Kabul Block is known as the Paghman fault in the literature (Abdullah & Chmyriov, 2008; Ruleman et al., 2007; Shroder et al., 2021) (Figure 3.2A). This fault is characterized by discontinuous and linear scarps on Quaternary deposits and landforms. In this research, the fault zone is considered to be a separate fault system rather than the northern extension of the Chaman fault zone. The relevant discussion and interpretations are presented in subsequent chapters.

The ~N–S trending Sarobi fault, with a length of ~150 km, is located in eastern Afghanistan. It bounds the northeastern edge of the Kabul Block and separates it from the adjacent Nuristan Block (Ruleman et al., 2007; Schreiber et al., 1972) (Figure 3.2A). The fault shows a clear topographic expression between the Gardiz and Chaman fault zone on aerial and Landsat imagery (Wellman, 1966).

Focal solutions carried out by Prevot et al. (1980) indicate right-lateral motion of the fault, but the fault type is still in question. The fault follows the contact between bedrock and colluvium, but there are no scarps on the adjacent piedmont alluvium. The fault has mainly vertical motion, but it may also have some right-lateral motion (Ruleman et al., 2007; Shnizai, 2020).

4. MATERIALS AND METHODS

The methodology adopted in this research involved a systematic literature review, remote sensing data analysis, and conventional data interpretation. A systematic literature review was conducted to review all relevant investigations of existing active faults in the Kabul Block and methodology, as published in journal articles, conference proceedings, books, reports, and discussions since the 1970s. This systematic review aimed to identify problem statements and scientific gaps in the existing knowledge about active faults in the Kabul Block.

The problem statements identified were addressed by the remaining two components of the methodology: data analysis and interpretation. In remote sensing data analysis, diverse imageries, including high-resolution images from Google Earth Pro, DEM-5m, Sentinel-1B, Sentinel-2MSI, and ASTER, were examined. These imageries were used to identify and map active faults, as well as to assess their potential for seismic hazard.

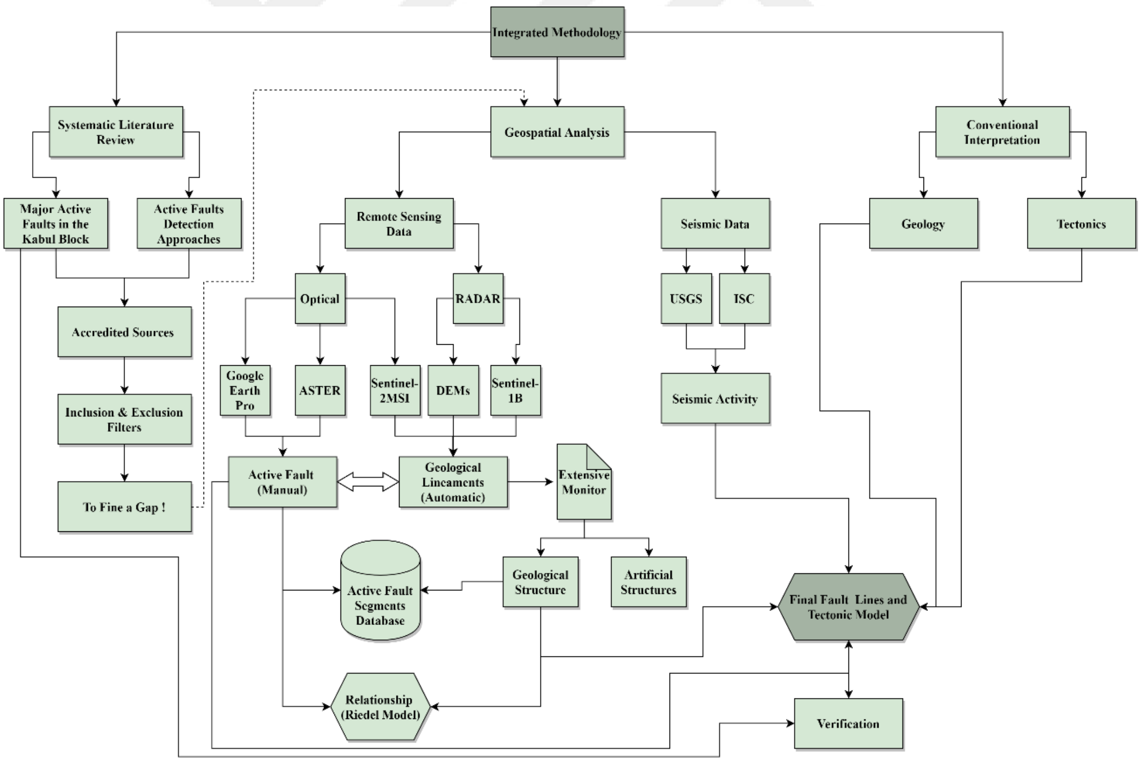

Figure 4.1. *General flowchart of methodology*

Previous geological and tectonic maps were used as conventional data and for verification purposes. These maps were used to provide context for the remote sensing data analysis and to verify the results of the analysis. Distinct data analysis approaches and methods were employed on the mentioned data to achieve the main objectives of this research. These approaches and methods included lineament extraction, structural analysis, and seismic hazard assessment.

The details of the methodology procedures are depicted in Figure 4.1. This figure provides a flowchart of the methodology, as well as a brief description of each step.

4.1. Data

4.1.1. Conventional

Conventional data comprises geological and tectonic maps and sketches, published and unpublished reports, journal articles, conference proceedings, and book chapters. The geological understanding of Afghanistan was initiated in the late 19th and early 20th centuries, but extensive geological mapping and prospecting operations began in 1955 after the establishment of the National Geological Survey. The Afghan Geological Survey (AGS) collaborated with geoscientists from Germany, Italy, France, the Soviet Union (USSR), and the United States Geological Survey (USGS) to create geological and tectonic maps of Afghanistan. Comprehensive geological studies on the Kabul crustal Block were conducted by Afghan and Soviet geologists between 1977 and 1980. In this study, the modified geological and structural map of Afghanistan compiled by Abdullah et al., (2008) was used. This work was originally carried out in 1977, but it was translated into English in 2008 by the British Geological Survey as part of their mission in Afghanistan. The USGS digitized the older 1:500,000 countrywide geological map made by the Soviet Union. In addition, the recent fault lines compiled by Ruleman et al. (2007) were considered, but due to the low accuracy of that work, the major fault zones surrounding the Kabul Block were redefined.

4.1.2. Remote sensing

4.1.2.1. High-resolution imagery

Google Earth is a powerful platform for providing high-resolution imagery globally. Unlike other imagery platforms, Google Earth allows users to view the Earth from various perspectives, including 2D and 3D. Recently, Google Earth Pro has become a focus of geoscientists for capturing and mapping geological structures, such as faults, folds, joints/shears, and dykes. Traditionally, during structural mapping, it is necessary to define the location, geometry, orientation, deduced deformation, and trace length of structures of interest. These tasks can all be performed using Google Earth imagery.

In this study, Google Earth Pro high-resolution imagery was used to interpret the geological structures of the study area, particularly fault segments, and their associated deformed lands. In addition, high-resolution imagery from ESRI Online, which is available in ArcMap as a basemap, was used to complement the interpretation. ESRI imagery with a spatial resolution of 2.5 m and 1 m is available online around the globe. In this work, these images were used to measure the associated deformation, including drainage offset and land displacement.

4.1.2.2. DEM-5m

A DEM (Digital Elevation Model) is a digital grid that represents the topographical visualization of the Earth's surface. It is created from terrain elevation data and is a generic term for DSM (Digital Surface Model) and DTM (Digital Terrain Model). DSMs and DTMs represent three-dimensional models of the Earth's surface.

DEMs are typically acquired using satellites, airplanes, or other flying objects. The spatial resolution of DEMs can vary depending on the capturing platform, but common resolutions include 90 m, 12.5 m, 5 m, 1 m, and larger. DEMs can also be produced from radar data (RADARSAT, TeraSAR-X, SRTM) or from stereoscopic pairs of optical data (e.g., SPOT 4 or ASTER). Additionally, DEMs can be generated by interpolating digital contour maps and elevation points collected by GPS or ground survey instruments.

Several other layers representing geomorphological properties of Earth's surface can be derived from DEMs, such as slope, aspect, and hillshade. DEM-derived hillshade, which visualizes the terrain as shaded relief by illuminating it with a hypothetical light source, is widely used in structural geology and neotectonics investigations.

In this study, a digital elevation model (DEM) with a spatial resolution of 5 meters was created on August 3, 2008 using an Intermap STAR-3i airborne interferometric synthetic aperture radar (SAR) system mounted on a LesarJet 35A aircraft. The DEM was used to interpret fault segments, automatically detect geological lineaments, and perform morphometric analysis. The data was obtained from the Ministry of Mines and Petroleum of Afghanistan.

4.1.2.3. Sentinel-1B SAR GRD

4.1.2.4. The Sentinel-1 SAR GRD, a dual-polarization C-band Synthetic Aperture Radar (SAR) instrument, was launched into orbit on April 3, 2014. The SAR instrument can acquire data at a frequency of 5.405 GHz. It is provided by two polar-orbiting satellites that operate day and night regardless of the weather.

Sentinel-1 can operate in four modes: Interferometric Wide Swath (IW), Extra Wide Swath (EW), Wave mode (WV), and Stripmap (SM). These modes can be operated in several polarization schemes (Copernicus, 2022b). The Wave mode operates in a single polarization (VV or HH), and the other modes can be operated in dual polarization (VV+VH or HH+HV) or as single polarization (HH or VV).

Each mode is produced in Level-0, Level-1 Single Look Complex (SLC), Level-1 Ground Range Detected (GRD), and Level-2. Sentinel-1 data is used in a variety of disciplines, including monitoring sea ice, oil spills, marine winds, waves, and currents; land-use change; land deformation; flood and earthquake assessment; and more (Copernicus, 2022a).

The Sentinel-1 collection includes Ground Range Detection (GRD) scenes, and the spatial resolution of each scene can be 10, 25, or 40 meters. In this study, Sentinel-1 data from July 20-30, 2021 was used. The data was acquired in C-band polarization, with both vertical–vertical (VV) and vertical–horizontal (VH) polarizations. The data was directly loaded from Google Earth Engine (GEE). The scripts are described in Appendix 6.

4.1.2.5. Sentinel-2A MSI

4.1.2.6. The Sentinel-2A MSI is a satellite-borne multispectral imager that was launched in 2015. It has 13 spectral bands that cover the visible and near-infrared (VNIR) and shortwave infrared (SWIR) regions. The spatial resolution of the MSI varies from 10 to 60 meters, making it a valuable tool for monitoring the Earth's surface (Table 4.1). The combination of high resolution (up to 10 m), novel spectral capabilities (three bands in the red edge), wide coverage (swath width of 290 km), and 10-day revisit time (five days after the launch of Sentinel-2B) provides extreme information and makes it possible for a wide range of applications in diverse fields, such as vegetation, water quality, geological studies, structural analysis, environmental studies, and rapid change detection (Mashkoor et al., 2022; van der Werff & van der Meer, 2016).

In this study, Google Earth Engine (GEE) was used to directly download the preprocessed Sentinel-2A MSI data used for structural analysis and geological lineaments for the entire study area. Only six bands (Edge-SWIR) that were appropriate for the given tasks were downloaded between the date interval of July 24–30, 2021. The script for dowloading Sentinel-2A MSI are described in the Appendix 7.

Table 4.1. *Details of Sentinel – 2A MSI data based on (Ahmadi & Pekkan, 2021)*

Band No	Band Name	Wavelength (μm)	Spatial Resolution (m)	Radiometric Resolution (bits)	Temporal Resolution (Days)
1	Coastal Aerosol	0.33-0.453	60	12	5-10
2	Blue	0.458-0.523	10		
3	Green	0.543-0.578			
4	Red	0.650-0.680			
5	Vegetation Red Edge	0.698-0.713	20		
6		0.733-0.748			
7		0.773-0.793			
8	NIR	0.785-0.900	10		
8A	Vegetation Red Edge	0.855-0.875	20		
9	Water Vapor	0.935-0.955	60		
10	SWIR-Cirrus	1.360-1.390			
11	SWIR	1.565-1.655	20		
12	SWIR	2.100-2.280			

4.1.2.7. ASTER

The Advanced Spaceborne Thermal Emission and Reflection Radiometer (ASTER) is one of the five instrumental sensors mounted on the Terra satellite. It was launched on December 18, 1999, in a sun-synchronous polar orbit. ASTER covers the visible, near-infrared, shortwave infrared, and thermal infrared regions, providing a combination of wide spectral and high spatial resolution. It is operated by NASA, Japan's Ministry of Economy, Trade, and Industry, the National Institute of Advanced Industrial Science and Technology, and Japan Space Systems (USGS, 2021).

The ASTER instrument can acquire images of the Earth in 14 different spectral bands, or wavelengths of light. The spatial resolution of the images varies depending on the band, with 15 meters for the visible and near-infrared bands, 30 meters for the shortwave infrared bands, and 90 meters for the thermal infrared bands (Ahmadi & Kalkan, 2021) (Table 4.2). ASTER data can be used in a wide variety of applications, including vegetation and ecosystem dynamics, hazard monitoring, geology and soils, hydrology, land cover change, glacier assessment, and DEM generation. It is available in three levels: Level-1A, Level-1B, Level-2, and Level-3.

Due to detector temperatures in the ASTER sensor, the SWIR detectors have not been operating since April 2008. All attempts to bring back the SWIR bands have failed. However, the VNIR and TIR bands still meet all the mission requirements and specifications (Caltech/JPL, 2004).

In this study, 9 bands of ASTER data (VNIR and SWIR) were obtained from Google Earth Engine (GEE) between July 1 and 20, 2007 using the script described in the Appendix 8.

Table 4.2. *Specification of ASTER data based on (Ahmadi & Pekkan, 2021)*

Band No	Band Description	Wavelength (μm)	Spatial Resolution (m)	Radiometric Resolution (Bits)	Temporal Resolution (Days)
1	VNIR	0.52-0.60	15	8	16
2		0.63-0.69			
3		0.78-0.86			
3B		0.78-0.86			
4	SWIR	1.60-1.70	30	8	
5		2.145-2.185			
6		2.185-2.225			
7		2.235-2.285			
8		2.295-2.365			
9		2.360-2.430			
10	TIR	8.125-8.475	90	12	
11		8.475-8.825			
12		8.925-9.275			
13		10.25-10.95			
14		10.95-11.65			

4.2. Methods

4.2.1. Active fault zone detection

Faults are fractures in the Earth's crust that have been displaced by movement along the fracture plane. They are indicators of crustal movement and an expression of stress concentration and energy release in crustal rocks. Faults can be classified as normal, thrust, or strike-slip faults, depending on the direction of movement along the fault plane.

1. Normal faults are characterized by the hanging wall moving down relative to the footwall. They are typically associated with extensional tectonics, such as rifting or the opening of an ocean basin.
2. Thrust faults are characterized by the hanging wall moving up relative to the footwall. They are typically associated with compressional tectonics, such as mountain building or the subduction of one tectonic plate beneath another.
3. Strike-slip faults are characterized by the hanging wall and footwall moving horizontally in opposite directions. They are typically associated with shearing tectonics, such as transform fault boundaries.

The diagnostic footprints of active faults on the Earth's surface include a variety of geomorphic features, such as:

Topographic changes: Faults can cause the formation of scarps, which are steep cliffs or slopes. They can also cause the formation of grabens, which are elongated depressions, and horsts, which are elongated ridges.

Geomorphic deformations: Faults can cause the deformation of preexisting landforms, such as rivers, lakes, and coastlines. They can also cause the formation of new landforms, such as fault-line scarps and sag ponds.

Displacement of rock formations: Faults can cause the displacement of rock formations, which can be seen in the offset of bedding planes, faults, and other geological features.

Existence of particular types of rocks: Faults can be associated with the presence of particular types of rocks, such as fault gouge, which is a fine-grained rock that forms when rocks are crushed along a fault plane.

Displacement of drainage networks: Faults can cause the displacement of drainage networks, which can be seen in the offset of streams, rivers, and lakes.

Particular types of geological structures: Faults can be associated with the presence of particular types of geological structures, such as pull-apart basins, which are formed when a fault segment splits apart.

Concentration of earthquake epicenters: Earthquakes are often associated with faults, and the concentration of earthquake epicenters can be a diagnostic indicator of active faults.

Subsurface or deep indicators of active faults include the occurrence of earthquake hypocenters and subduction zones. Earthquake hypocenters are the points on the Earth's surface directly below the epicenter of an earthquake. They are typically located along active faults. Subduction zones are regions where one tectonic plate is subducting beneath another. They are typically associated with active faults and earthquakes.

Surface-active faults are determined using remote sensing and trenching approaches. Remote sensing techniques, such as satellite imagery and aerial photography, can be used to identify geomorphic features that are diagnostic of active faults. Trenching is a field technique that involves digging a trench across a fault to expose the fault plane and the rocks that have been displaced along the fault.

Subsurface active faults are also identified using geophysical methods, such as seismic reflection, gravity, and magnetics. Seismic reflection methods use sound waves to image the subsurface. Gravity methods measure the strength of gravity at different points on the Earth's surface. Magnetic methods measure the strength of the Earth's magnetic field at different points on the Earth's surface.

The determination of surface faults can also help lead to the identification of subsurface or deep faults. For example, the presence of a surface scarp may indicate the presence of a subsurface fault that extends to depth.

Detection of regional active faults using geophysical or other conventional methods is costly and time-consuming. In arid and semi-arid regions, remote sensing is considered one of the best and most reliable methods for active fault detection.

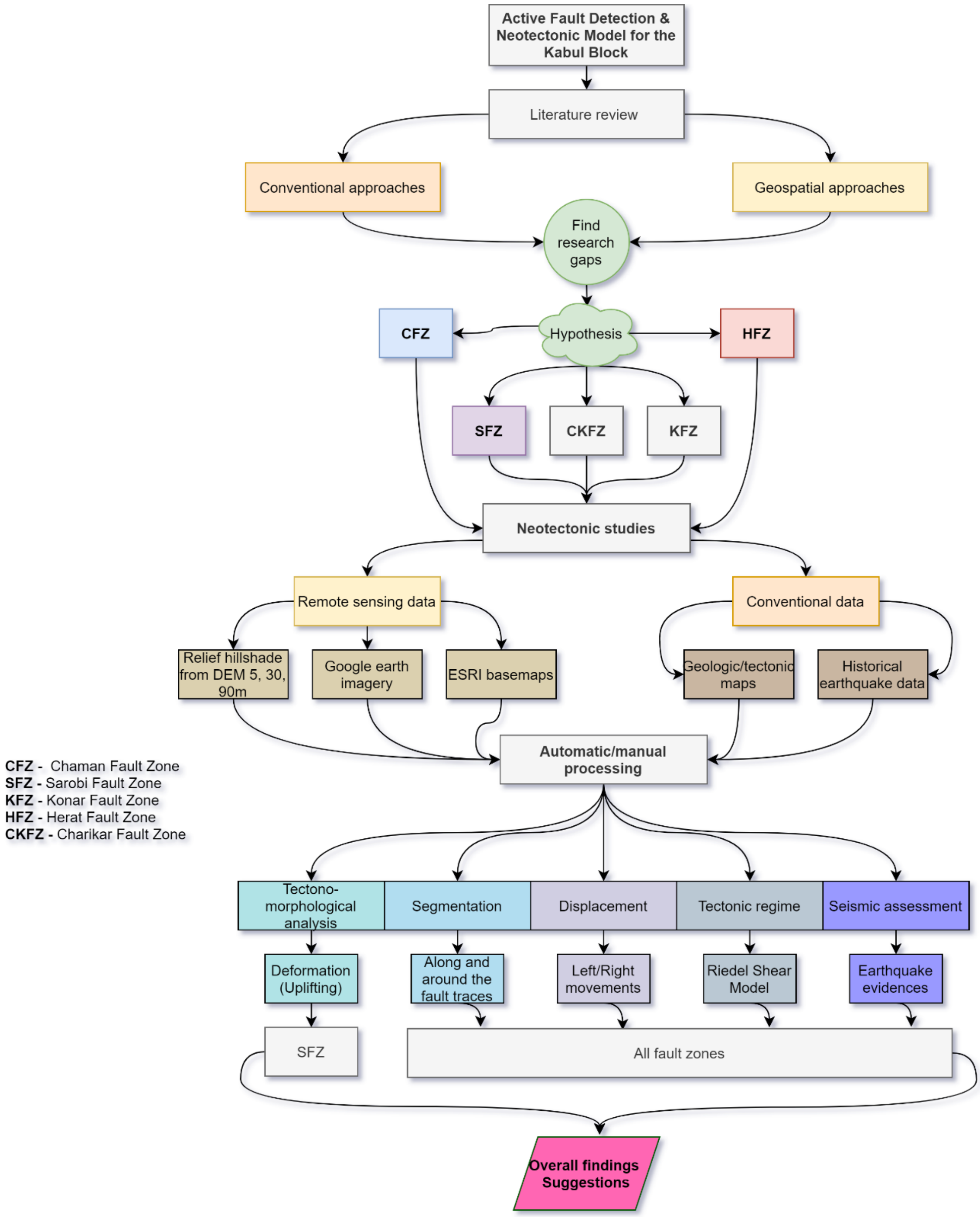

Figure 4.2. *Flowchart for the active fault zone detection and neotectonics of the Kabul Block*

Diverse remote sensing data and techniques are used to identify fault traces. In this research work, Google Earth and Esri imageries were applied to detect the main active fault zone in the Kabul Block and surroundings, and to interpret their associated geomorphic expression, and deflected streams within the valleys. Once the active faults were detected, attempts were made to measure the structures.

The exact determination of active faults in a region can lead to the definition of the active tectonics framework of the region. Therefore, this research redefined the major active fault zone in the Kabul Block and surrounding areas and consequently proposed a neotectonic model for this crustal Block. The overall methodology procedures are illustrated in Figure 4.2.

This research redefined the major active fault zones that were previously considered as the Chaman, Sarobi, Herat, and Konar faults by past studies. The Kabul Block is limited by the Chaman, Gardiz (an eastern splay of the Chaman fault zone), and Sarobi faults. However, to characterize the neotectonics of this Block, further faults, including the Konar and Herat faults, were considered to the east and west, respectively.

The previous fault traces of these zones were matched using Google Earth Engine and evaluated based on the regional tectonic settings of the Kabul crustal Block and adjacent terranes. Due to the inconsistency between the fault traces and the reality of the field, the fault segments resulting in stream deflection were redefined. Then, a tectonic model for the study area was proposed. The details of these modifications and the tectonic model are discussed in the following chapters.

4.2.2. Morphotectonic analysis

The Earth's surface is constantly changing due to ongoing tectonic and geologic processes. Morphometric analysis is the quantitative measurement and mathematical analysis of landforms and landscapes. Tectonic geomorphology analysis is the quantitative measurement of landscape shape, including size, elevation, and slope. Morphotectonic analysis is a powerful tool for assessing the effects and intensity of tectonic activity in a region (Khalifa, 2018; Merritts & Vincent, 1989; Wells et al., 1988). Researchers can use geomorphic indices to evaluate the impact of tectonic activity on the landscape or landforms.

Based on Khalifa (2018), geomorphic indices can be used to identify areas experiencing rapid tectonic deformation. This information can be used to plan research and collect detailed information about active tectonics. Other geomorphic indices have been developed to quantify the description of landscapes.

Geomorphic indices are crucial in neotectonics studies because they can be used to assess large regions. The data required for geomorphic indices can be easily obtained from topographic maps and remote sensing data.

Some of the geomorphic indices that are commonly used in active tectonics include:

- **Hypsometric integral**: This index measures the overall shape of a landscape and can be used to identify areas that have been uplifted or eroded.
- **Basin asymmetry factor:** This index measures the asymmetry of a drainage basin and can be used to identify areas that have been tilted or deformed.
- **Stream length-gradient index**: This index measures the relationship between the length and gradient of a stream and can be used to identify areas that have been actively eroding.
- **Mountain front sinuosity:** This index measures the sinuosity of a mountain front and can be used to identify areas that have been actively uplifting.
- **Ratio of valley floor width to valley height**: This index measures the width of a valley relative to its height and can be used to identify areas that have been actively eroding.
- **Isobase analysis:** This analysis uses the elevation of landforms to identify areas that have been uplifted or eroded.
- **Swath profile analysis:** This analysis uses the shape of a swath to identify areas that have been uplifted or eroded.

These are just a few of the many geomorphic indices that can be used to study active tectonics. The choice of which indices to use will depend on the specific research question being addressed.

In the present research, three morphotectonic analyses, including the Basin Asymmetry Factor Index, Isobase analysis, and Swath Profile analysis, were tested over the selected areas in the northern, eastern, and western margins of the Kabul Block to verify the hypothesized neotectonic model.

4.2.2.1. Basin Asymmetry Factor Index (A_F)

The basin asymmetry factor (AF) index examines tectonic tilting based on the assessment of the left and right areas of a drainage basin's trunk (Rawat et al., 2021). It is expressed using the following formula:

$$A_F = 100 * \left(\frac{A_r}{A_t}\right) \quad (4.1)$$

Where Ar is the area of the drainage basin to the right of the trunk stream in the downstream direction and At is the total area of the drainage basin (Figure 4.3).

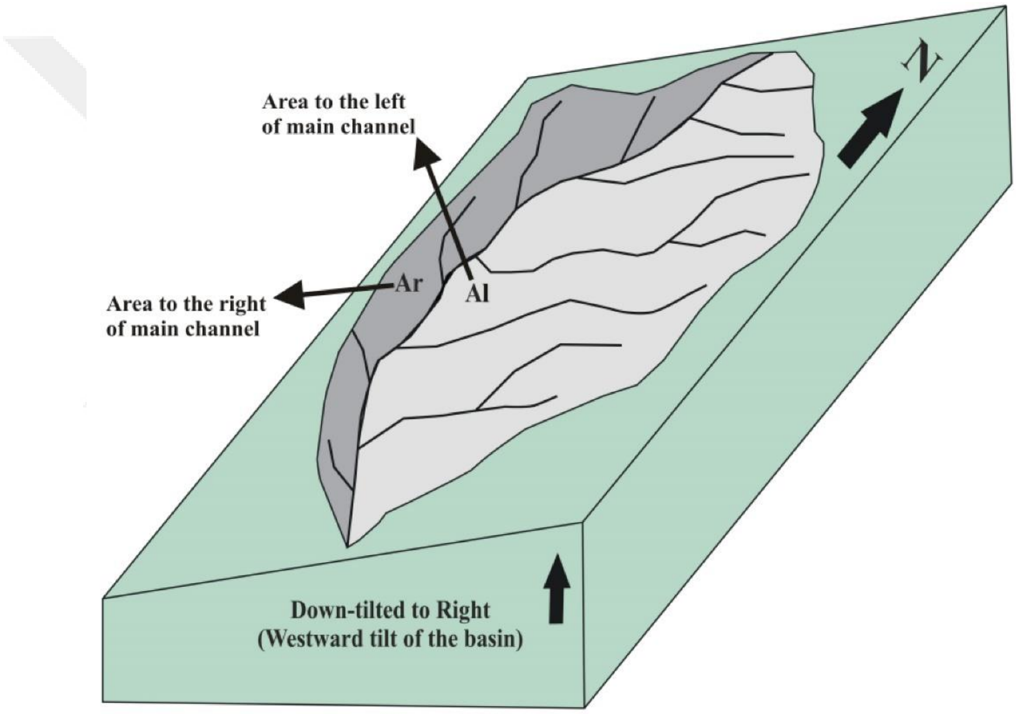

Figure 4.3. *Schematic illustration of drainage basin asymmetry factor adapted from* (Rawat et al., 2021)

The tectonic tilting of a drainage basin can be evaluated based on the basin asymmetry factor (AF) value. An AF value of 50 indicates that the areas to the left and right of the basin are symmetrically placed, and thus that the basin has developed in a tectonically stable environment. Any deviation from the AF value of 50 suggests that the basin has developed on a tilted Block. AF values less than 50 indicate rightward tilting, while AF values greater than 50 indicate leftward tilting. These values suggest that the basin has been developed under active tectonics (Keller & Pinter, 1996; Khalifa, 2018; Rawat et al., 2021).

In this study, the AF index was used in a region along the west edge of the Kabul Block, near the Sarobi fault zone. The goal was to determine the uplifting of the region by quantifying the eastward or southward tectonic tilting.

4.2.2.2. Isobase analysis

Isobase analysis is a method of mapping the distribution of erosional surfaces formed due to active tectonics and other erosional events. Isobases are imaginary contour lines on a map that show points of equal elevation in a surface that was formerly level but has been deformed at the present.

The concept of isobase analysis was first introduced by (Powell, 1875) and further developed by (Filosofov, 1960). According to (Farrand, 2006), an isobase is an imaginary contour line on a map that shows points of equal elevation. These lines were once level, but have been deformed over time. A drainage basin is typically composed of several stream segments, which can be classified according to the Strahler stream order system (Strahler, 1957). Changes in stream order are strongly correlated with topography, as streams of the same order are associated with similar geological events and age (Figure 4.4).

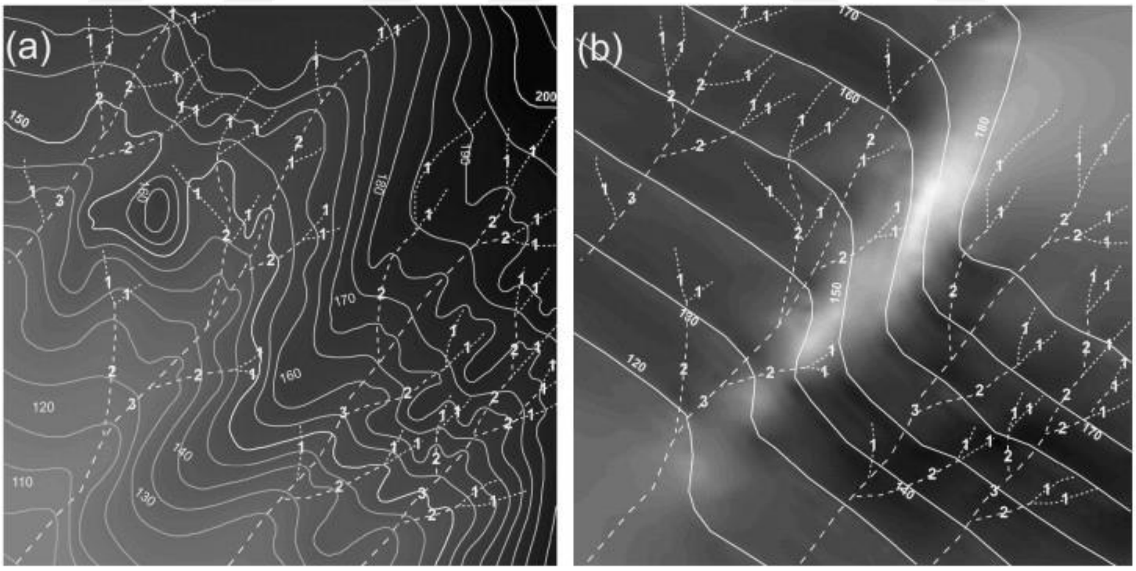

Figure 4.4. *Schematic illustration showing the isobase map adapted from* (Shahzad & Gloaguen, 2011). *a)Digital Elevation model overlain by contour lines and extracted 2nd and 3rd orders stream and b) Isobase lines generated from the elevation points of 2nd and 3rd order streams superimposed on shaded relief of isobase grid. The brightest regions clearly highlight the position of a morphotectonic feature.*

Isobases are typically generated by interpolating the elevation points of 2nd and 3rd stream orders (Grohmann et al., 2011; Shahzad & Gloaguen, 2011). The valley order represents the relative position of stream segments in a drainage basin, and streams of similar orders are associated with similar geological events and age. Sharp variations in the isobase map can indicate the possible location of faults and/or lithological contacts. For example, a sharp increase in the elevation of an isobase may indicate the presence of a fault that has caused the surface to be uplifted.

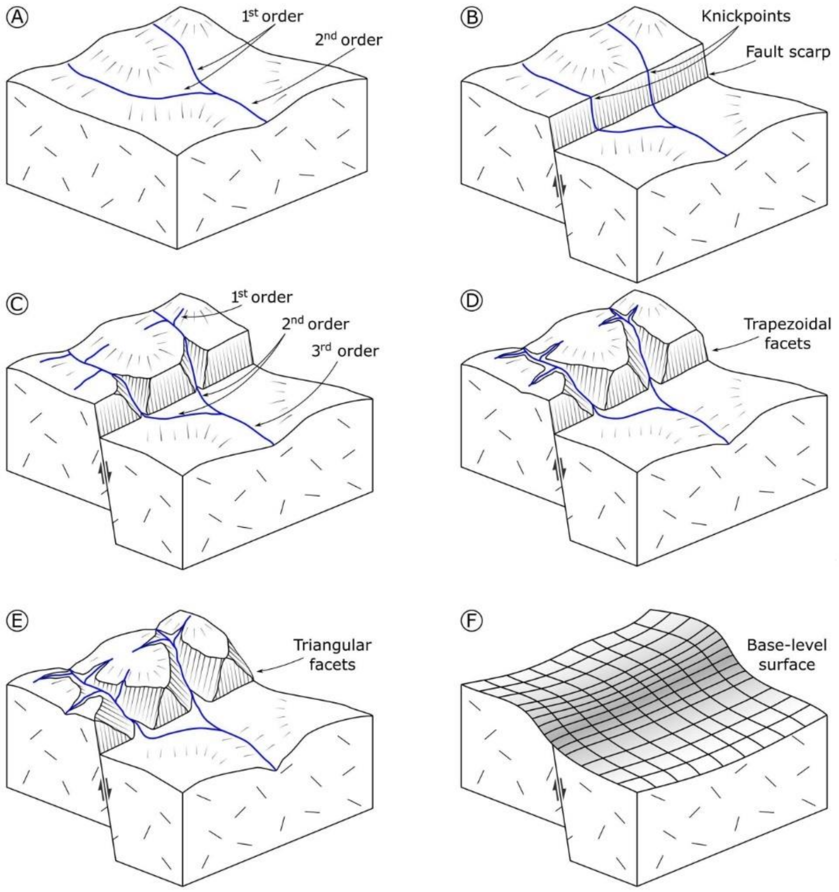

Figure 4.5. *Schematic progression of normal fault scrap indicated by the isobase map. A) Two orders stream in a simple topography, B) development of knick points and normal fault, C) development of new 1st–order stream, D) segmentation of scrap into series of trapezoidal facets, E) development of triangular facets and eroded areas, and F) base-level surface illustrating the elevation of 2nd and 3rd order streams which highlights the distribution of fault trace area by a darker color.*

The evolution of faults is also marked by the existence of stream orders and characteristic geometrical shapes. For example, triangular facets are indicators of a normal fault scarp. The order of streams is increased by the deformation of the basin due to tectonic activities. Therefore, the isobase interpretation of stream orders can be used to delineate active fault traces in a given region. As illustrated in Figure 4.5, the stream orders progress in association with the normal fault trace.

In areas with a higher population of stream orders, the 4th and 5th orders are also used to create isobase maps. Additionally, differential maps (DEM – isobase) are produced to better interpret morphotectonic features (Slama et al., 2015). In this study, the 4th and 5th order streams in a limited region, including northern and western Chaman and along the Sarobi fault zones, were considered for the isobase map. The interpolation process of the elevated points was performed in ArcMap 10.7.1. Afterward, the differential map (DEM – isobase map) was generated for further interpretation.

4.2.2.3. Swath profile analysis

Topographic swath profiles are built by projecting equally spaced topographic profiles within a strip or swath (Pérez-Peña et al., 2017). These profiles are used to highlight the characterization of the regional landscape and to correlate with other spatial data such as geological structures, tectonic activity, or precipitation (Jaiswara et al., 2020). According to Pérez-Peña et al. (2017), these profiles can be used to characterize the general view of a topographic feature and for regional-scale topographic analysis.

Swath profiles can be constructed as linear, nonlinear (e.g., mountain fronts or river valleys), or curvilinear (Pérez-Peña et al., 2017; Telbisz et al., 2013). They can be used to extract maximum, minimum, and mean topographic elevation for each transverse. These parameters can be used to visualize the topographic pattern within the profile strip. Mean elevation is a significant clue for the analysis of the general topographic trend of the landscape, while maximum and minimum can visualize the topographic variation perpendicular to the swath profile. In addition, another parameter called local relief (maximum elevation – minimum elevation) can also be obtained from these profiles to describe the topographic variations. According to Pérez-Peña et al. (2017), stable regions are characterized by low to moderate incision, having low local values, and the lines in the swath profiles will almost merge together. In contrast, high values of local relief or wider variations of swath profiles will characterize active regions (mountain ranges) or highly dissected landscapes deduced by tectonic activities exposed to high incision and/or uplifting.

Another interpretation by (Keller & Pinter, 1996; Wobus et al., 2006) conceptualizes the relationship between mean elevation, maximum elevation, and minimum elevation, which can present significant information about the landscape pattern. For a stable landscape, the mean elevation will be closer to the minimum than to the maximum. However, if the mean elevation approaches the maximum elevation, this deflection represents an unstable state of the region, particularly due to higher uplifting.

The swath profile can be constructed using different plugins and software. In this research, the Swath Profiler plugin was added to ArcMap 10.7.1 to generate profiles within a specific swath. The swath profiles were tested over the regions in the Kabul Block to reveal the uplifting (Sarobi Fault Zone) and down-warping of hanging blocks of normal faults in the Charikar Fault Zone.

4.2.3. Geological lineaments extraction

The term "lineament" was used in the early 20th century to describe a variety of linear features on the Earth's surface. These features could be ridge crest, drainage line, coastline, or boundary between different rock types. In other word, a lineament is a linear feature on the Earth's surface that can be mapped. It can be simple or composite, meaning that it can be made up of a single line or multiple lines. The parts of a lineament are aligned in a straight or slightly curved pattern, and they form distinct patterns that are different from the surrounding features. (Ahmadi & Pekkan, 2021).

According to Ahmadi and Pekkan (2021), lineaments can be classified into two main types based on their origin: genetical and topological. Genetically, lineaments can be classified into three types: geologic (They are caused by tectonic activities, such as faulting, folding, and uplift), geomorphological (They are caused by geomorphological processes, such as erosion and deposition), and pseudo (are not caused by any geological or geomorphological process. They are often the result of the alignment of random features, such as roads or rivers). Topologically, lineaments can be classified into two types: positive (linear features that are higher than the surrounding area and they include linear ridges, hills, and mountains) and negative (linear features that are lower than the surrounding area and they include linear valleys, depressions, drainages, faults, fractures, and joints).

In geological studies, the tectonic linear features (lineaments) which might be faults, fractures, joints, dykes, and shear zones are considered essential for achieving the targets in most of the surface and subsurface related studies, for example, lithological mapping (Abdelouhed et al., 2021; Ahmadi & Kalkan, 2021; Yamusa et al., 2018), hydrothermal alteration zone mapping (Ahmadi & Uygucgil, 2021; Farah et al., 2021; Maleki et al., 2021; Sheikhrahimi et al., 2019), morphotectonics and active fault detections (Akram et al., 2019; Msaddek et al., 2019; Viveen et al., 2021), ore deposits and mineral prospecting and exploration (Ahmadi & Uygucgil, 2021; Guha & Vinod Kumar, 2016; Shirazi et al., 2022; Andongma W. Tende et al., 2021), hydrogeology and groundwater exploration (Ahmadi et al., 2021; Epuh et al., 2020; Tagnon et al., 2020), hydrocarbon prospecting and exploration (Akanji et al., 2020; Ngoroyemoto, 2021; Saha, 2022), geothermal potentials (Awoyemi et al., 2022; Barkah & Daud, 2021; Joel et al., 2022), landslides mapping (Lahai et al., 2021; Mallick et al., 2018; Sadiq et al., 2022), and construction engineering project (Mallick, 2021; Othman et al., 2020; Sigtryggsdóttir & Snæbjörnsson, 2019).

Geological lineaments are linear features on the Earth's surface that appear brighter or darker than the surrounding area in satellite or aerial images. This is because they reflect or absorb light differently than the surrounding material. Geological lineaments can include faults and fractures that have displaced the Earth's surface, as well as ruptures that have not caused any significant displacement like joint zones, cleavage belts, structural fissures, and tectonic crush zonesOther types of geological lineaments include linear traces reflecting abnormal hues, linear micro-geomorphological features, deep faults, large crustal fractures, and buried faults (Ahmadi & Pekkan, 2021).

According to Ahmadi and Pekkan, 2021, geological lineaments are often indicative of fault systems. A fault is a break in the Earth's crust where two blocks of rock have moved relative to each other. The surface along which the rocks have moved is called the fault plane. The identification of geological lineaments can help to characterize and identify active faults, tectonic units, and seismically active regions.

Conventional methods of detecting geological lineaments on the field, such as field mapping and geophysical surveys, can be costly, time-consuming, and sometimes even impossible due to physical and geographical challenges. Therefore, In the last decade, the use of remote sensing to detect geological lineaments has become increasingly widespread (Ahmadi & Pekkan, 2021). A variety of remote sensing techniques can be used to delineate and analyze lineament data. These techniques can be manual or automated. The choice of the appropriate remote sensing technique for delineating and analyzing lineament data depends on the specific analysis objectives and the type of remote sensing data available. Optical and radar remote sensing data are commonly used to extract and characterize active faults. In Table 4.3, Ahmadi and Pekkan (2021) provided a summary of the prevalent types of remote sensing data employed for the extraction of lineaments.

Table 4.3. *Details about the typical remote sensing data utilized in the detection of geological lineaments, as per the research modified from Ahmadi and Pekkan in 2021.*

Satellite/ Senor	Lunch Year	Band Number	Band Name	Wavelength (μ)	Spatial Resolution	Radiometric Resolution	Spectral Resolution	Temporal Resolution	Swath Width (km)
Landsat 1–MSS	1972	4	Green	0.5–0.6	80	6 bits	4 bands	18 days	185
		5	Red	0.6–0.7					
		6	Near–IR	0.7–0.8					
		7	Near-IR	0.8–1.1					
Landsat 2–MSS	1975	4	Green	0.5–0.6	80	6 bits	4 bands	18 days	185
		5	Red	0.6–0.7					
		6	Near–IR	0.7–0.8					
		7	Near-IR	0.8–1.1					
Landsat 3–MSS	1978	4	Green	0.5–0.6	80	6 bits	5 bands	18 days	185
		5	Red	0.6–0.7					
		6	Near–IR	0.7–0.8					
		7	Near-IR	0.8–1.1					
		8	TIR	10.4–12.6					
Landsat 4–TM	1982	1	Blue	0.45–0.52	30	8 bits	7 bands	16 days	185
		2	Green	0.52–0.60					
		3	Red	0.63–0.69					
		4	Near–IR	0.76–0.90					
		5	SWIR-1	1.55–1.75					
		6	TIR	10.40–	120				
		7	SWIR-2	2.08–2.35	30				
Landsat 5–TM	1984	1	Blue	0.45–0.52	30	8 bits	7 bands	16 days	185
		2	Green	0.52–0.60					
		3	Red	0.63–0.69					
		4	Near–IR	0.76–0.90					
		5	SWIR-1	1.55–1.75					
		6	TIR	10.40–	120				
		7	SWIR-2	2.08–2.35	30				
Landsat 7–ETM+	1999	1	Blue	0.45–0.52	30	8 bits	8 bands	16 days	185
		2	Green	0.52–0.60					
		3	Red	0.63–0.69					
		4	NIR	0.77–0.90					
		5	SWIR–1	1.55–1.75					
		6	TIR	10.40–	60 (30)				
		7	SWIR–2	2.09–2.35	30				
		8	Panchrom	0.52–0.90	15				
Landsat 8 OLI	2013	1	Coastal/	0.43–0.45	30	12 bits Level 1– 16 bits	11 bands	16 days	185
		2	Blue	0.45–0.51					
		3	Green	0.53–0.59					
		4	Red	0.64–0.67					
		5	NIR	0.85–0.88					
		6	SWIR–1	1.57–1.65					
		7	SWIR–2	2.11–2.29					
		8	Panchrom	0.50–0.68	15				
		9	Cirrus	1.36–1.38	30				
		10	TIRS–1	10.60–	100 (30)				
		11	TIRS–2	11.50–					

Table 4.4. ***(Continued)*** *Details about the typical remote sensing data utilized in the detection of geological lineaments, as per the research modified from Ahmadi and Pekkan in 2021*

ASTER	1999	1	VNIR	0.52–	15		8 bits	14 bands	16 days	60
		2		0.63–						
		3N		0.78–						
		3B		0.78–						
		4	SWIR	1.60–	30		8 bits			
		5		2.145–						
		6		2185–						
		7		2.235–						
		8		2.295–						
		9		2.360–						
		10	TIR	8.125–	90		12 bits			
		11		8.475–						
		12		8.925–						
		13		10.25–						
		14		10.95–						
Sentinel 2	2017	1	Coastal	0.433–	60		12 bits	12 bands	5 days	29 0
		2	Blue	0.458–	10					
		3	Green	0.543–						
		4	Red	0.650–						
		5	Vegetati	0.698–	20					
		6	Vegetati	0.733–						
		7	Vegetati	0.773–						
		8	NIR	0.785–	10					
		8A	Vegetati	0.855–	20					
		9	Water	0.935–	60					
		10	SWIR–	1.360–	60					
		11	SWIR	1.565–	20					
		12	SWIR	2.100–						
SPOT 5	2002	1	Panchro	0.51-0.73	2.5 & 5		8 bits	5 bands	2–3 days	12 0
		2	Green	0.50–	10					
		3	Red	0.61–						
		4	NIR	0.79–						
		5	Mid IR	1.58–	20					
ASTER	-	1	-	-	1 arc-sec		-	-	-	1°
SRTM	-	1	-	-	3 arc-sec		-	-	-	5° × 5°
CartoDE	2005	1	-	-	1 arc-sec		-	-	-	1° × 1°
JERS-1	1992	1	L	2.35e + 7	18		3 bits	1 band	44	75
IRS LISS III	1995	2	Green	0.52–	23.5		7 bits	5 bands	24	142
		3	Red	0.62–						
		4	NIR	0.77–						
		5	SWIR	1.55–	70					14
ERS-1	1991	1	C	5660000	10-30		5 bits	1 band	35	100
ERS-2	1995	1	C	5660000	10-30		5 bits	1 band	35	100
PALSAR	2006	1	L	2.29e+7	10		5 bits	1 band	45	30
Sentinel 1	2014	1	C	3.75 0	5×5			1 band	12	80

4.2.3.1. Geological lineaments extraction techniques

A detailed literature review of the techniques of lineament extraction was undertaken as part of this thesis by the author (Ahmadi & Pekkan, 2021). This review identified three approaches for extracting lineaments:

- Manual lineament extraction
- Automated lineament extraction
- Semi-automated lineament extraction

1. Manual lineament extraction

This process is particularly suitable for spatial assessment, as it allows the operator to take into account the spatial context of the lineaments. This extraction method uses a variety of image enhancement techniques to improve the visibility of lineaments in satellite or aerial images. These techniques include directional filtering, band ratio transformation, and visual interpretation (Ahmadi & Pekkan, 2021). The effectiveness of manual lineament extraction relies on the skills of the analyst and the specific area of interest. According to existing literature, the earliest instances of manual interpretation of lineaments involved the use of stereoscopic aerial photos. In this approach, lineament patterns were first delineated on transparent overlays. Transparent overlays are thin sheets of plastic or glass that can be placed over images to make it easier to identify and trace features. Once the lineament patterns were delineated on the overlays, they were then transferred onto a map. This could be done by tracing the lineament patterns onto the map by hand or by using a digitizer. This approach is a manual method of lineament extraction that is relatively simple and inexpensive to implement. However, it can be time-consuming and labor-intensive, especially for large areas (Ahmadi & Pekkan, 2021; Azman et al., 2020; Chaabouni et al., 2012).

Many researchers recommend the use of high-resolution images or the Digital Terrain Model (DTM) for the manual interpretation of lineaments, particularly when analyzing geological features. Recent advancements in hardware and technology have allowed for the direct interpretation of lineaments from enhanced imagery. The main clues to understanding the Earth's surface from visual interpretation are the differences in brightness (tonal contrast) and the patterns of texture. These clues can be used to identify a variety of geomorphological features, such as rivers, the hardness of rocks, landforms, layers of rock, and surface covers such as vegetation and crops (Ahmadi & Pekkan, 2021). Manual extraction of lineaments is employed when the primary objective is to emphasize geological structures (Scheiber et al., 2015).

Lineaments in satellite or aerial imagery are typically represented as straight or curved lines or edges that stand out from the surrounding pixels due to tonal gradients (Ahmadi & Pekkan, 2021; SARP, 2005). The analyst's field experience plays a crucial role in accurately interpreting and segmenting broken lines into longer lineaments. Furthermore, the quality of the image is important for getting better results. The diagnostic features of lineaments, which are linear features on the Earth's surface, have been proposed by Wang and Howarth (1990) and described in detail by Ahmadi and Pekkan (2021). These features include topographic characteristics such as straight valleys, continuous scarps, straight rock boundaries, systematic stream offsets, sudden changes in brightness, and alignment of vegetation. Koike et al. (1995) highlighted the importance of continuous straight valleys as the most significant feature in image processing for extracting lineaments. Various remote sensing data have been employed for lineament detection, with the earliest manual approaches dating back to the launch of Landsat in 1972. A comprehensive overview of the most relevant studies on manual lineament extraction between 1975 and 2021 can be found in the published review paper by Ahmadi & Pekkan (2021), which is also a part of this thesis.

2. Automated lineament extraction

The automated extraction of lineaments utilizes computer-aided software to perform the task. The process involves several steps, including enhancement, filtering, edge detection, and the extraction of linear features from the lineaments (Ahmadi and Pekkan, 2021). Scientists have developed various algorithms to automatically extract linear features from remote sensing data. These algorithms include the Hough Transform (Wang & Howarth, 1990), Lineament Extraction and Stripe Statistical Analysis (LESSA) (Zlatopolsky, 1992), Segment Tracing Algorithm (STA) (Koike et al., 1995), Canny Algorithm (Marghany & Hashim, 2010), ADALGEO (Soto-Pinto et al., 2013), TecLines (Rahnama & Gloaguen, 2014), and Lineament Detection and Analysis (LINDA) (A. Masoud & Koike, 2017).

The resulting lineaments map produced by these algorithms is obtained in vector format for subsequent analysis and modeling. Compared to manual extraction approaches, the automated lineament extraction approach allows analysts to obtain the lineaments in a shorter time. However, it is important to note that at times, the lineaments extracted through automated algorithms may not accurately correspond to geological structures or may include artificial linear features. In such cases, it is necessary for the user to evaluate the final results and potentially integrate them with manual interpretations (Ahmadi and Pekkan, 2021).

The extraction of lineaments that represent geological faults poses a significant challenge because they are often mistakenly identified as non-geological structures. However, it is important to note that lineaments, regardless of their origin, are formed due to potential tectonic activities. In certain cases, the density of lineaments becomes a crucial factor in identifying active faults. For example, Abdullah et al. (2013) developed a map of fault potential by considering four key factors: drainage patterns, previously mapped faults, lineaments, and lithological contacts. Subsequently, the authors assigned weights to these layers based on their importance in relation to active faults.

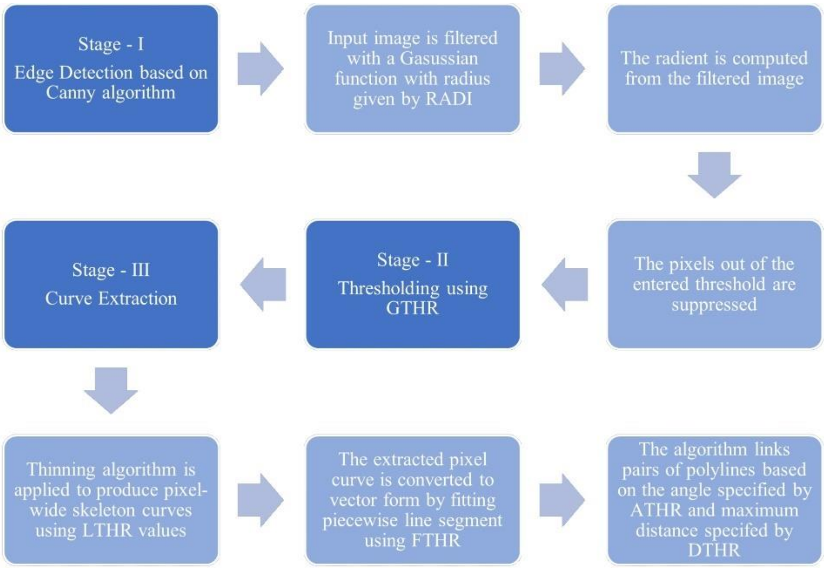

Figure 4.6. *Stages and substages of automated lineament extraction using LINE module based on Ahmadi and Pekkan, (2021)*

Recently, the LINE module of Geomatica has emerged as a powerful tool for the automated extraction of geological lineaments (Ahmadi and Pekkan, 2021). This module uses the logic of the Segment Tracing Algorithm (STA) to trace line segments in images, but it uses the Canny algorithm in the initial stages to detect edges in the image. By considering six parameters, the LINE module can extract linear features as vector segments. These parameters include the Filter Radius (RADI) with recommended values between 3-8, Edge Gradient Threshold (GTHR) with accepted values between 10-70, Curve Length Threshold (LTHR) commonly set to 10 in most cases, Line Fitting Error Threshold (FTHR) with recommended values between 2-5, Angular Difference Threshold (ATHR) with an appropriate angle ranging from 3 to 20 degrees, and Linking Distance Threshold (DTHR) with efficient values between 10 to 45 (Adiri et al., 2017; Ahmadi & Pekkan, 2021). According to Ahmadi and Pekkan (2021), the automated lineament extraction using the LINE module works in three stages, as shown in Figure 4.6.

3. Semi-automated lineament extraction

The semi-automated method is a compromise between the fully automated method, which is faster but less accurate, and the fully manual method, which is more accurate but slower. It is a good choice for applications where accuracy is important but speed is also a consideration. After performing preprocessing and enhancement of the imagery, the analyst undertakes manual editing of the lineaments following digital image analysis (Ahmadi & Pekkan, 2021; Ayten KOÇ, 2005; Suzen & Toprak, 1998). According to Abdullah et al. (2013), the semi-automated approach to lineament extraction can identify more lineaments than human-based interpretation because image processing can enhance the image and linear features more effectively.

In this thesis, a combination of manual and automated (semi-automated) techniques was applied to detect the active fault zone and associated segments with their tectonic implications. Additionally, geological lineaments were extracted, evaluated, and then correlated with the identified active fault zone. The spatio-temporal distribution of geological lineaments was also assessed based on the lithological units, which will be discussed in subsequent chapters.

4.2.3.2. Preprocessing and filtering

1. Image enhancement

Remote sensing detectors typically record reflected or emitted radiation from Earth's surface materials. These materials can be distinguished because one material type will reflect or emit more energy than another material in a particular wavelength. This difference in energy reflection or emission creates a contrast between the two materials, which can be recorded by remote sensing sensors.

However, in some cases, different materials may reflect or emit a similar amount of energy, resulting in low contrast. This can make it difficult to determine the materials or identify structures in the image. In these cases, image enhancement can be used to increase the variation in reflected energy, leading to higher contrast. Image enhancement can be used to improve the visibility of weak edges or linear features in an image, which can improve the accuracy of image interpretation. (Ahmadi & Pekkan, 2021; Han et al., 2018).

Image enhancement is a primary preprocessing step for lineament extraction. Contrast in imagery is determined by the radiometric range, which is the range of brightness values that can be recorded by a sensor. For example, an 8-bit sensor can record a total of 256 brightness values, from 0 (the darkest) to 255 (the brightest). However, the radiometric sensitivity of the sensor may limit its ability to record the full range of intensities of reflected or emitted energy. This can result in imagery with relatively low contrast (Han et al., 2018). Image contrast enhancement can be divided into two main categories: linear and nonlinear methods. Linear contrast enhancement methods, such as contrast stretching, minimum-maximum contrast stretch, and piecewise contrast stretch, adjust the contrast of an image by stretching or compressing the grayscale levels in a linear manner. Nonlinear methods, such as histogram normalization, adjust the contrast of an image by redistributing the grayscale levels in a more uniform way (Jensen, 2015).

2. Spatial Convolution Filtering

Spatial frequency is a measure of the amount of change in brightness values in an image over a unit distance. It is a key characteristic of remotely sensed data, as it can be used to identify different features in the image (Perfetto et al., 2020). Two ranges of spatial frequency can be distinguished in image data: low-frequency and high-frequency. Low-frequency areas have fewer changes in brightness value over a given area, while high-frequency areas have a dramatic change over a short distance (Ahmadi & Pekkan, 2021; Jensen, 2015). Edges, lines, and some types of noise are the common examples of high-frequency areas.

In the realm of digital image processing for remote sensing data, there are two distinct methods for either boosting or diminishing spatial frequency: spatial convolution filtering and fourier analysis can be employed. Spatial convolution filtering works by applying a convolution mask to an image, which alters the spatial frequency content of the image. Fourier analysis is a mathematical technique that decomposes an image into its spatial frequency components. This means that the image is broken down into a series of sine waves of different frequencies and amplitudes. The spatial frequency components are represented by a Fourier transform, which is a mathematical function that describes the frequency content of the image (Jensen, 2015). Spatial convolution filtering is commonly used for lineament extraction, as it can be used to enhance the edges of lineaments in an image.

Spatial convolution filtering is a linear filtering technique that works by weighting the neighboring pixel values in an image to produce a new image (Ahmadi & Pekkan, 2021; W. Pratt, 1991). The brightness value of a pixel in the output image is determined by a weighted average of the brightness values of the pixels in a surrounding region, called the kernel. The kernel is a small matrix of weights that is applied to the surrounding region. The weights determine how much each pixel in the surrounding region contributes to the brightness value of the output pixel. This process is known as two-dimensional convolution filtering.

Utilizing high-frequency linear filtering can enhance the sharpness of image edges, whereas low-frequency linear spatial filtering is employed to mitigate image noise. Based on the systematic literature review by Ahmadi and Pekkan (2021), there are four common spatial convolution filters:

- Low-pass filter
- High-pass filter
- Linear edge detection
- Non-linear edge detection

a) ***Low pass filtering***

This image enhancement technique is commonly employed to reduce high spatial frequencies in image data (Ahmadi & Pekkan, 2021; Jensen, 2015). These filters serve a practical purpose in eliminating noise from images. A basic low-pass filter evaluates the brightness value of a given pixel and those neighboring it, producing a fresh brightness value that represents the average of this convolution process (Ahmadi & Pekkan, 2021). The convolution mask or kernel can have different sizes, such as 3 × 3, 5 × 5, 7 × 7, or 9 × 9. An example of a typical low-frequency convolution filter is depicted in Figure 4.7. According to Jensen (2015), the common coefficients in a low-frequency mask are selected as 1. The equation below represents a typical low-pass filter:

$$\text{Convolution mask template} = \begin{bmatrix} C_1 & C_2 & C_3 \\ C_4 & C_5 & C_6 \\ C_7 & C_8 & C_9 \end{bmatrix} \tag{4.2}$$

$$\text{Low frequency filter} = \begin{bmatrix} 1 & 1 & 1 \\ 1 & 1 & 1 \\ 1 & 1 & 1 \end{bmatrix} \tag{4.3}$$

$$\text{Mask Template} = \begin{bmatrix} C_1 \times V_1 & C_2 \times V_2 & C_3 \times V_3 \\ C_4 \times V_4 & C_5 \times V_5 & C_6 \times V_6 \\ C_7 \times V_7 & C_8 \times V_8 & C_9 \times V_9 \end{bmatrix} \tag{4.4}$$

$$LFF = Int \frac{\sum_{i=1}^{n=9} C_i \times V_i}{n} \quad (4.5)$$

Where C_i is the coefficient, V_i is the individual pixel value, and n is the number of pixel covered by the convolution mask.

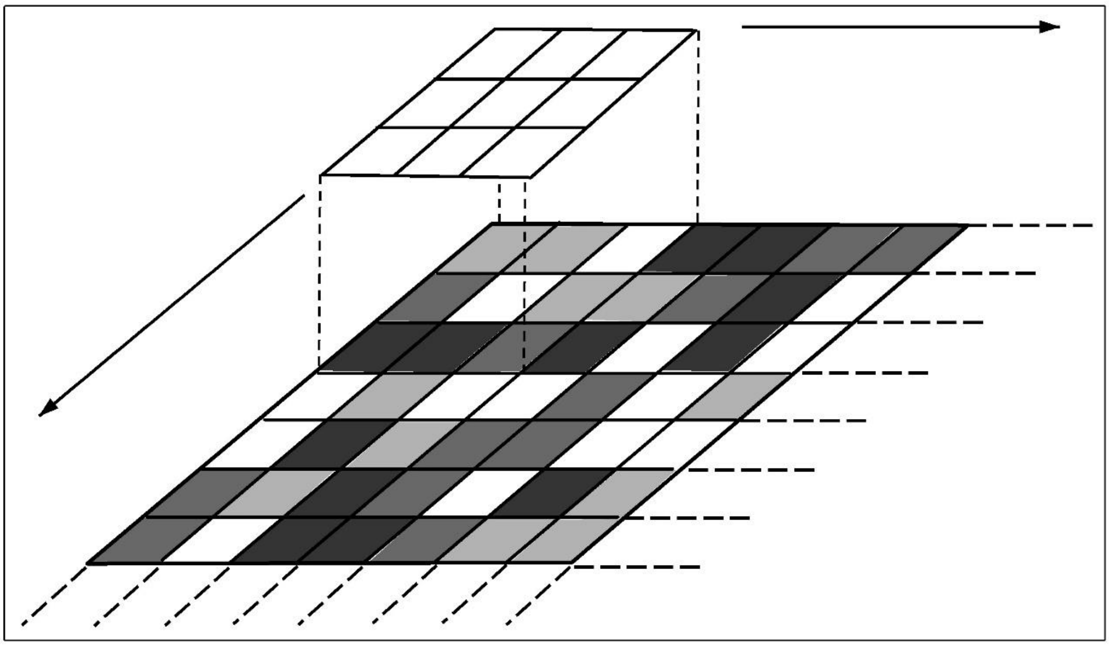

Figure 4.7. *Moving window in the spatial convolution filtering adapted from* (Ahmadi & Pekkan, 2021)

Figure 4.8 visually depicts the graphical representation of the low-pass filter mechanism as per the equation mentioned earlier. In the context of lineament extraction, the use of low-pass filters is not recommended. These filters tend to reduce the overall image quality by blurring not only the noise but also the lineaments of interest. This blurring effect can lead to confusion and hinder effective lineament detection.

0	1	3	4	7
2	5	4	9	7
8	3	1	6	4

Original image

1	1	1
1	1	1
1	1	1

Mask A

	3	4	5

Filtered image

Figure 4.8. *Input and output of image data in low pass filtering*

b) High-pass filtering

A high-pass filter is employed to enhance the intensity of high-frequency components in an image while reducing the low-frequency components (Ahmadi & Pekkan, 2021). The calculation of high-pass filtering is typically performed using the following formula:

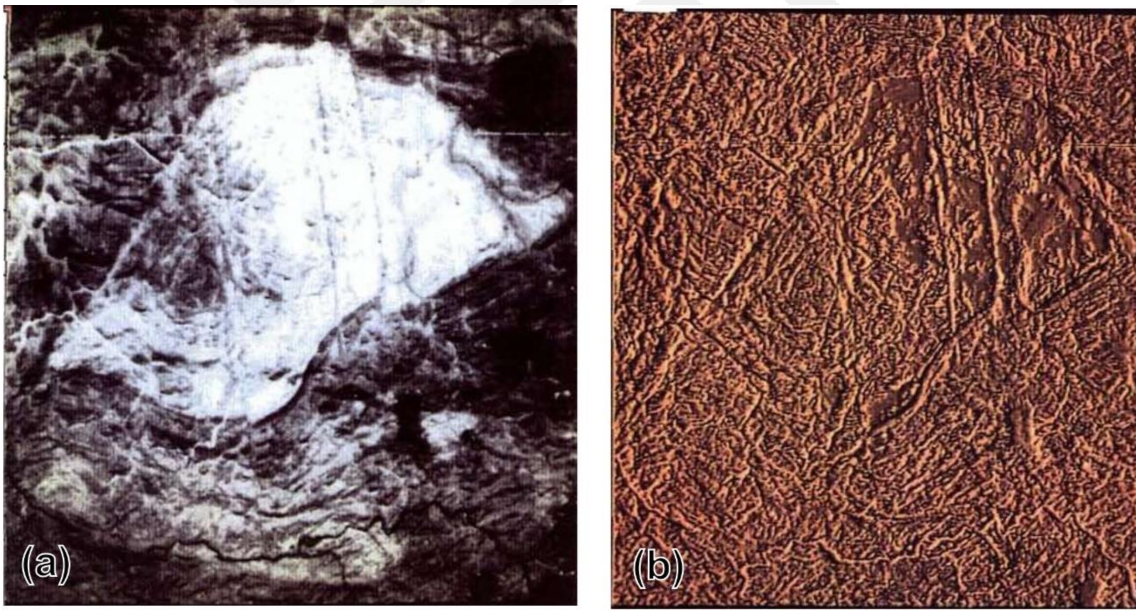

Figure 4.9. *Application of a high-pass filter to a Landsat TM image, showing: a) the original image, and b) the filtered image.*

$$HPF = (2 \times BV) - LPF \tag{4.6}$$

Where BV represents the brightness value and LPF denotes the output of the low-pass filter. Jensen (2015) elucidates that a high-pass filtered image is distinguished by having a relatively compressed intensity histogram, a result of the strong connection between brightness values and a nine-element kernel. When using a common kernel window for filtering, such as a 3 × 3 matrix, the coefficients provided below result in edge sharpening.

$$\text{High-frequency filter} = \begin{bmatrix} 1 & -2 & 1 \\ -2 & 5 & -2 \\ 1 & -2 & 1 \end{bmatrix} \tag{4.7}$$

High-pass filtering is frequently used to enhance edges, thus boosting the probability of identifying lineaments, particularly in manual extraction methods (Figure 4.9).

c) Linear edge detection filtering

Edge detection is a commonly applied method in remote sensing to extract geological lineaments because linear characteristics are defined by abrupt alterations in brightness values among neighboring pixels (Ahmadi & Pekkan, 2021; Campbell, 1996). Therefore, it is recommended to employ edge enhancement techniques to make shapes and details more prominent and facilitate analysis. Without edge enhancement, the identification of distinct and sharp lines between adjacent regions becomes challenging due to noise and coarse resolution.

Among the linear detection filters, emboss filtering is considered effective in achieving edge enhancement using a specific convolution weighted kernel (Jensen, 2015). This method converts the image into a shaded-relief format resembling a sculpted surface, utilizing embossing effects in both the east and northwest directions, and the coefficients for this operation are detailed as follows:

$$\text{Emboss East} = \begin{bmatrix} 0 & 0 & 0 \\ 1 & 0 & -1 \\ 0 & 0 & 0 \end{bmatrix} \tag{4.8}$$

$$\text{Emboss NW} = \begin{bmatrix} 0 & 0 & 1 \\ 0 & 0 & 0 \\ -1 & 0 & 0 \end{bmatrix} \tag{4.9}$$

Compass gradient masks represent an alternative category of linear filtering methods for edge detection, serving the purpose of accentuating discrete directional variations for enhanced edge perception. This method utilizes eight separate gradient mask orientations, encompassing N, E, S, W, NE, SE, SW, and NW directions (W. K. Pratt, 2014). The specific coefficients associated with each directional mask are outlined in Table 4.4.

Table 4.5. *Compass gradient mast into eight directions with their coefficient adapted from* (Ahmadi & Pekkan, 2021)

North	1	1	1	Northeast	1	1	1
	1	−2	1		−1	−2	1
	−1	−1	−1		−1	−1	1
East	−1	1	1	Southeast	−1	−1	1
	−1	−2	1		−1	−2	1
	−1	1	1		1	1	1
South	−1	−1	−1	Southwest	1	−1	−1
	1	−2	1		1	−2	−1
	1	1	1		1	1	1
West	1	1	−1	Northwest	1	1	1
	1	−2	−1		1	−2	−1
	1	1	−1		1	−1	−1

Furthermore, (Richards, 2013)suggests four additional alternative directional filters with a size of 3 × 3. The corresponding coefficients for these filters are provided below:

$$\text{Vertical} = \begin{bmatrix} -1 & 0 & 1 \\ -1 & 0 & 1 \\ -1 & 0 & 1 \end{bmatrix} \tag{4.10}$$

$$\text{Horizontal} = \begin{bmatrix} -1 & -1 & -1 \\ 0 & 0 & 0 \\ 1 & 1 & 1 \end{bmatrix} \tag{4.11}$$

$$\text{Diagonal} = \begin{bmatrix} 1 & 1 & 1 \\ -1 & 0 & 1 \\ -1 & -1 & 1 \end{bmatrix} \tag{4.12}$$

$$\text{Diagonal} = \begin{bmatrix} 1 & 1 & 1 \\ 1 & 0 & -1 \\ 1 & -1 & -1 \end{bmatrix} \tag{4.13}$$

The final linear edge detection filter recommended by Jensen (2015) is Laplacian filtering, which is applied to images to enhance edge sharpness. The Laplacian filter is a second derivative edge enhancement filter that is not concerned with edge direction. The Laplacian filters and their associated coefficients are as follows:

$$\text{Laplacian 4} = \begin{bmatrix} 0 & -1 & 0 \\ -1 & 4 & -1 \\ 0 & -1 & 0 \end{bmatrix} \tag{4.14}$$

$$\text{Laplacian 7} = \begin{bmatrix} 1 & 1 & 1 \\ 1 & -7 & 1 \\ 1 & 1 & 1 \end{bmatrix} \tag{4.15}$$

$$\text{Laplacian 5} = \begin{bmatrix} 0 & -1 & 0 \\ -1 & 5 & -1 \\ 0 & -1 & 0 \end{bmatrix} \tag{4.16}$$

$$\text{Laplacian 8} = \begin{bmatrix} -1 & -1 & -1 \\ -1 & 8 & -1 \\ -1 & -1 & -1 \end{bmatrix} \tag{4.17}$$

d) Nonlinear edge detection filtering

Nonlinear edge detection filtering methods function by nonlinearly combining pixels. The most frequently employed filters in this category encompass the Sobel Filter, Prewitt Filter, and Robert Filter (Ahmadi & Pekkan, 2021; Davis, 1975; Rosenfeld, 1970). The Sobel filter, which is commonly employed for edge detection, utilizes a 3 × 3 kernel and is computed using the following formula:

$$\text{Sobel} = \sqrt{X^2 + Y^2} \tag{4.18}$$

Where

$$X = (V_3 + 2V_6 + V_9) - (V_1 + 2V_4 + V_7) \tag{4.18a}$$

$$Y = (V_1 + 2V_2 + V_3) - (V_7 + 2V_8 + V_9) \tag{4.18b}$$

Where V represents the individual pixel value. This filter can be calculated along four main orientations (N-S, NE-SW, E-W, and NW-SE) for a single band with an extended wavelength, which is less influenced by moisture and atmospheric haze (refer to Table 4.5). The Prewitt filter consists of two sets of 3 × 3 kernels, one for horizontal and one for vertical edge detection. However, edges and lineaments can have multiple directions. Therefore, it is recommended to utilize a Prewitt filter with six or eight directions, as described in (refer to Table 4.5).

Table 4.6. *The prevailing directions and corresponding coefficients for the Sobel and Prewitt filters, sourced from* (Ahmadi & Pekkan, 2021).

	N-S			**NW-SW**			**E-W**			**NW-SE**		
Sobel filter window	−1	0	1	−2	−1	0	−1	−2	−1	0	1	[illegible]
	−2	0	2	−1	0	1	0	0	0	−1	0	[illegible]
	−1	0	1	0	1	2	1	2	1	−2	−1	[illegible]
Prewitt filter window	−1	0	1	−1	−1	0	−1	−1	−1	0	1	[illegible]
	−1	0	1	−1	0	1	0	0	0	−1	0	[illegible]
	−1	0	1	0	1	1	1	1	1	−1	−1	

3. Multiband analysis

Multiband preprocessing of remote sensing data is essential for the delineation of lineaments, which are linear features that can be interpreted visually. The process of multiband preprocessing involves transforming the data into different color composites, which can help to highlight the lineaments. The prevalent multiband approaches employed for identifying lineaments include principal component analysis (PCA), false color composite (FCC), and band ratio (BR).

a) Principle component analysis (PCA)

Principal component analysis (PCA) is a statistical method for multivariate data that is employed to decrease the data's dimensionality. This is accomplished by converting the chosen data into a fresh set of principal component axes. The resulting image contains uncorrelated data and exhibits higher contrast compared to the original data (Ahmadi & Pekkan, 2021; Ali & Pour, 2014). According to Jensen (2015), PCA can be considered a form of spectral enhancement wherein the information from multiple spectral bands is condensed into two or three transformed images. Furthermore, PCA finds application in lithological mapping, specifically when considering selected minerals. In essence, features such as lineaments or faults that delineate boundaries between adjacent lithologies can be easily interpreted by analysts using the principal component (PC) images.

b) False color composite (FCC)

A band combination or composite refers to the merging of three different bands in the red, green, and blue (RGB) channel orders. When the combined bands are red, green, and blue, it is referred to as a true color composite, where each object is displayed in its natural color. However, if other portions of the electromagnetic spectrum are combined in the red, green, and blue order, it is called a false color composite (Ahmadi & Uygucgil, 2021). Often, the Optimum Index Factor (OIF) introduced by Chavez and colleagues in 1982 is employed to rank all conceivable combinations within a specified set of spectral bands. Furthermore, the choice of a suitable band composite is influenced by deterministic methods that consider the spectral characteristics of the objects under investigation.

c) Band ratio (BR)

Band ratioing is a spectral enhancement technique used to mitigate environmental effects and potentially provide spatial information that cannot be obtained from a single band alone. The band ratio (BR) is calculated by dividing one spectral band by another, taking into account the spectral properties of the targeted object.

$$BV_{i,j,r} = \frac{BV_{i,j,k}}{BV_{i,j,l}} \quad \textbf{(4.19)}$$

In the equation, BVi,j,r represents the output result for a single pixel at row i and column j. BVi,j,k corresponds to the brightness value in band k at the same location, while BVi,j,l represents the brightness value in band l. Band ratioing (BR) has been utilized to emphasize linear features in images, and the combination of three BRs is often arranged in the RGB order (Ahmadi & Kalkan, 2021; Ahmadi & Pekkan, 2021; Jensen, 2015).

This thesis incorporates a combination of single and multiband enhancement approaches, including directional filtering and principal component analysis (PCA), to automatically and manually identify geological lineaments, which will be discussed in subsequent chapters.

4.2.4. Summary

In this research, semi-automated geological lineaments were used to determine the active fault zones within the Kabul Block and their associated segments, fractures, and stream deflection. Manual interpretation was also undertaken to refine the active fault zone definition and better assess the proposed neotectonics model. The automated geological lineaments approach consists of three steps: preprocessing/filtering, processing/extraction, and post-processing/tectonics implication. In the second phase, the chosen parameters and initial procedures are specified, and the outcomes are then passed on to the post-processing stage for validation and additional examination. A visual representation of the complete methodology can be found in Figure 4.10.

Google Earth Engine (GEE) was employed for obtaining and fetching remote sensing datasets. ENVI 5.3, PCI Geomatic 2016, and Global Mapper Pro were utilized for improving, filtering, and automating the extraction and analysis of lineaments. For structural analysis, descriptive statistics, temporal-spatial interpretation, and creating visual representations, IMB SPSS Statistics 22 and ArcGIS Desktop 10.7.1 were utilized.

The results acquired were cross-referenced with manually identified fault segments, with the assistance of Google Earth Pro and Esri base map images for validation purposes.

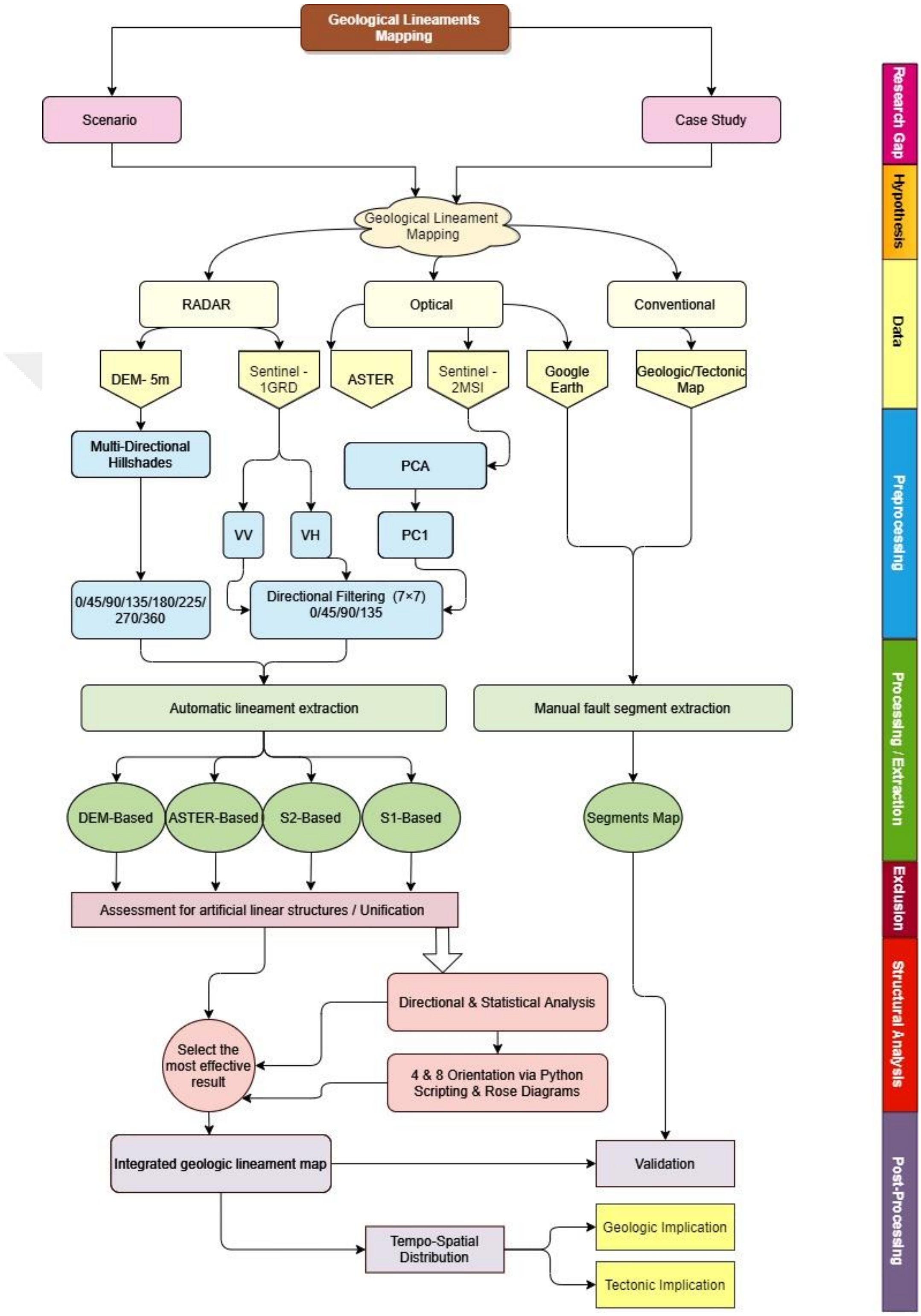

Figure 4.10. *Illustration depicting the step-by-step process of automated extraction of geological lineaments and subsequent tectonic analysis.*

Manual identification of geological lineaments is a more subjective process compared to automated extraction, demanding additional time and expertise from analysts. Nevertheless, automated lineament extraction can present difficulties since lineaments may be mistaken for artifacts due to factors like vegetation cover, urban development, and other environmental influences. In order to tackle this issue, a combination of data sources, such as radar and optical sensors, was employed in this research. Radar data, specifically DEM-5m and Sentinel-1 GRD, along with optical data sources like Sentinel-2 MSI and ASTER, were analyzed. All of these datasets underwent spatial and spectral filtering processes to amplify and visualize the indicated geomorphological features, as depicted in Figure 4.10.

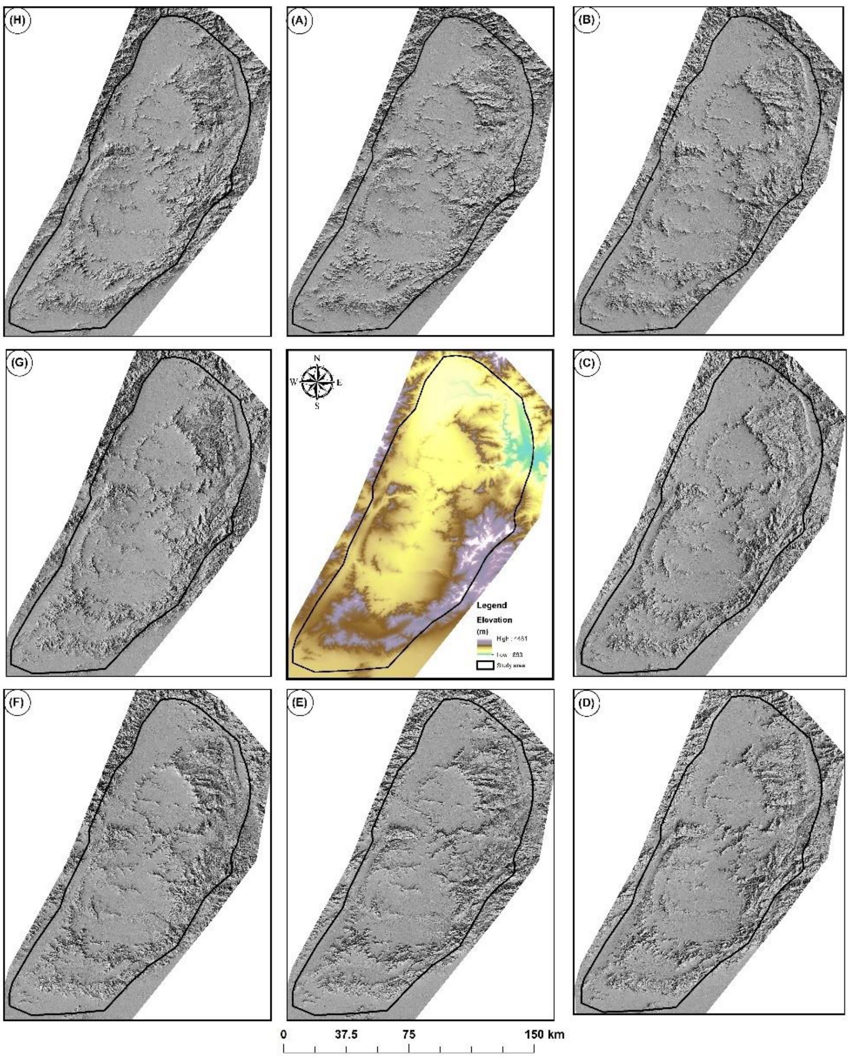

Figure 4.11. *Shaded relief images were created by applying directional/azimuthal filtering to a 5-meter Digital Elevation Model (DEM). The filtering was performed in eight different directions, resulting in the following images: A) 0 degrees, B) 45 degrees, C) 90 degrees, D) 135 degrees, E) 180 degrees, F) 225 degrees, G) 270 degrees, and H) 315 degrees.*

The high-resolution DEM data underwent spatial filtering and was used to create shaded relief images. Shaded relief images were generated in eight different directions, covering angles of 0º, 45º, 90º, 135º, 180º, 225º, 270º, and 315º, by employing azimuthal directions (Figure 4.11). The advantages of employing these azimuthal directions were to efficiently extract lineaments throughout the entire 360-degree range.

Ground Range Detected (GRD) data from the Sentinel-1 Synthetic Aperture Radar (SAR) were obtained through the utilization of Google Earth Engine (GEE). The data had previously undergone a series of preparatory procedures, which encompassed tasks such as applying the orbit file, eliminating RGD border noise, eliminating thermal noise, executing radiometric calibration, and conducting terrain correction. Following this, the acquired Sentinel-1 data was subjected to Prewitt filtering, which is a non-linear technique for detecting edges. A 7 × 7 Prewitt filter was employed in four distinct orientations: North-South (N-S), Northeast-Southwest (NE-SW), East-West (E-W), and Northwest-Southeast (NW-SE). This filtering technique was employed to boost the identification of directional edges indicative of geological lineaments. (refer to Figure 4.12).

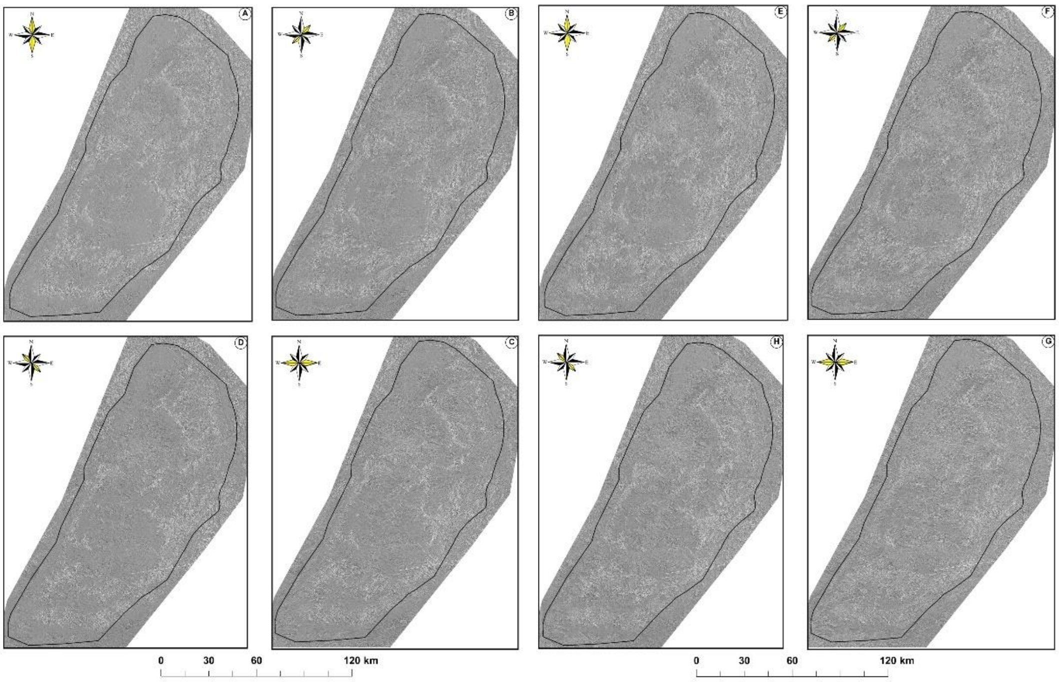

Figure 4.12. *GRD data with VV polarization were processed using a Prewitt filter applied in four different directions: A) 0 degrees (North-South), B) 45 degrees (Northeast-Southwest), C) 90 degrees (East-West), and D) 135 degrees (Northwest-Southeast). Similarly, Sentinel-1 data with VH polarization underwent Prewitt filtering in the same four directions: A) 0 degrees (North-South), B) 45 degrees (Northeast-Southwest), C) 90 degrees (East-West), and D) 135 degrees (Northwest-Southeast).*

The multispectral bands found in Sentinel-2 MSI and ASTER data underwent a two-step improvement process. In the initial stage, Principal Component Analysis (PCA) was employed, and in the subsequent stage, directional filtering was applied. PCA is a widely utilized statistical method for multivariate data reduction, resulting in an uncorrelated image with enhanced contrast compared to the original image. The first three principal components (PCs) capture the highest variation in the data. Hence, PC1 was chosen and subjected to additional processing through directional filtering. A 7 × 7 directional filter was used in four orientations: North-South (N-S), Northeast-Southwest (NE-SW), East-West (E-W), and Northwest-Southeast (NW-SE). This filtering was carried out on the generated PC1 images of both Sentinel-2 MSI and ASTER data (Figure 4.13).

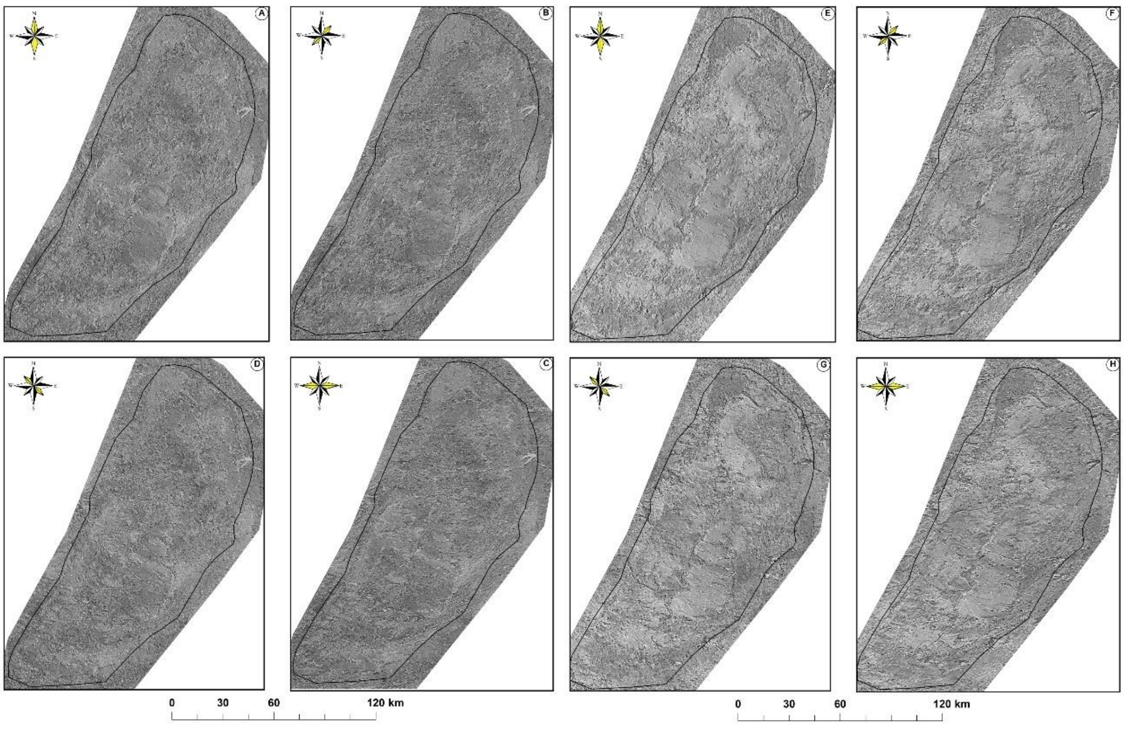

Figure 4.13. *The first principal component (PC1) of Sentinel-2MSA data was processed with directional filtering in four different directions: A) 0 degrees (N-S), B) 45 degrees (NE-SW), C) 90 degrees (E-W), and D) 135 degrees (NW-SE). Similarly, PC1 of ASTER data underwent directional filtering in the same four directions: A) 0 degrees (N-S), B) 45 degrees (NE-SW), C) 90 degrees (E-W), and D) 135 degrees (NW-SE).*

Extracting lineaments automatically involves two main steps:

1. Finding edges: This step identifies abrupt changes in pixel values between neighboring pixels.

2. Tracing lines and curves: This step builds upon the detected edges to identify linear features.

In this study, we used PCI Geomatica's LINE module, which relies on the Segment Tracing Algorithm (STA) and the Canny algorithm for these tasks. Importantly, this module requires setting six parameters before running the algorithms. These parameters were defined as follow:

Edge detection

- RADI (filter radius): Measured in pixels, typically between 3 and 8.
- GTHR (Edge Gradient Threshold): A value between 10 and 70.

Line/curve detection

- LTHR (Curve Length Threshold): Minimum length of a curve, set to 10 pixels.
- FTHR (Line Fitting Threshold): Maximum allowed deviation from a straight line, set between 2 and 5 pixels.
- ATHR (Angular Difference Threshold): Maximum allowable angle between line segments, set between 3 and 20 degrees.
- DTHR (Linking Distance Threshold): Maximum separation between connected line segments, set between 10 and 45 pixels.

Due to the vast size of the research area, it was impractical to display all identified lineaments on a single map. As a result, the study region was divided into four clockwise zones, and the identified lineaments were detailed separately for each zone, relying on the chosen dataset.

To ensure precision, assessments of the extracted lineaments' accuracy were carried out, followed by a substantial manual elimination process. This process was aimed at concentrating solely on naturally occurring geological lineaments. The orientation of extracted lineaments was determined using Python-based code within the ArcMap Desktop environment. The code was structured to categorize the lineaments into four and eight quadrants. Detailed explanations of the codes can be found in Appendix 9. Afterward, the most successful of these extracted lineaments were chosen for subsequent temporal and spatial analysis. Once the definitive geological map was chosen, the relationship between active fault zones and their tectonic implications was interpreted using the Riedel shear model within the selected areas of interest. Additionally, the spatio-temporal interpretation of geological lineaments was carried out based on the geological units present in each of the four zones.

5. RESULTS AND DATA ANALYSIS

The Kabul Block is enclosed by three geological fault regions, namely the Chaman Fault Zone (CFZ), which comprises the Gardiz, Sarobi Fault Zone (SFZ), and Charikar Fault Zone (CKFZ). However, in this research, two other adjacent fault zones, the Konar Fault Zone (KFZ) and the Herat Fault Zone (HFZ), were also considered for a more detailed regional tectonic interpretation. This led to the proposal of a hypothesized tectonic model for the Kabul Block, which reveals the tectonic meaning of the existing geomorphic expressions.

5.1. Manual Determination of Active Fault Zones

5.1.1. The Chaman fault zone (CFZ)

The Chaman Fault Zone (CFZ), a significant fault characterized by left-lateral movement, displaying an oblique motion, is situated in the southeastern region of Afghanistan between the Indian and Eurasian tectonic plates. In the western direction, it acts as a division between the Indian plate, which is moving northward, and a jutting part of the Eurasian plate that extends southward (Ruleman et al., 2007; Shnizai, 2020; Wellman, 1966) (Figure 5.1). This boundary-scaled strike-slip fault zone has caused extensive regional deformation ranging from 150 to 300 km in Afghanistan and Pakistan (Ambraseys & Bilham, 2003). Makran accretionary prism over the western end of the Chaman fault zone, through eastward transition from subduction to transform motion, thrust faults within this prism bend northward, forming oblique fault systems with higher slip rates and accommodate part of the compression in accordance with the lateral slip rate variations identified on the Chaman transform fault zone (Shah et al., 2021). Scientists have hypothesized that the major earthquakes in the Makran onshore region (MKOR) are caused by transform faults, such as the Chaman fault zone (CFZ), Ghazaband fault (GF), Ornach-Nal fault (ONF), and Minab fault (MF), as well as their associated fault splays and the megathrust of the Makran subduction zone (M. J. Khan et al., 2020).

Based on the literature, this fault zone has been referred to by different names, such as the Chaman fault and the Chaman-Mokur fault. Ruleman et al. (2007) subdivided it into four separate sections from south to north: Chaman, Mokur, Gardiz, and Paghman. Lawrence et al. (1992) considered this fault to be the major continental strike-slip structure in the region, with an orientation of N10°E to N35°E. The total length of this fault is 860 km, of which 650 km are located within Afghanistan. It begins in the southern Shorabak district of Kandahar province in the southern area, traverses the southeastern zones, and concludes its course close to the southern outskirts of Kabul city (See Figure 5.1).

The eastern continuation of the Chaman Fault Zone (CFZ) is represented by the Gardiz fault, which spans 300 kilometers in length and follows an east-northeastern direction. It acts as a boundary, creating a division between the Kabul Block and the nearby Katawaz basin in the southeastern direction (Abdullah & Chmyriov, 2008). The Gardiz fault displays distinct features, including straight, intermittent scarps on alluvial foothills and displacement of river channels (Ruleman et al., 2007).

Table 5.1. *Summary of the slip rates along the Chaman fault zone, as measured by different methods.*

No	Slip Rate –mm/yr.	Type	Reference	Description
1	2 – 20	Geologic	Wellman, (1965)	-
2	25 – 35		Beun et al. (1979)	Based on the correlation of Pliocene offset of volcanic over the northern
3	19 - 35		Lawrence & Yeats, (1979)	According to the estimation of plate closure for the last 25 My
4	40		DeMets et al. (1990)	NUVEL – 1 global plate motion
5	19 - 24		Lawrence et al. (1992)	For the last 20 – 25 My
6	20 - 30		Molnar et al. (2010)	-
7	~ 33		(Ul-Hadi et al., 2013)	Based on the ^{10}Be exposure age of the left-lateral offset of the alluvial fan within the Afghanistan and Pakistan border
8	3.5 – 4.5		(Shnizai et al., 2020)	Based on ^{10}Be TCN dating on two offsets of an alluvial fan in the south of Kabul.
9	8	Geodetic	(Furuya & Satyabala, 2008)	Based on the GPS and InSAR data
10	18±1		Mohadjer et al. (2010)	Based on the difference in velocities between installed GPS
11	15.1		Szeliga et al. (2012)	Based on India's relative velocity with Eurasia at the Chaman fault zone
12	16.8 ± 2.7		Szeliga et al. (2012)	Near Qalat, Afghanistan, InSAR
13	16.8 ± 0.51		Szeliga et al. (2012)	Near Kabul, GPS
14	10		Jay et al. (2017)	Modeled slip rate

The geologic and geodetic slip rates of the CFZ have been estimated using a variety of methods, including conventional and remote sensing approaches. Most of the estimated slip rates are associated with the southern sections of the CFZ. The geologic slip rate ranges from 2 to 40 mm/yr, while the geodetic slip rate ranges from 5.4 to 16.8 mm/yr. The entire estimated slip rate for the CFZ is summarized in Table 5.1.

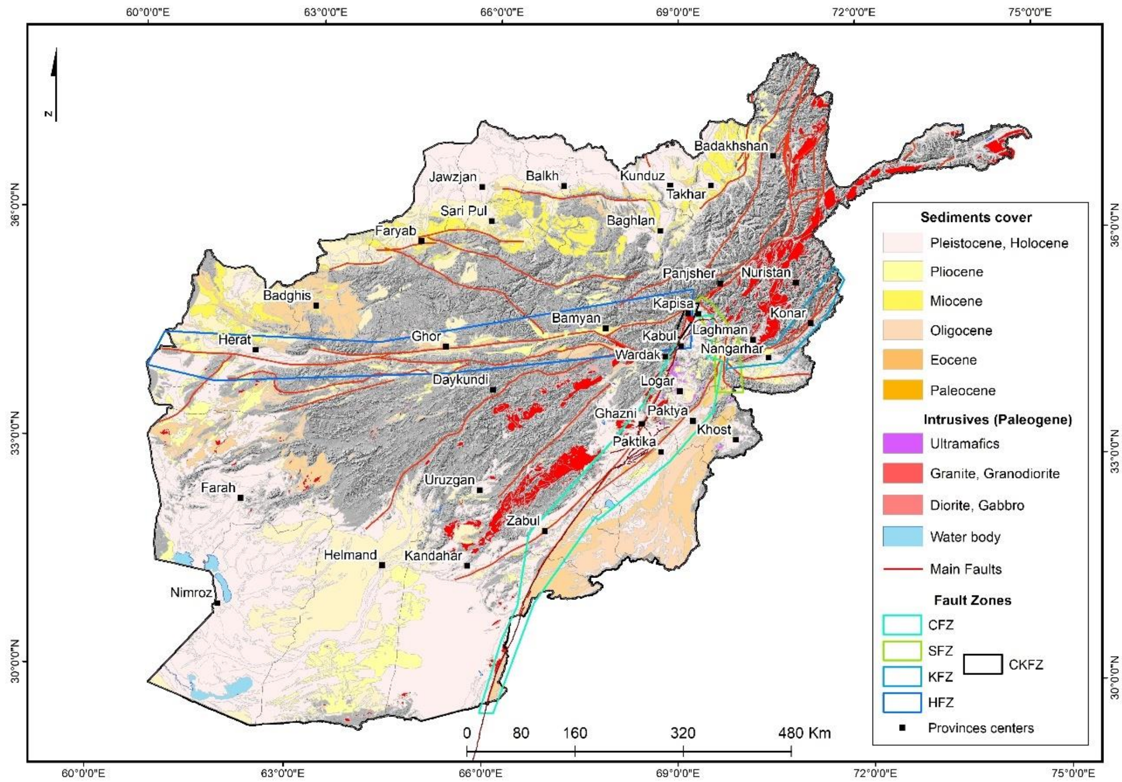

Figure 5.1. *Simplified geological map showing the distribution of Cenozoic sediments and igneous rocks and location of the active fault zones surrounding the Kabul Block and adjacent terranes and basins modified from* (Abdullah et al., 2008; Ruleman et al., 2007; Wheeler et al., 2005). *CFZ; Chaman Fault Zone, CKFZ; Charikar Fault Zone SFZ; Sarobi Fault Zone, KFZ; Konar Fault Zone, HFZ; Herat Fault Zone.*

Based on the research conducted by Ruleman et al. (2007) and Shnizai (2020), the Chaman Fault Zone (CFZ) is identifiable through unbroken, straight scarps on alluvial foothills. Additionally, it exhibits various morphotectonic features, including displaced and truncated stream channels, shifted alluvial fans, shutter ridges, and tilted alluvial fans. (Ruleman et al., 2007; Shnizai, 2020).

Ruleman et al. (2007) describe the CFZ as having a distinct fault trace, ranging from linear zones less than 1 km wide to wider zones of multiple strands where conjugate and Riedel shear systems merge with the main trace.

In this research, within the extent of the Kabul Block, 345 fault segments were determined along the main fault zone using manual interpretation of Google Earth imagery (Figure 5.2). Several segments of different scales related to the south splay of the CFZ were mapped over the Qarabagh, Giro, Deh Yak, Andar, Waghaz, and Wali Mohammad Shahid districts of Ghazni province (Figure 5.3A).

The morphotectonic expression and the earth's surface deformation are considered indicators of fault zone activity. These deformations differ based on the nature and intensity of the fault zone activity. Strike-slip faults can result in stream deflection, stream bending, and landform offsets, which can be measured in different ways.

In this research, in addition to determining fault traces, the measurement of morphotectonic structures, particularly stream channel deflection, was undertaken along the CFZ.

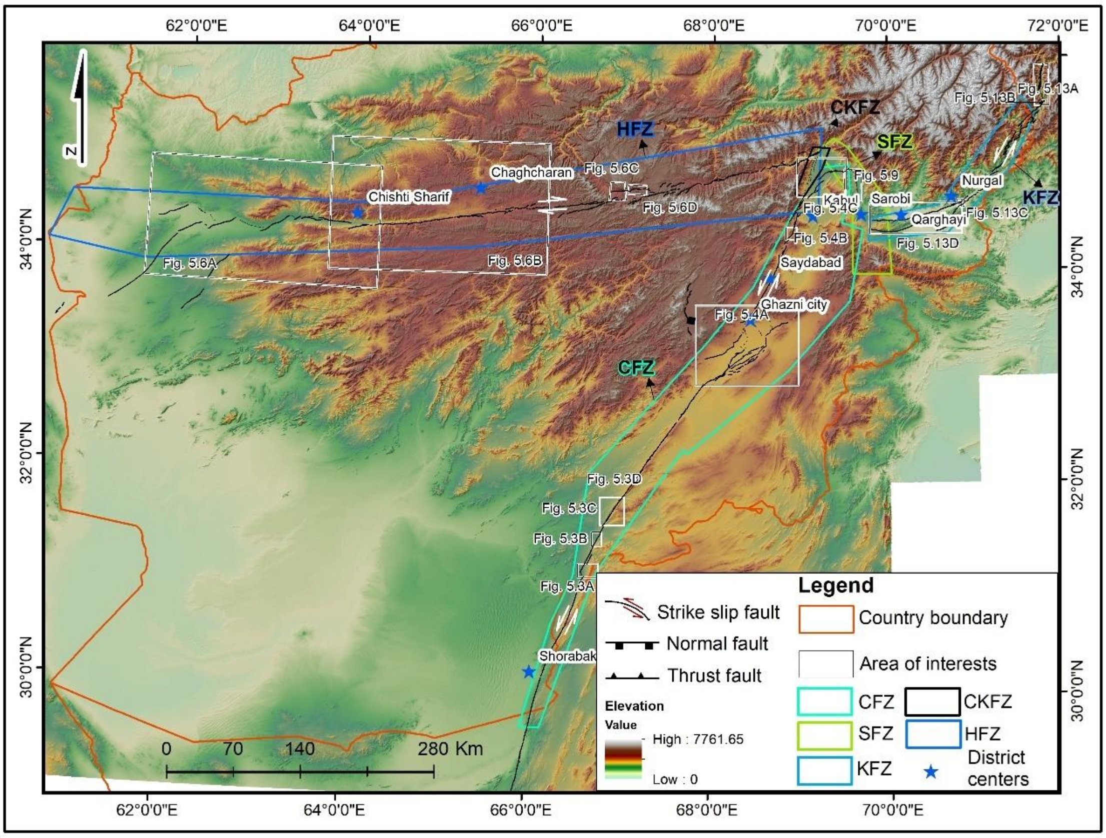

Figure 5.2. *Thematic illustration of the mapped fault segments along the Chaman, Charikar, Sarobi, Konar, and Herat fault zones, overlaid on shaded relief and a digital elevation model (DEM). The black lines represent the main mapped faults by this study.*

Within the northeast of Chaman along the Afghanistan-Pakistan border, well-developed drag folds represent the left-lateral motion of the Chaman Fault Zone (CFZ) (Ahmadi et al., 2022) (Figure 5.3A).

The NNE trending of fault segments of the CFZ over the Haji Jalal Kalay and Kelizay settlements form a releasing stepover (Segments Chm-39a-c). An active left-lateral movement of the CFZ (Segments Chm-35b-d) is marked by the 7.40 km left-lateral offset of the Arghistran River within the Malekzay village (Figure 5.3B). Moreover, the (Segments Chm-32a to 34d) control the linear route of major rivers as long as 35 km for the Lura River around the Deresha, Khodadkhil, and Kuz Komandi localities (Figure 5.3C). Moving to the northeast, the CFZ forms large landslides at the southwest of the Lowy Makhay settlement between the segments Chm-30e and Chm-31b (Figure 5.3D).

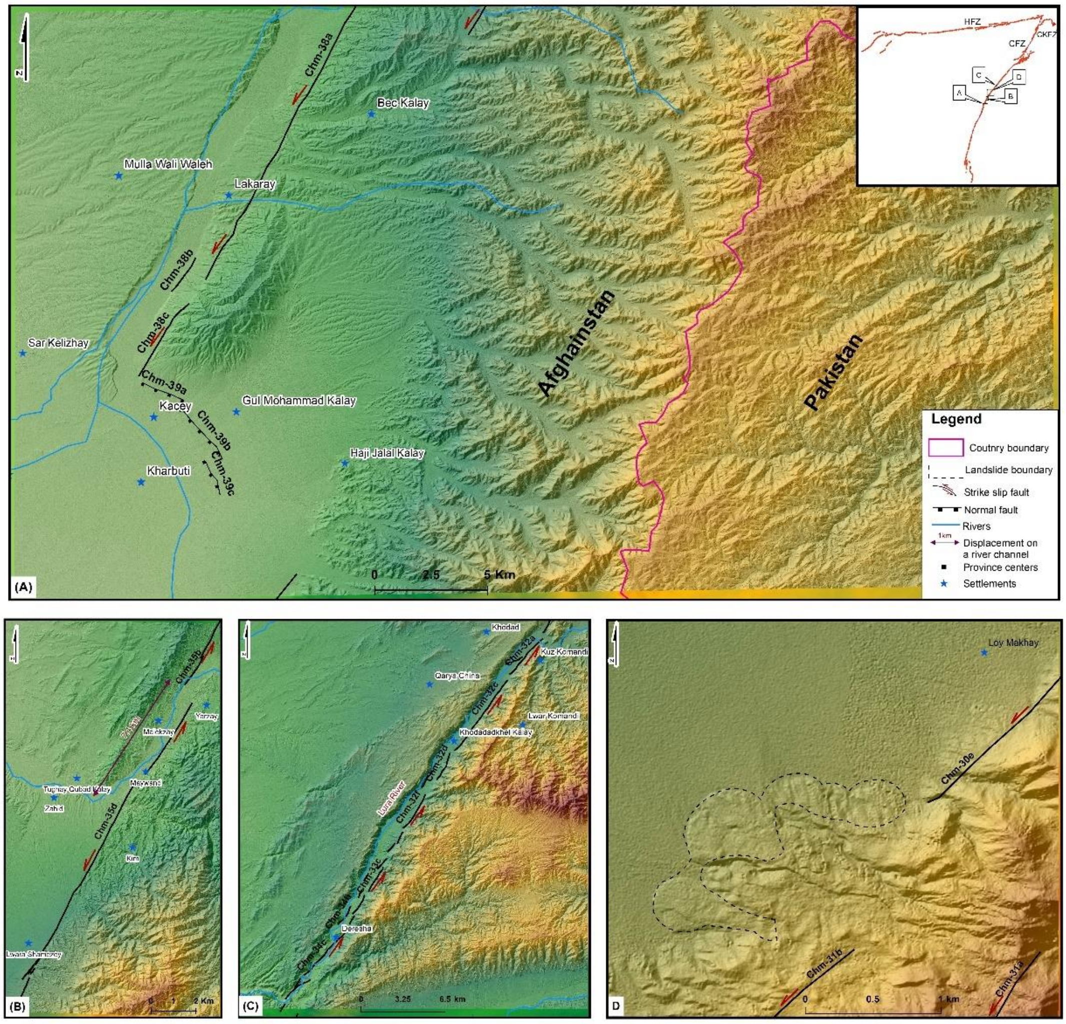

Figure 5.3. *The southern splay of CFZ; A) Formation of regional drag fold and NNE possible normal faults creating releasing stepover zone, B) activity of left-lateral movement represented by the channel displacement of Arghistan River, C) Continuation of CFZ segments controlling the Lura River, and D) Development of large landslides resulted by the left-lateral CFZ.*

The Chaman Fault Zone (CFZ) creates another major releasing stepover zone, where Ghazni City is situated on the northwest corner. The existence of north-south (N-S) and northwest-southeast (NW-SE) trending possible normal fault segments in this area indicates that the main splay of the CFZ does not extend northeastward as the Gardiz fault, but instead, it may have jumped to the north of the Ghazni province. (Figure 5.4A)

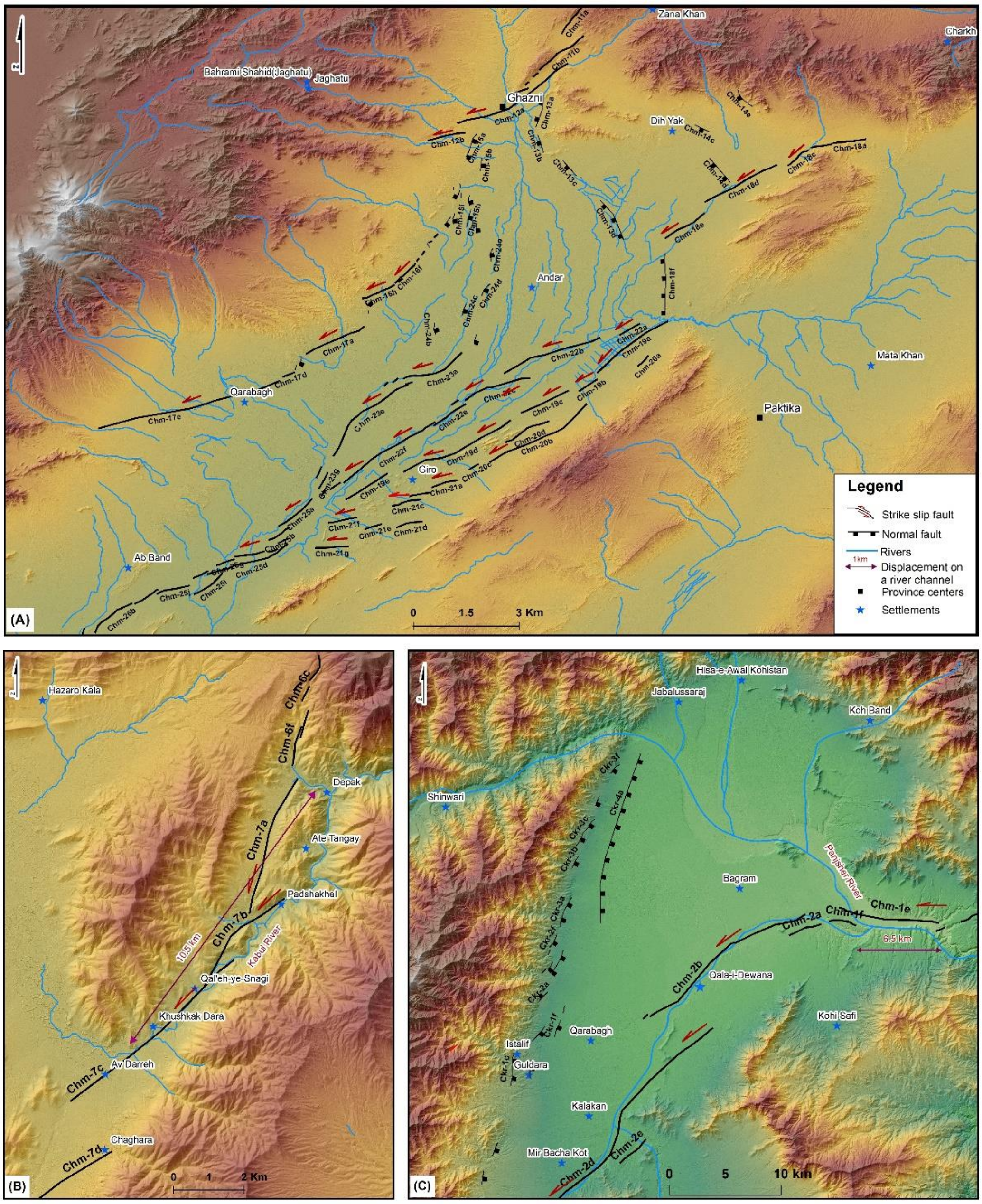

Figure 5.4. *The norther extension of CFZ; A) Formation of possible N-S and NE-SE oriented normal faults resulting the expansion of releasing stepover zone, B) left-lateral displacement along the branches of CFZ over the southwest of Kabul city, and C) Changing the direction of CFZ from NNE to NE and distribution of Charikar Fault Zone (CKFZ) within the NW of the Kabul Block.*

To examine the trends of the developed possible normal faults, swath profiles perpendicular to them with a 2-kilometer width were calculated (Figure 5.5). The maximum, minimum, mean elevation and local relief were calculated in the profiles to quantify the topographic trend and show the topographic expressions influenced by the normal faults within the releasing stepover zone.

Basically, the main section of the Chaman Fault Zone (CFZ) extends from the north of Ghazni to the southwest of Kabul, where a 10.5-kilometer left-lateral displacement of the western splay of the Kabul River is developed within the Av Darreh and Depak localities along the Chm 7a-c segments (Figure 5.4B). The orientation of the CFZ changes from NNE to NE in the northwest of Kabul between Paghman and Qala-i-Diwana through Mir Bacha Kot district (Figure 5.4C). Within this region, in the south of Bagram Air Base, the morphological expression of the Chm-2b segment is distinguished. Further to the ENE direction, a total of 6.5 kilometers of left-lateral displacement of the Panjshir River can be measured over the Dingak locality (Segment Chm-1e) (Figure 5.4C). The Appendix 1 summarizes the additional dominant left-lateral shifts of river channels along the CFZ with the smaller lengths.

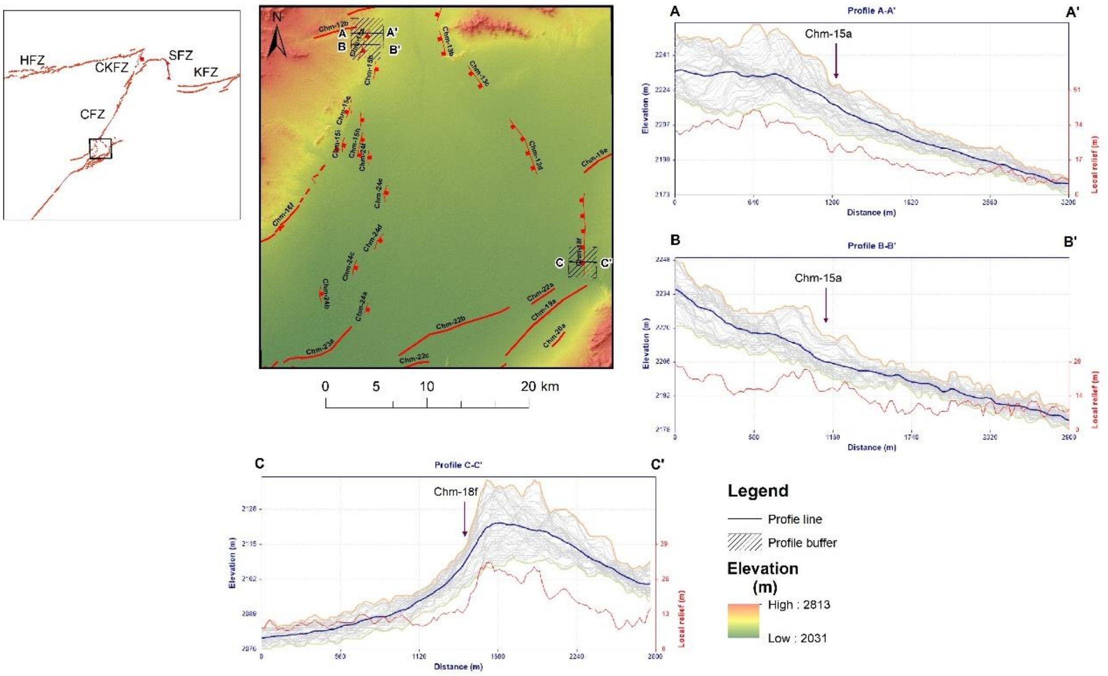

Figure 5.5. *Swath profile analysis of possible normal fault segments of the Chaman Fault Zone (CFZ) with a 2-kilometer width perpendicular to the fault segments. Light orange-colored lines represent maximum elevation, light green line marks the minimum elevation, and dark blue line represents mean elevation.*

According to the Riedel shear model developed by (Hancock, 1994; wilcox et al., 1973), the compressional stress (σ_1) trends NW-SE over the orientation of N03°W, while the extensional stress (σ_3) is oriented NE-SW trending N42°E. Within the eastern branch of the Chaman Fault Zone (CFZ) (Gardiz fault), the same mechanism of the Reidel shear model is accommodated with only changes in the direction of the stress axes. The compressional stress directs N19°E, whereas the extensional stress trends N73°W.

5.1.2. The Herat fault zone (HFZ)

The right-lateral Herat Fault Zone (HFZ), also known as the Hari Rud fault, has a length of approximately 1,100 kilometers. It is located about 30 kilometers east of the Iran-Afghanistan border and extends eastward, passing through Herat city, Ghor, Bamyan, and Parwan provinces, before terminating 70 kilometers north of Kabul city. It finally connects with the Panjsher-Badakhshan fault (Wellman, 1966) (Figure 5.6).

The fault zone is a major tectonic boundary that separates the relatively stable Eurasian plate to the north from the extensively deformed and accreted terrains to the south (Ruleman et al., 2007; Tapponnier et al., 1981). The elongated fault basins filled with Oligocene and Miocene sediments are believed to suggest the strike-slip motion of this fault zone during that period (Tapponnier et al., 1981).

Studies by Ruleman et al. (2007) and Shnizai (2020) indicate that young displacement of small landforms and streams has been observed along the entire length of the HFZ. The geodetic slip rate along the fault zone is estimated to be less than 2 mm/yr by Mohadjer et al. (2010), whereas (Sborshchikov et al., 1981) confirm a geologic slip rate of 2–3 mm/yr.

Accurate mapping of the Herat Fault Zone (HFZ), along with other bounding fault zones of the Kabul Block, remains a challenge. However, by utilizing high-resolution imagery, I was able to examine the fault's geomorphic expression and precisely trace its segments. My mapping effort identified a total of 215 segments, which included both right-lateral strike-slip faults and normal faults, as depicted in Figure 5.6.

The mapped segments of the HFZ exhibit well-defined structures associated with the right-lateral strike-slip system, as illustrated in Figure 5.6. At the north of Herat city, the fault forms a releasing stepover zone, where the fault trace has shifted from the western corner to the southeast of Herat city. This area potentially features NW-SE-oriented normal faults, such as Segment Hrt 33a-d, as shown in Figure 5.6A.

Moving further east, another extensional area expressing the releasing stepover can be observed, which is inferred from the jumping of the HFZ from Khwaje Darrah to Qala-i-Dast village. This has resulted in the development of possible WNW-ESE trending normal faults, such as Segment Hrt-32d, as depicted in Figure 5.6B.

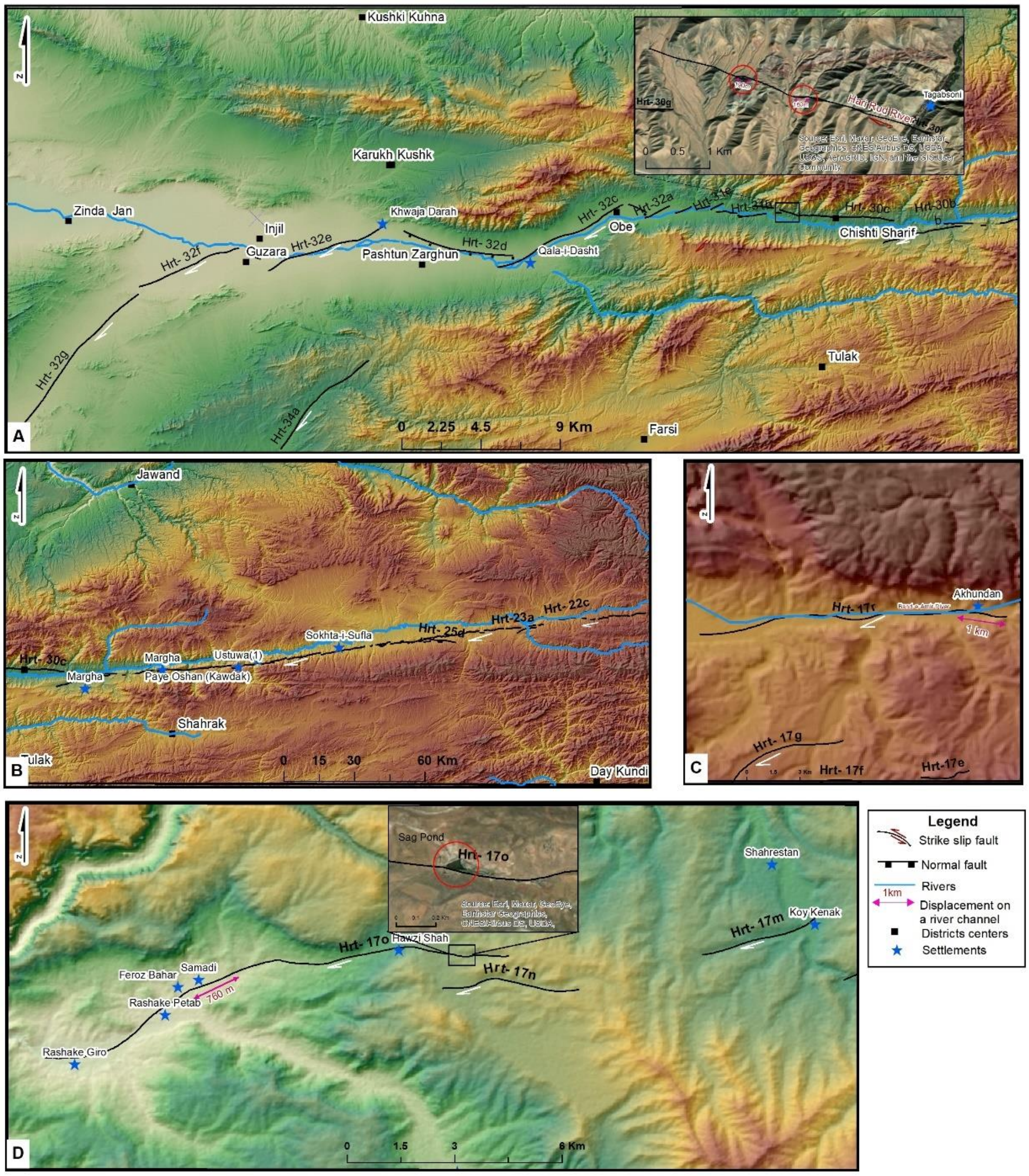

Figure 5.6. *Segmented areas of the Herat Fault Zone (HFZ) are illustrated in the following: A) distribution of normal and right-lateral segments in the western section, B) right-lateral drainage shift in the central section, C) right-lateral displacement of a section of Band-e-Amir river in the Yakawlang district, and D) development of linear valleys and sag ponds in the eastern section.*

The HFZ plays a crucial role in controlling the course of the Hari Rud River, and it is also responsible for causing several stream deflections, which confirms its right-lateral motion. At the Tagab-Soni locality, a right-lateral 190-meter lithological displacement and 150-meter drainage shift can be observed, as seen in Segment Hrt-30f (Figure 5.6C).

In this area, the right-lateral shift of drainages and the triangular facets of ridges are prominent features indicating the recent movement of the HFZ (Figure 5.6C).

As the Herat Fault Zone (HFZ) extends to the east, it crosses the Ghor province, where right-lateral displacements of 1.36 kilometers, 3.5 kilometers, 800 meters, and 150 meters have been measured in local drainages (Segments Hrt 28e-f & 28c-d) (Figure 5.6B). The most significant impact of the HFZ in the Yakawlang district of Bamyan province is a large right-lateral displacement of 1 kilometer in the Band-e-Amir River at the Akhunda area (Segment Hrt-17r) (Figure 5.6C).

As we move towards the eastern end of the Herat Fault Zone (HFZ), a 760-meter right-lateral drainage shift is observed near the Reshake Betab settlement. In addition, Segment Hrt-17o shows the development of a linear valley and sag pond. More information on the displacement of minor river channels along the HFZ can be found in the Appendix 2.

5.1.3. The Charikar fault zone (CKFZ)

According to Ruleman et al. (2007) and Shnizai (2020), this fault zone exhibits discontinuous, linear, and arcuate fault scarps on Quaternary deposits and landforms. It is considered the northern extension of the Chaman Fault Zone (CFZ), a part of the Paghman fault. The Paghman Fault is a major fault line that runs for about 80 kilometers. It starts in the Paghman district and ends in the Shutul and Unaba districts of Panjsher province. The fault line terminates at the northern margin of the Kabul Block. (see Figure 5.2).

In this study, we redefined the Charikar Fault Zone (CKFZ) as a separate fault with normal fault character, rather than considering it as the northern extension of the CFZ as the Paghman fault. The CKFZ is a 40-kilometer-long fault trending NNE with normal motion, passing through the districts of Guldara (Güldere), Istalif, Bagram, and Charikar. We named the redefined fault trace as the Charikar Fault Zone since it already passes through this locality (Figure 5.4C). Alluvial fans developed along the CKFZ and the sequence of lithological units in cross-sections A–D confirm the vertical offset (normal) type motion in the area (Figure 5.7).

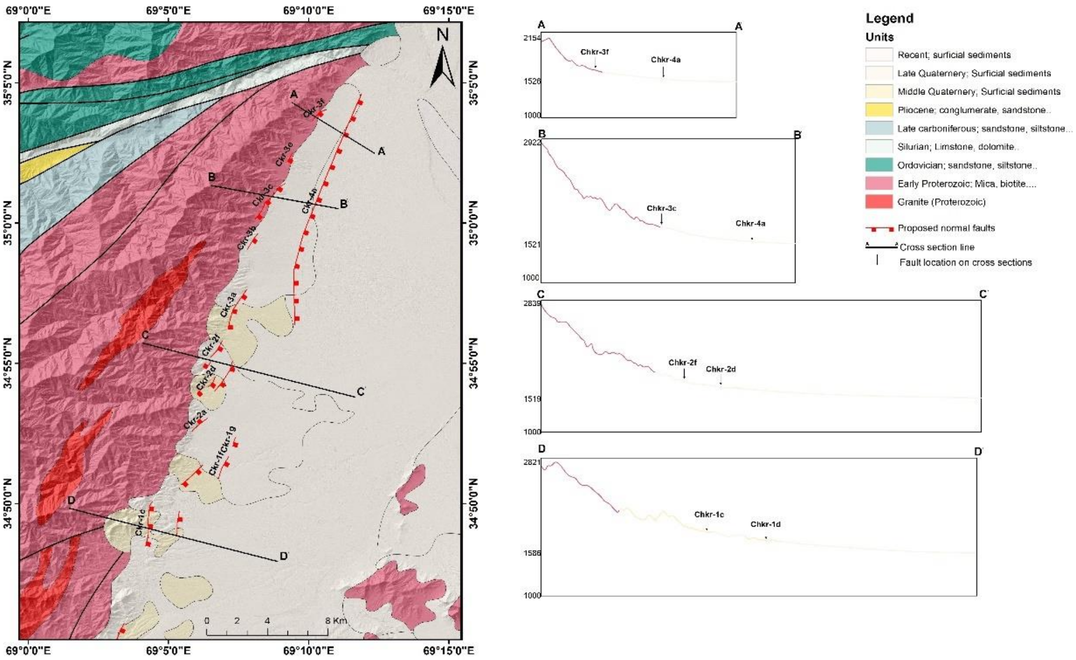

Figure 5.7. *This simplified geological map, modified from Abdullah et al. (2008), showing cross-sections perpendicular to the Charikar Fault Zone.*

Geomorphologically, the northern parts of Bagram Air Base, known as the Shomali Plain (Bohannon, 2010b), have an oval or plane shape. The area is situated on an escaping wedge between the right-lateral Herat Fault Zone and the left-lateral Chaman Fault Zone, and it is controlled by the normal fault segments of the Charikar Fault Zone (CKFZ). The cross-sections perpendicular to the CKFZ exhibit step-like topography, corresponding to the normal faults (Figure 5.7). Additionally, three swath profiles with a width of 2 km were calculated perpendicular to the CKFZ, indicating the topographic trend affected by the developed normal faults (Figure 5.8). The maximum elevation represents the rigid block, while the minimum elevation represents the possible hanging wall block. Furthermore, typical alluvial fans are observed over the eastern boundary of Shomali Plain, starting from the central parts of Hisa-i-Awal Kohistan (over the Gölbahar and Albironi University areas), which may indicate a normal fault in this area as antithetics of the Charikar fault (Figure 5.8).

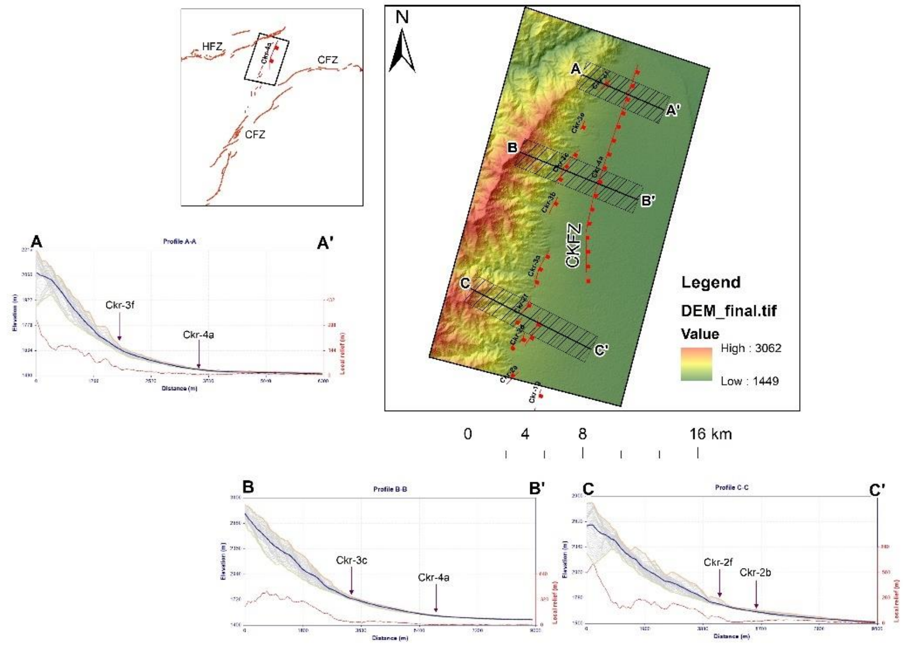

Figure 5.8. *Thematic map showing topographic swath profiles perpendicular to the Charikar Fault Zone (CKFZ), with a width of 2 km. The light orange line represents the highest elevation, the light green line indicates the lowest elevation and the dark blue line represents the mean elevation.*

5.1.4. The Sarobi fault zone (SFZ)

The Sarobi fault is a 150-kilometer-long fault that trends in a north-south direction and is located in eastern Afghanistan. It forms the northeastern edge of the Kabul Block, a relatively stable area, and separates it from the adjacent Block of Nuristan. The fault line is active and has been documented by geomorphic features, such as offset drainages and fault scarps (Schreiber et al., 1972; Shnizai, 2020). The Sarobi fault is considered to be connected to the Panjsher and Paghman faults, and it continues eastward where it joins the Spinghar fault (Figure 5.2).

According to Schreiber et al. (1972) and Shnizai (2020), the fault trends approximately north-south with its northern section deflecting to the north-northwest direction and the southern section deflecting towards the east. A study by Prevot et al. (1980) suggests that the Sarobi fault is a right-lateral strike-slip fault. The study was based on the analysis of earthquake focal mechanisms, which are the directions and amounts of slip on faults that cause earthquakes. Although the fault has scarps along the bedrock-colluvium contact, no scarps have been reported on the adjacent piedmont alluvium. The fault's movement appears to be primarily dip-slip (vertical), with a possible small dextral motion (Ruleman et al., 2007; Shnizai, 2020).

The Sarobi fault, situated between the Gardiz and Chaman fault zones, is clearly expressed topographically on aerial and Landsat images, as well as on the ground (Wellman, 1966). In this research, we propose a thrust-type motion for the Sarobi Fault Zone based on our interpretations. Within the mapped area, typical landslide marks were found on the eastern side of the SFZ, indicating a disruption of slope stability that contributes to an uplift in the region, as illustrated in Figure 5.9.

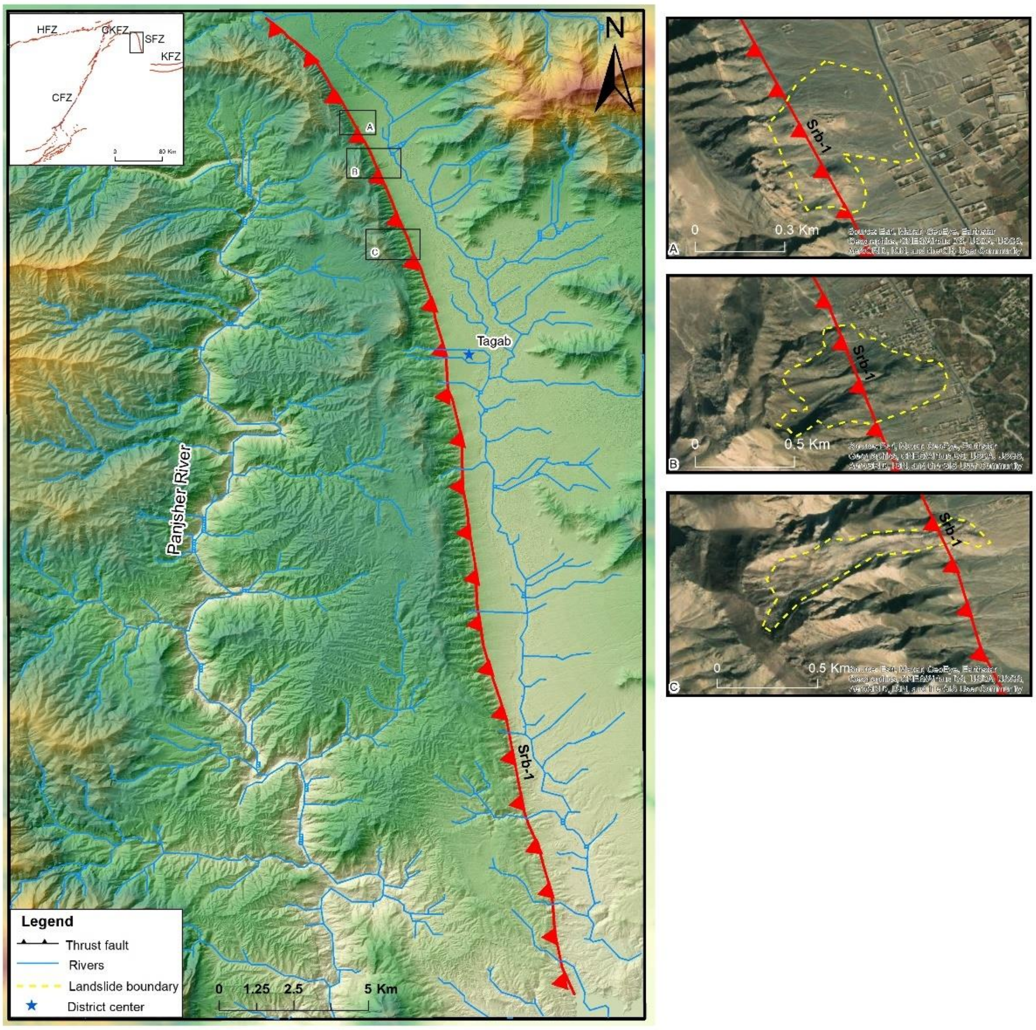

Figure 5.9. *The central section of the Sarobi Fault Zone exhibiting a thrust-type motion, with highlighted areas where landslides have occurred.*

A detailed examination of the fault trace on the topography reveals that the fault surface has a strike of N20W with a dip of 23° southwest in the southern section of the SFZ. In the northern section, the same strike is found with a minor change in angle to N24W and a dip of 27° southwest. Since this fault zone lies between the left-lateral Konar and Chaman fault zones, it is suggested that it is a restraining stepover zone in this region.

To further understand the uplifting of the SFZ, we conducted a detailed morphotectonic analysis by examining cross-sections perpendicular to the fault zone at different intervals. We also calculated two asymmetry factors (AFs) between two points along the Panjsher River west of the fault boundary between Kohe Safi and Tagab districts to assess the drainage basin asymmetry and identify the tectonic tilting on the hanging wall of the thrust fault. We deployed the AF indices for two types of basins, regional and local, on both scales. The first calculated AF for the region-wide drainage basin indicated eastward tectonic tilting (Figure 5.10a). However, the second calculated AF for basins on a local scale revealed westward tilting, confirming the uplifting along the SFZ (Figure 5.10b).

The examination of the cross-sections revealed that the eastward tectonic tilting related to the main basin represents a regional uplift from west to east, which may be associated with specific faulting in region 1 (shown by the blue dashed line in the cross-section), such as the Charikar Fault Zone. In contrast, the westward tectonic tilting calculated from local basins indicates an uplift from east to west in region 2 (shown by the red dashed line in the cross-section).

The uplift caused by the SFZ also affects the geomorphic features of the Panjsher River in this region. Although the river flows from northwest to east, it suddenly turns southward at the intersection of the boundaries of the Bagram and Tagab districts (AF 1 in Figure 5.10b) instead of flowing to the east of the fault into a valley. This change in direction could be associated with the uplift of the SFZ in the area. The thrust fault extends north over the central parts of the Koh Band district in the Malekar area, but active uplift due to the thrust faulting is not observed in this region.

The detailed morphological investigation indicates that the current uplift due to the SFZ has ceased after the Nijrab district. Based on the morphology and stream patterns, as illustrated in Figure 5.10d, we have defined the boundary between the active (1) and inactive parts (2 and 3) of the SFZ. The river stream can act as a natural boundary that overcomes the uplift and is directed to the east of the fault zone. In area 2 of Figure 5.10e, another stream network cuts the fault, indicating that the fault is inactive in this area. The prominent stream channels confirm the situation within area 3, as shown in Figure 5.10e.

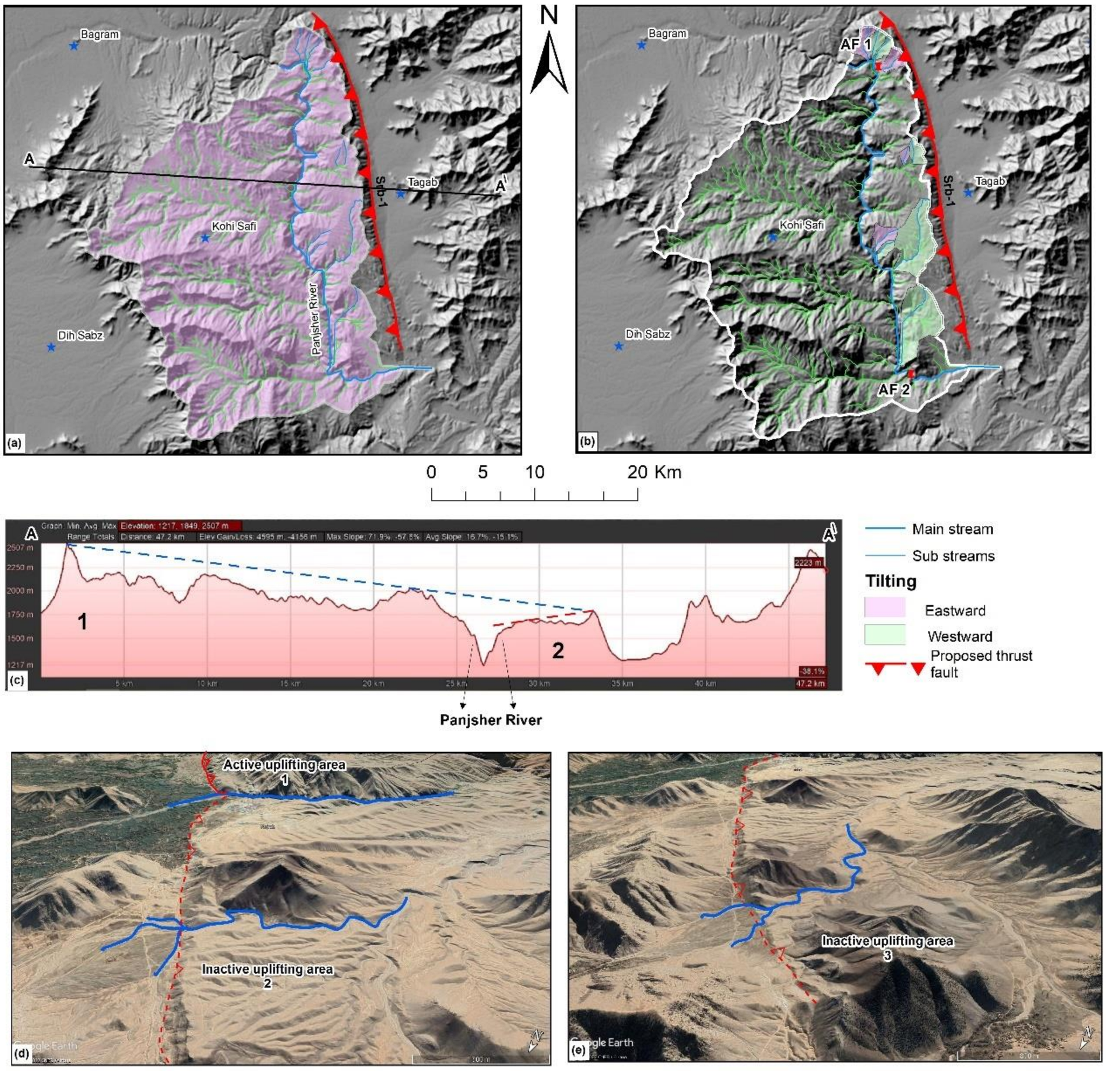

Figure 5.10. *Thematic map illustrating the asymmetry factor (AF) measurements along the Sarobi Fault Zone, demonstrating its thrust-type motion. (a) shows the AF measurements for the regional basin, while (b) displays the local basin measurements. (c) is a schematic cross-section taken from a perpendicular direction to the regional and local basins, with blue and red dash lines indicating slope directions. (d) and (e) show the active and inactive parts of the Sarobi Fault Zone, respectively, as captured from Google Earth Pro.*

Furthermore, the cross-sectional analysis reveals a discernible degree of uplift along the trace of the fault zone (Figure 5.11). Additionally, we calculated five swath profiles with a width of 2 km perpendicular to the SFZ to determine the maximum, minimum, mean elevation, and local relief. The topographic signature of uplift is noticeable in all profiles, especially in (A-A', B-B', and D-D'), as depicted in Figure 5.12. Our proposed model is strongly supported by the results of the AF measurements, graphical cross-sections, and swath profiles, which all demonstrate a high degree of consistency. In addition, high-resolution satellite imagery of the SFZ reveals a minor right-lateral displacement of the drainage systems, potentially indicating an oblique motion of the fault zone. Further details of these observations can be found in the Appendix 3.

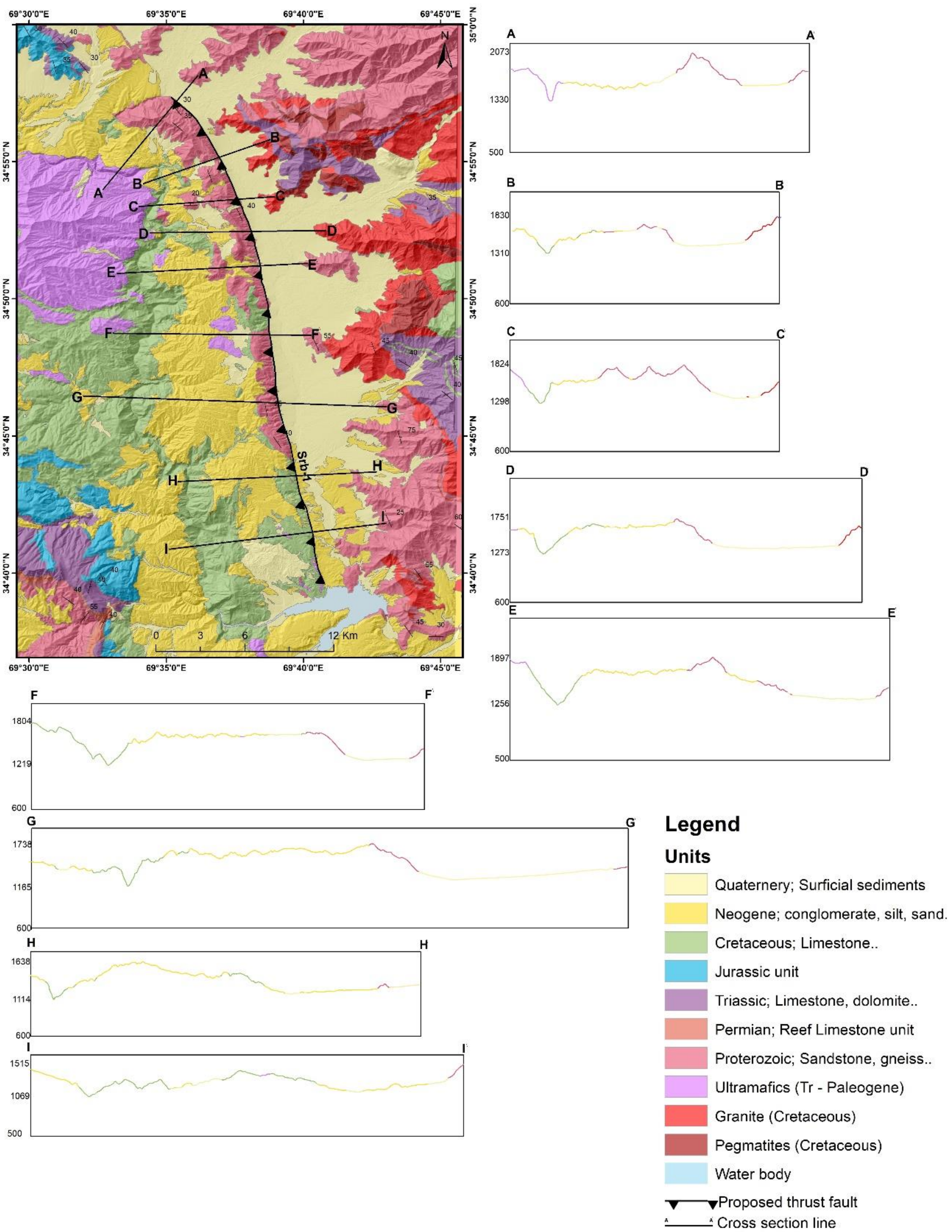

Figure 5.11. *Graphical illustrations showing the uplifting and tectonic tilting along the Sarobi Fault Zone through graphical cross-sections. The geologic map has been simplified and adapted from previous studies (Abdullah et al., 2008; Bohannon, 2010a).*

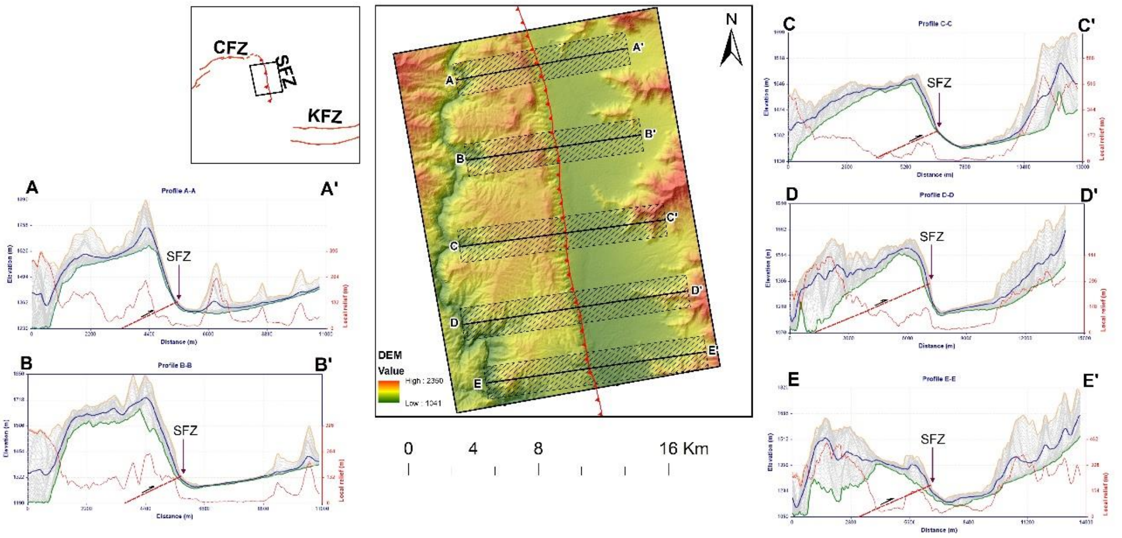

Figure 5.12. *Swath profiles perpendicular to SFZ with a width of 2km, showing maximum elevation (light orange line), minimum elevation (light green line), mean elevation (dark blue line), and the presumed thrust fault (red dashed lines).*

5.1.5. The Konar fault zone (KFZ)

The left-lateral Konar Fault Zone (KFZ) in eastern Afghanistan trends in a northeast direction and acts as a boundary between the Konar/Jalalabad tectonic zones and the Nuristan-Pamir Block. Its length has been estimated to be between 156 and 200 km within Afghanistan's territory (see Figure 5.2). The fault zone is a major tectonic feature that originates from the left bank of the Kabul River near the settlement of Sarobi. It then follows the Konar River, a tributary of the Kabul River, and extends beyond Afghanistan's borders into the Chitral region of Khyber Pakhtunkhwa, Pakistan. It is possible that the fault zone merges with the main Karakoram and Tirich Mir Thrust system (Mahmood & Gloaguen, 2012).

Arcuate scarps trending in an east-northeast direction and occurring on piedmont landforms of various ages have been documented in the literature (Ruleman et al., 2007; Shnizai, 2020). Ruleman et al. (2007) estimated the slip rate of the KFZ to be between 1 and 10 mm/yr, based on its resemblance to faults found in other parts of the world, such as the Karakoram fault in western China and East Anatolian Fault in Türkiye.

We attempted to trace the previous path of the Konar Fault Zone (KFZ) using high-resolution imagery, but we found that many of the trace lines did not match the surface features in the selected regions. Instead, we used imagery from Google Earth Pro to map out 92 different segments of various lengths and types, including left-lateral strike-slip faults and normal faults located in the releasing stepover areas along the KFZ (Figure 5.2). As part of our segmentation analysis, we identified several distinctive morphotectonic features, including stream deflections, shutter ridges, and alluvial fans. We observed that the (NNE) trending KFZ (Segments 1a-2e) shifted from the Sandikdeh region to the Drosh settlement, creating a releasing stepover zone between these two areas. As a result of this shift, several possible normal fault segments were observed (Segments 3a-f) (Figure 5.13).

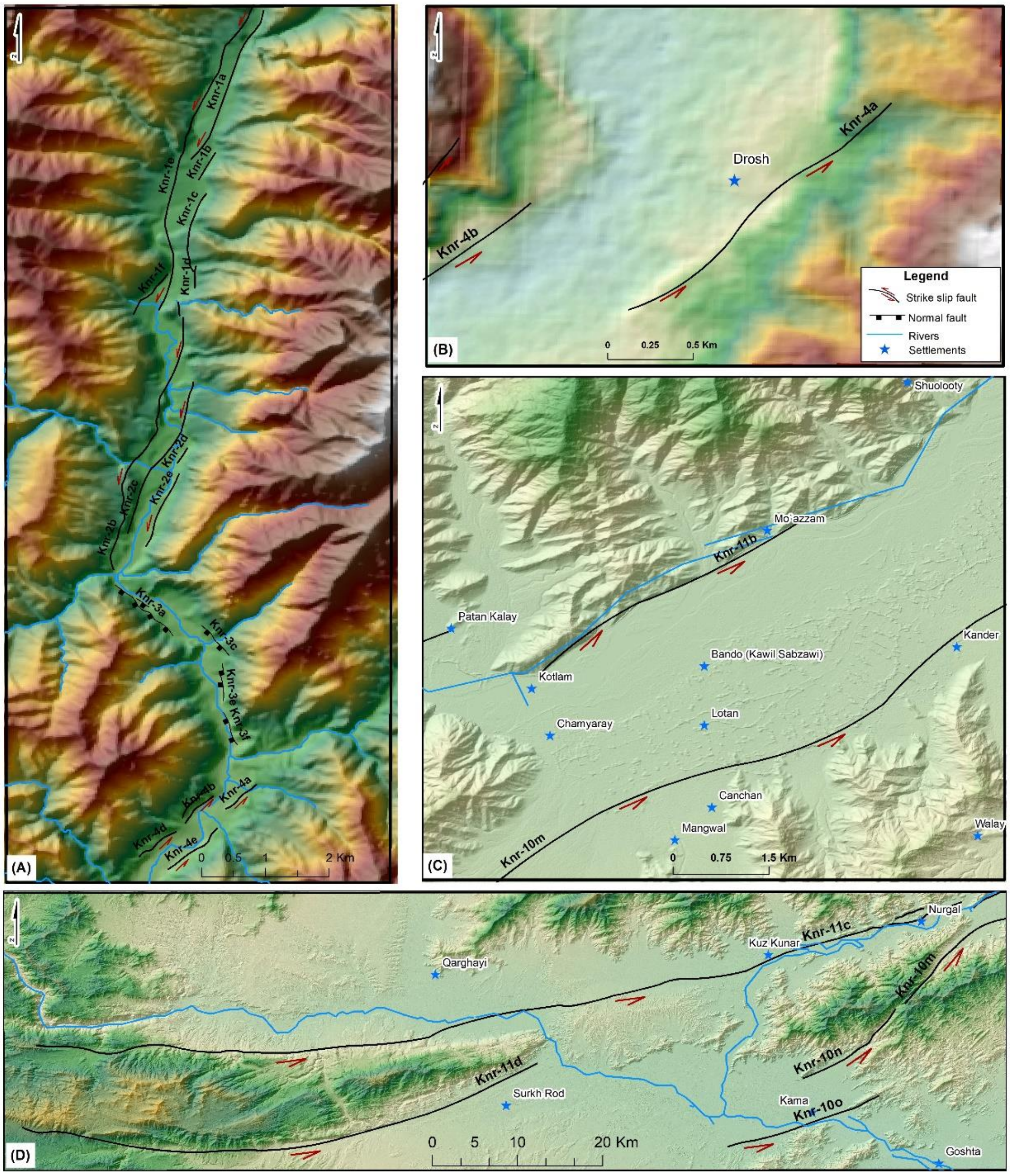

Figure 5.13. *The Konar Fault Zone (KFZ) segmentation magnified from (Figure all fault zone). A) representing the Chitral Region in Pakistan, B) the area outside of Afghanistan within the Drosh settlement, C) the southeastern area of Nurgal district in Konar province, and D) the eastern end of the KFZ spanning across the southern Laghman and western Nangarhar provinces.*

Furthermore, the trend of the Konar Fault Zone (KFZ) appears to be shifting towards the northeast. The segments that trend in a northeast-southwest direction generally follow linear valleys and cause significant left-lateral displacements in the drainage pattern. The overall structure of the KFZ consists of left-stepping segments located between the settlements of Drosh, Mo'azzam, and Kutlam (Segments Knr-4a and Knr-11b) (Figures 5.13 B and C). In the northeast and west of Jalalabad, the segments of the KFZ bend in an ENE-WSW direction (i.e., Segments Knr-11c-d) (see Figure 5.13 D). These segments likely have a thrust component, as expected from a left-lateral fault zone that bends towards the right. Further details about the geomorphic expression of the KFZ can be found in the Appendix 4.

5.2. Automatic Extracted Lineament and Structural Analysis

The automated extraction of geological lineaments within the Kabul Block is a large-scale extend that has been divided into four different zones. The results of each zone are summarized as follows:

5.2.1. Zone-I

Zone-I is a geologically diverse region located on the northeast margin of the Kabul Block. It is characterized by the Sarobi fault zone, a major tectonic. The zone also contains a variety of igneous, metamorphic, and sedimentary rocks, which provide evidence of its complex geological history. Table 5.2 summarizes the statistical data for the extracted lineaments in this zone. Radar data e.g. DEM-5m and Sentinel-1B GRD was able to extract more lineaments than optical data because radar data is better at detecting linear features, such as faults and fractures, than optical data e.g. Sentinel-2A MSI and ASTER. Radar data can penetrate clouds and darkness, so it can be used to image areas that are not visible to optical sensors. Radar data also has a higher resolution than optical data, which allows for the detection of smaller lineaments.

Figures 5.14a and b show that the main orientation of lineaments extracted from radar data is northwest-southeast (NW-SE), with a secondary orientation of northeast-southwest (NE-SW). In contrast, the primary extracted lineaments from optical data are predominantly oriented northeast-southwest (NE-SW), while the secondary lineaments are oriented northwest-southeast (NW-SE). The magnified regions in Figures 5.15a and b show that the lineaments can be divided into two types: positive and negative. Positive lineaments are associated with elevated topography or ridges, while negative lineaments typically represent valleys, trenches, fractures, and joints. The lineaments extracted from both types of data are concentrated in the northeast, center, and south of Zone-I. This is because these areas are characterized by tectonic deformation and rapid changes in topography. In contrast to the northeast, center, and south of Zone-I, the northwest, east, and west of Zone-I exhibit a significantly lower number or complete absence of lineaments. This is because these areas are characterized by flat topography and artificial structures. (Figures 5.14a and b and 5.15a and b). The consistent pattern of the extracted lineaments confirms their accuracy.

Table 5.2. *Quantitative overview of the lineaments detected in each zone using radar and optical data*

Data	**Zones**	**No of lineaments**	**Length (m)**				
			Max.	Min.	Mean	Median	Sum
DEM	I	156488	948.31	10	129.56	113.36	20274739.79
	II	59498	834.87	10	132.02	115.43	7854784.37
	III	131782	876.58	10	134.69	119.27	17750222.90
	IV	67448	906.23	10	135.44	120.42	9135303.91
Sentinel – 1GRD	I	28693	2018.5	32.77	344.55	290.8	9886235.45
	II	10510	2197.62	33.1	349.40	295.85	3672224.02
	III	30614	2469.92	16.62	343.78	290.99	10524518.99
	IV	17014	1925.68	32.83	329.99	280.86	5614307.99
Sentinel – 2MSI	I	22697	2388.14	40	372.2	316.23	8445492.79
	II	8151	2436.47	40	384.88	322.49	3137182.02
	III	35807	2183.3	40	372.08	316.23	13323142.64
	IV	13963	2145.6	40	358.39	305.94	5004150.07
ASTER	I	12511	3421.31	2.15	527.85	447.82	6603985.93
	II	4594	3722.17	5.31	532.43	443.19	2445998.63
	III	17812	3719.84	0.87	519.86	436.98	9259744.63
	IV	7839	2753.49	0.46	497.44	421.87	3899437.95

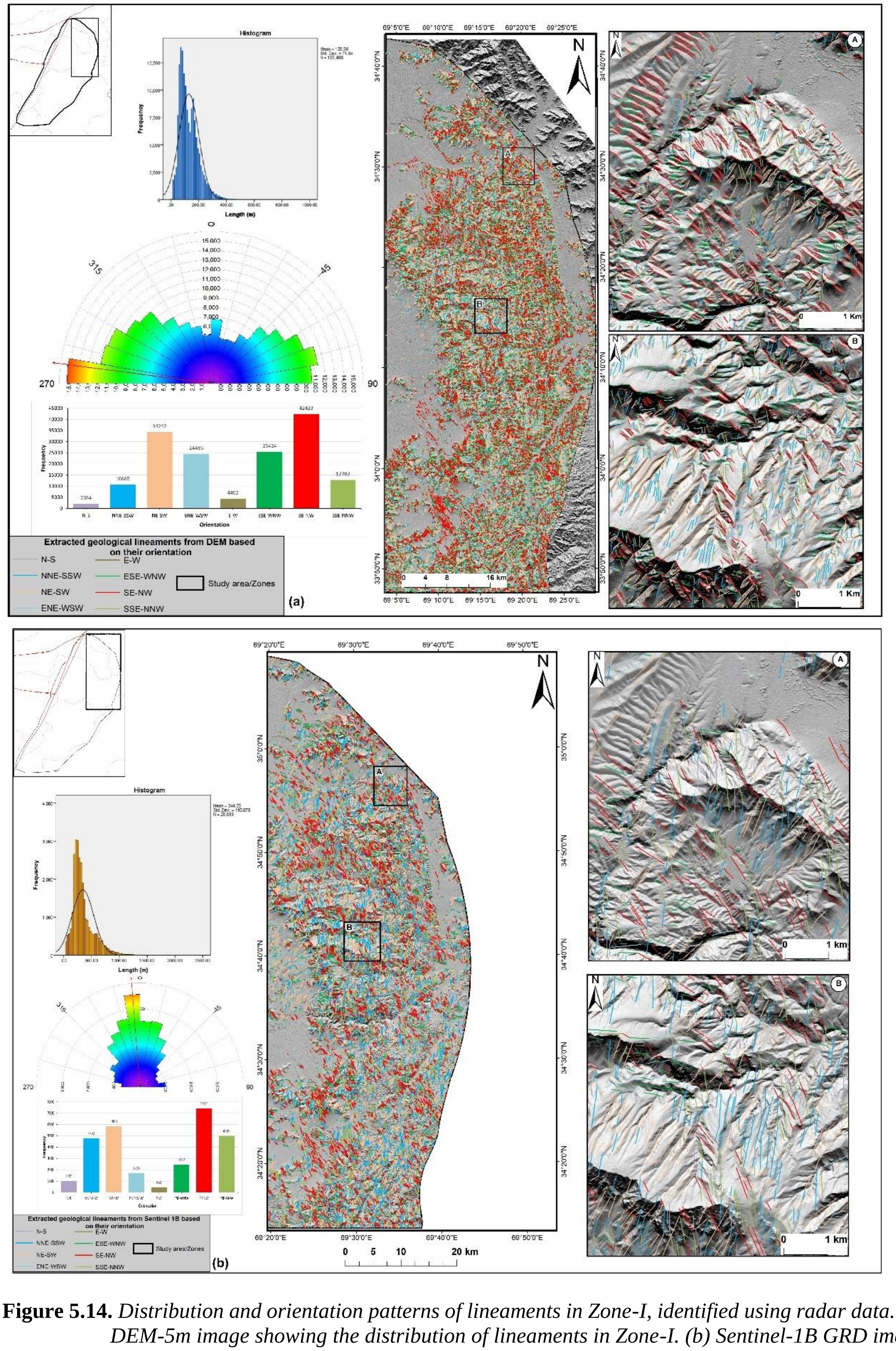

Figure 5.14. *Distribution and orientation patterns of lineaments in Zone-I, identified using radar data. (a) DEM-5m image showing the distribution of lineaments in Zone-I. (b) Sentinel-1B GRD image showing the orientation of lineaments in Zone-I.*

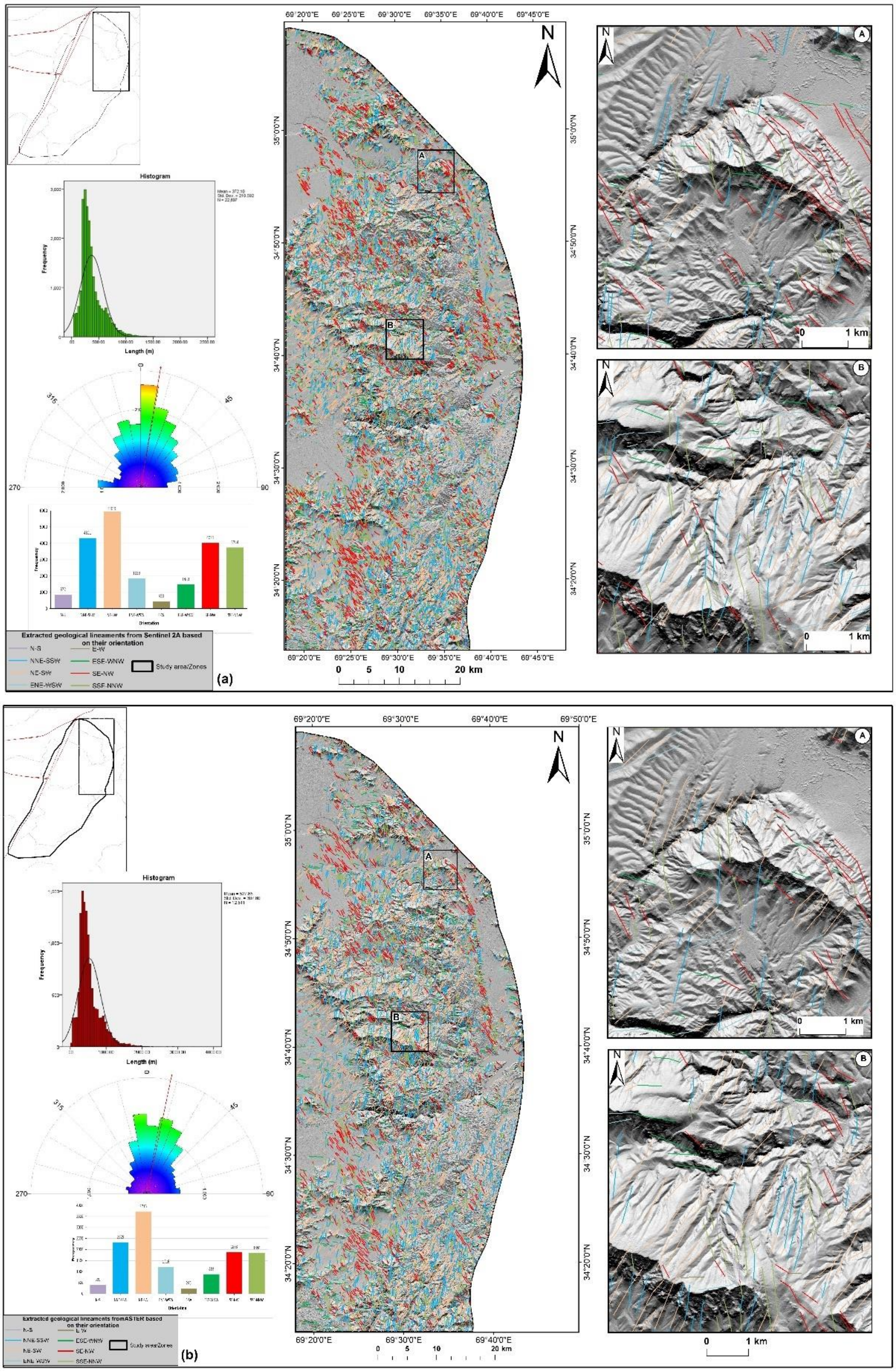

Figure 5.15. *Spatial pattern of extracted lineaments in Zone-1 of the Kabul Block.(a) Sentinel-2A MSI image showing the spatial pattern of extracted lineaments in Zone-1 of the Kabul Block, superimposed on a shaded relief image. (b) ASTER image showing the spatial pattern of extracted lineaments in Zone-1 of the Kabul Block, superimposed on a shaded relief image.*

5.2.2. Zone-II

Zone-II is located in the southern region of the Kabul Block. It spans the northeast-southwest (NE-SW) trending edge of the Block, and is bounded by the Gardiz fault, which is considered to be a northeast-southwest (NE-SW) splay of the Chaman Fault Zone. (Table 5.2) (Figures 5.16 a and b). A notable discrepancy was observed in the number of lineaments detected using radar and optical data in Zone-II. DEM-5m and Sentinel-1B GRD detected more lineaments than Sentinel-2A MSI and ASTER data. DEM-5m detected 59,498 lineaments, Sentinel-1B GRD detected 10,510 lineaments, Sentinel-2A MSI detected 8,151 lineaments, and ASTER detected 4,594 lineaments (Figures 5.16 and 5.17).

The number of extracted lineaments and their length are inversely related. The lineaments extracted from DEM-5m have an average length of 132.02 meters, while those extracted from ASTER data have an average length of 532.43 meters. The lineament orientation pattern in Zone-II is similar to that of Zone-I, with the primary trend being NW-SE and the secondary trend being NE-SW for radar data (Figure 5.16), and the primary trend being NE-SW and the secondary trend being NW-SE for optical data (Figure 5.17). The majority of the detected lineaments are concentrated in the northeast, east, and southwest regions, covering the entire data set.

5.2.3. Zone-III

Zone-III is located in the southern and southwestern extensions of the Kabul Block. It is bounded by the Chaman Fault Zone to the west and the Gardiz Fault to the east. Analysis of the structural features and descriptive statistics of the detected lineaments revealed that 13,782 lineaments were identified from DEM-5m. The average length of the lineaments detected from DEM-5m is 119.27 meters. In contrast to the number of lineaments detected from DEM-5m, which is 13,782 lineaments with an average length of 119.27 meters, Sentinel-1GRD detected 30,614 lineaments with an average length of 290.99 meters. Similarly, Sentinel-2MSI detected 35,807 lineaments with an average length of 316.23 meters, and ASTER data detected 17,812 lineaments with an average length of 519.86 meters (Table 5.2). Figures 5.18 and 5.19 show that there is an inverse relationship between the mean length of the lineaments and the number of lineaments. This means that as the mean length of the lineaments increases, the number of lineaments decreases. The frequency distribution of the lineaments shows that most of the lineaments have a length of less than 200 meters for DEM-5m and less than 400 meters for Sentinel-1GRD and Sentinel-2MSI.

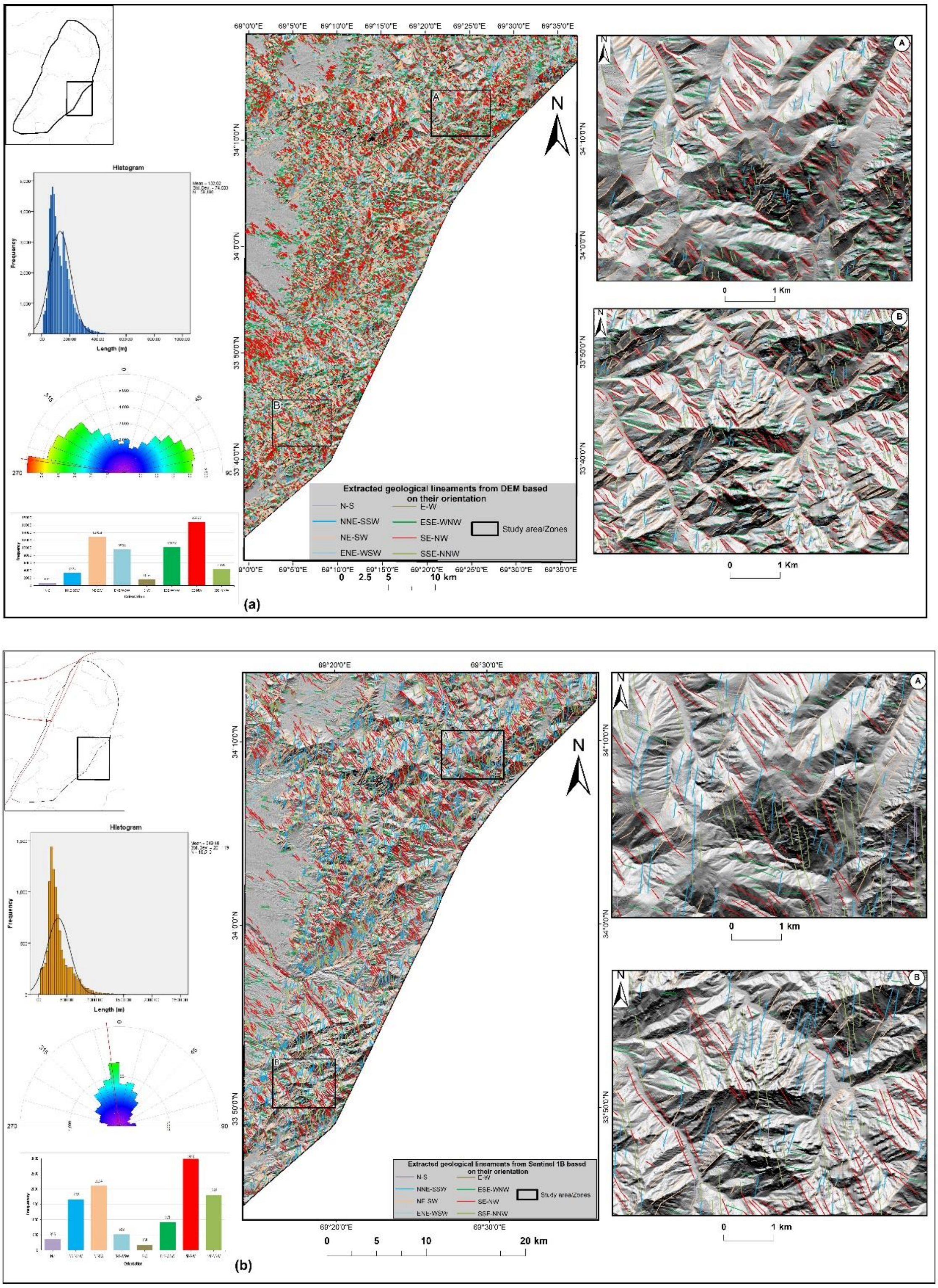

Figure 5.16. *Geospatial arrangement of identified lineaments throughout the Zone-II of the Kabul Block through remote sensing data analysis: a) DEM-5m and b) Sentinel-1B GRD imagery.*

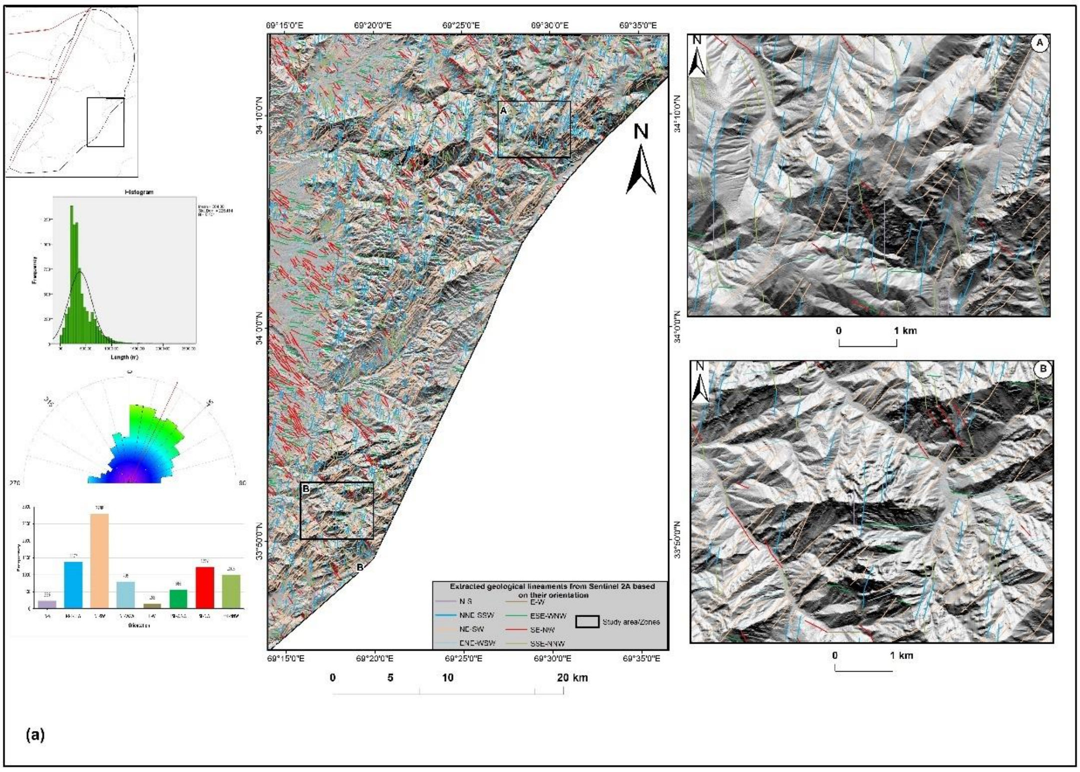

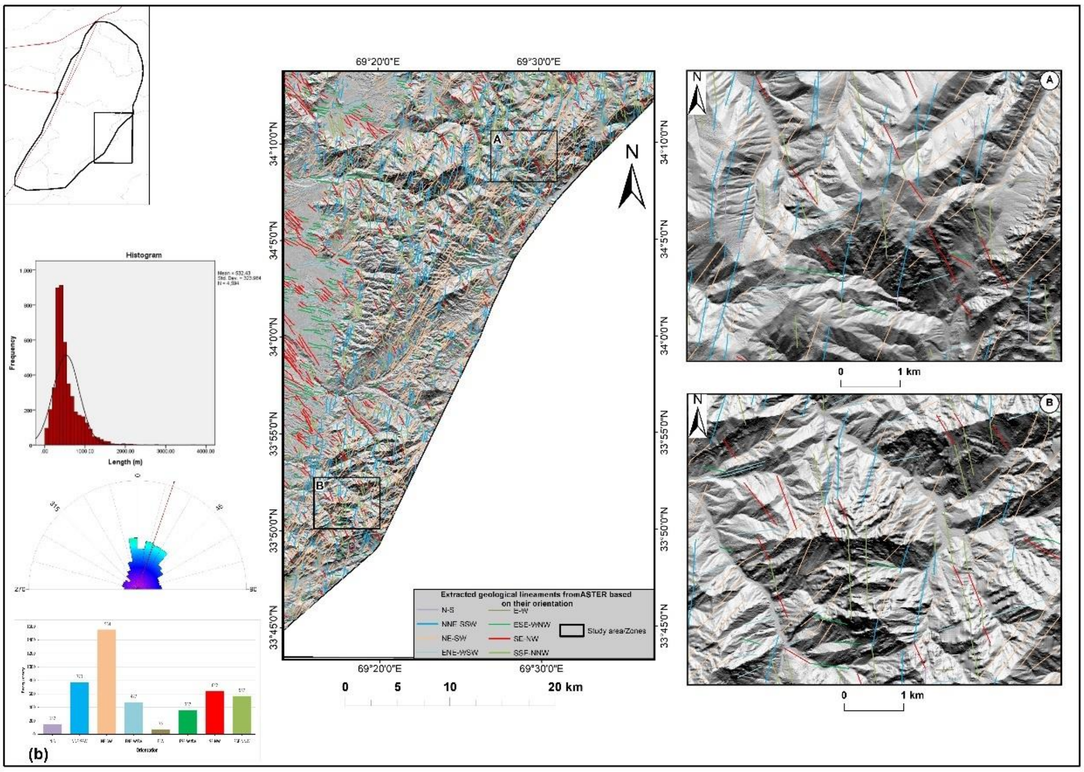

Figure 5.17. *Distribution of extracted geological lineaments over the Zone-II of the Kabul Block using remote sensing data: a) Sentinel-2A MSI and b) ASTER.*

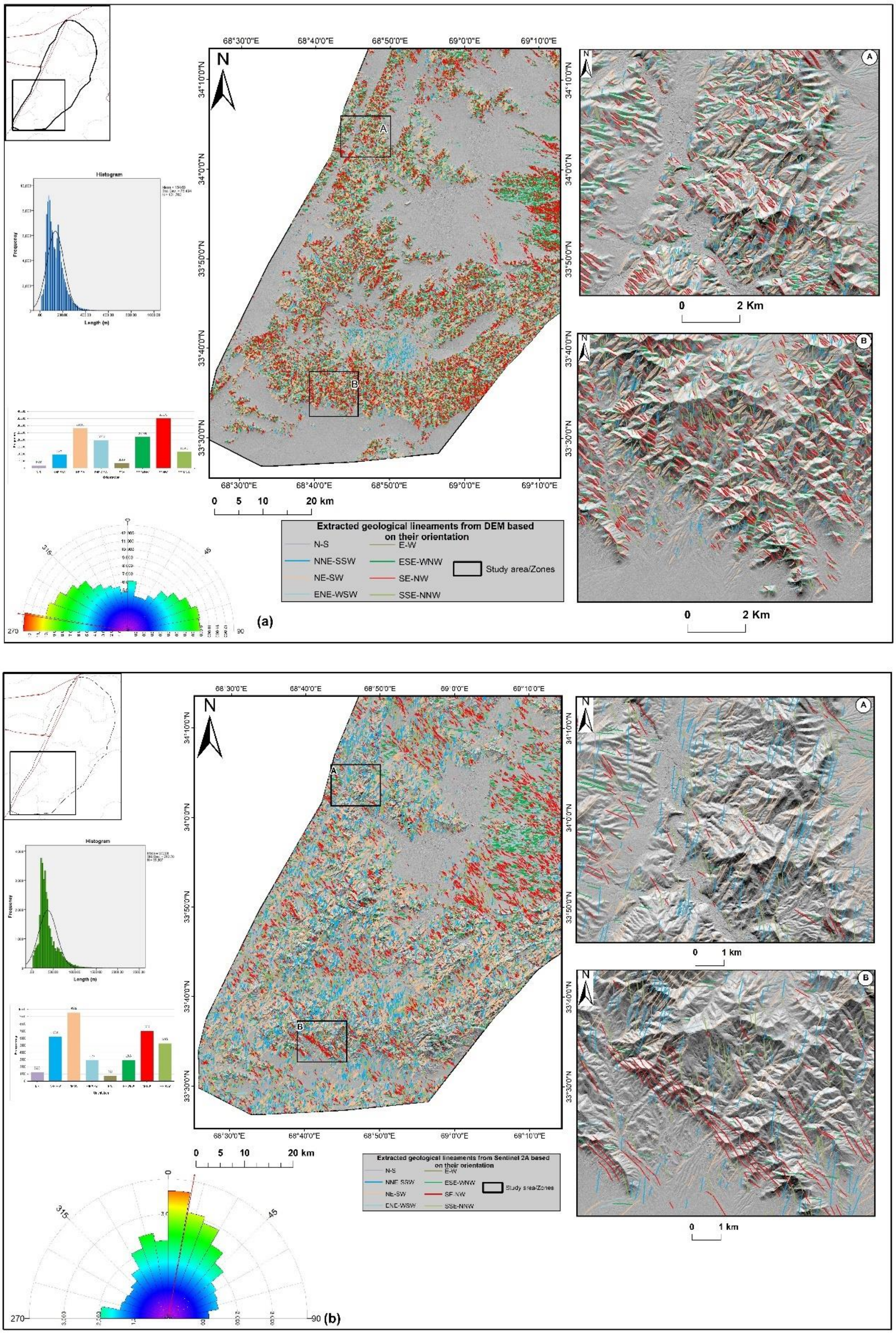

Figure 5.18. *Spatial distribution of mapped lineaments throughout the Zone-III, with magnified regions overlaid on hill-shaded images: a) DEM-5m and b) Sentinel-1B GRD.*

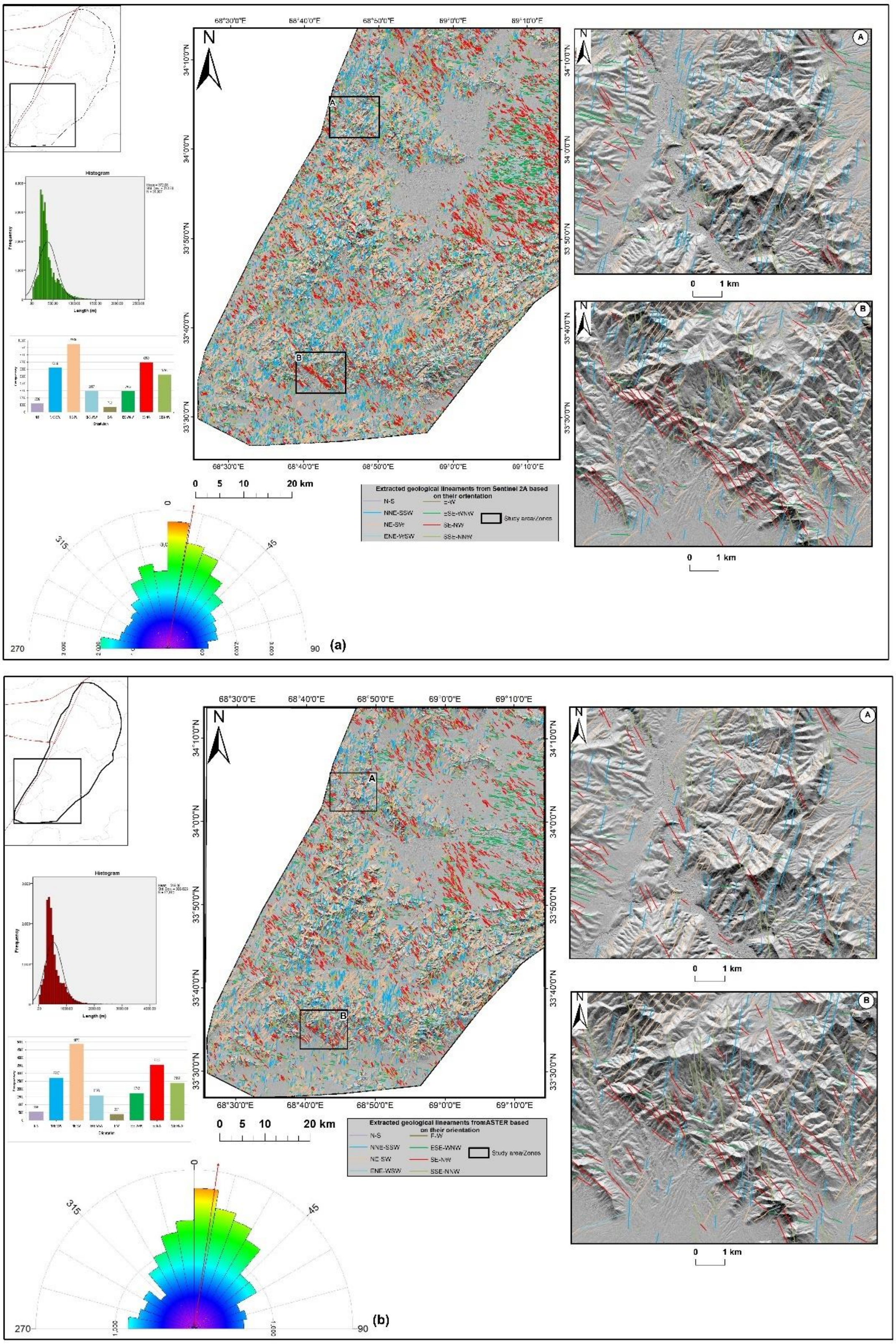

Figure 5.19. *Geospatial distribution and pattern of identified lineaments within Zone-III, depicted with magnified views, superimposed on hill-shaded images using Sentinel-2B MSI and ASTER data.*

5.2.4. Zone-IV

Zone-IV is located in the northern part of the Kabul Block and is bordered by the northern extension of the Chaman Fault Zone. The area is characterized by a diverse landscape, with a relatively flat area called the Shomali Plain, as well as urban sites and high rugged terrain, such as the Hindu Kush Mountains. A vast expanse of vegetation is present in the northwest part of Zone-IV. This makes it challenging to detect lineaments using optical data. As presented in Table 5.2, The largest number of lineaments with the shortest length were detected in Zone-IV using DEM-5m. The smallest number of lineaments with the longest length were found in the ASTER data (Figures 5.20 and 5.21).

The primary trend of the lineaments detected in Zone-IV using both radar and optical data is similar to that in other zones. The lineaments in Zone-IV have a northwest-southeast (NW-SE), west-northwest-east-southeast (WNW-ESE), and north-northwest-south-southeast (NNW-SSE) trend (Figure 5.20). In Zone-IV, the secondary trend of the lineaments detected using radar data is northeast-southwest (NE-SW), east-northeast-west-southwest (ENE-WSW), and north-northeast-south-southwest (NNE-SSW). The secondary trend of the lineaments detected using optical data is the opposite, with a southwest-northeast (SW-NE), west-southwest-east-northeast (WSW-ENE), and south-southwest-north-northeast (SSW-NNE) trend (Figure 5.21). The majority of the extracted lineaments are located in the eastern, southern, and southwestern regions of the study area accompanied by the igneous complexes.

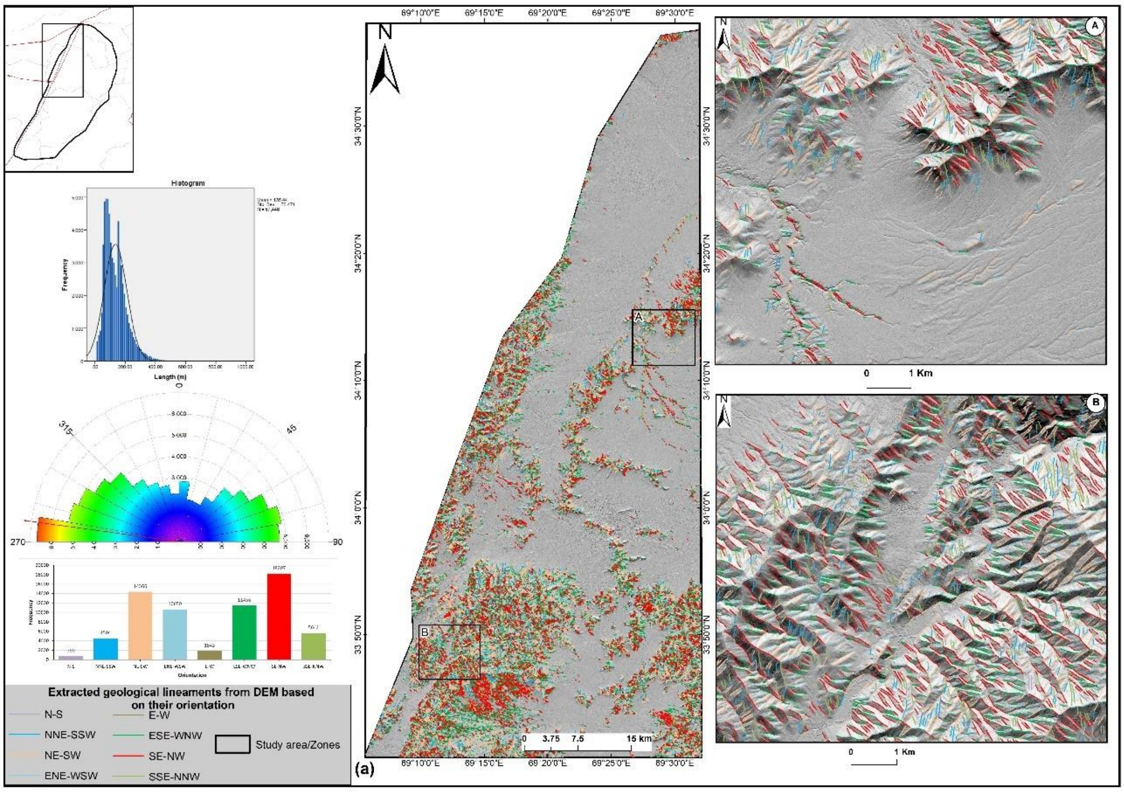

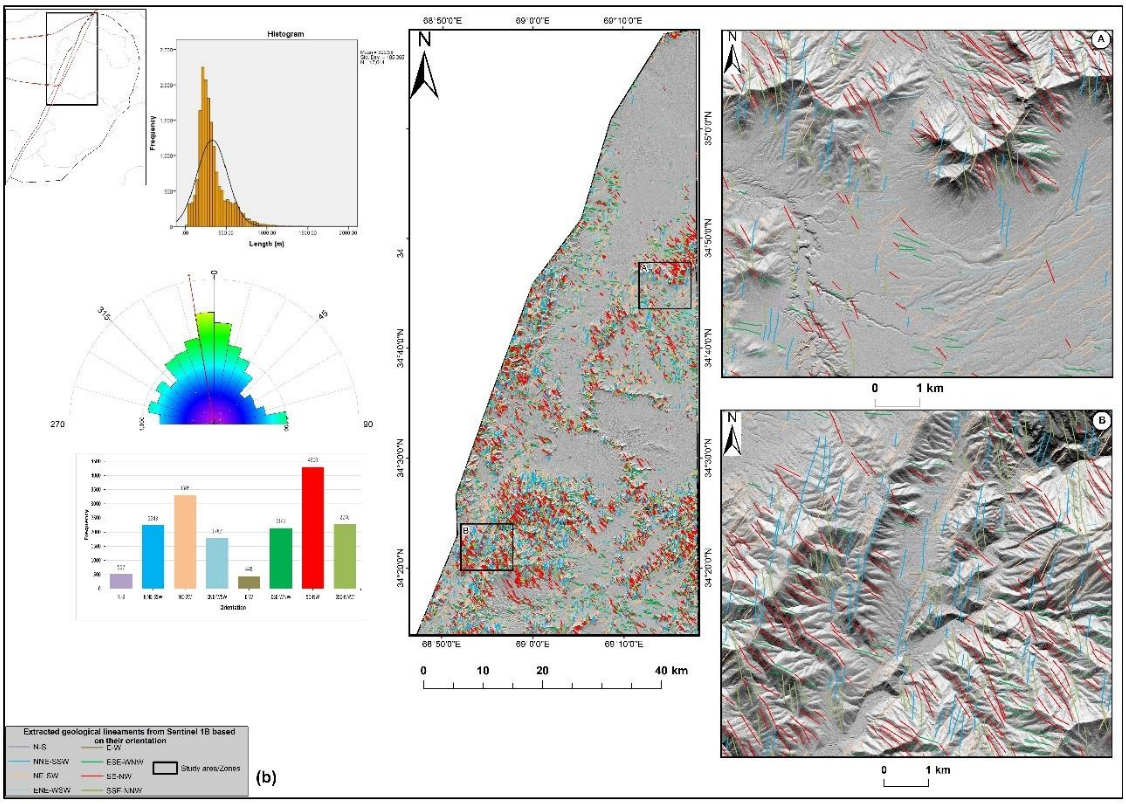

Figure 5.20. *Geospatial representation of the detected lineament patterns overlaid on a shaded relief map across Zone-IV, generated using a) DEM-5m and b) Sentinel-1B GRD.*

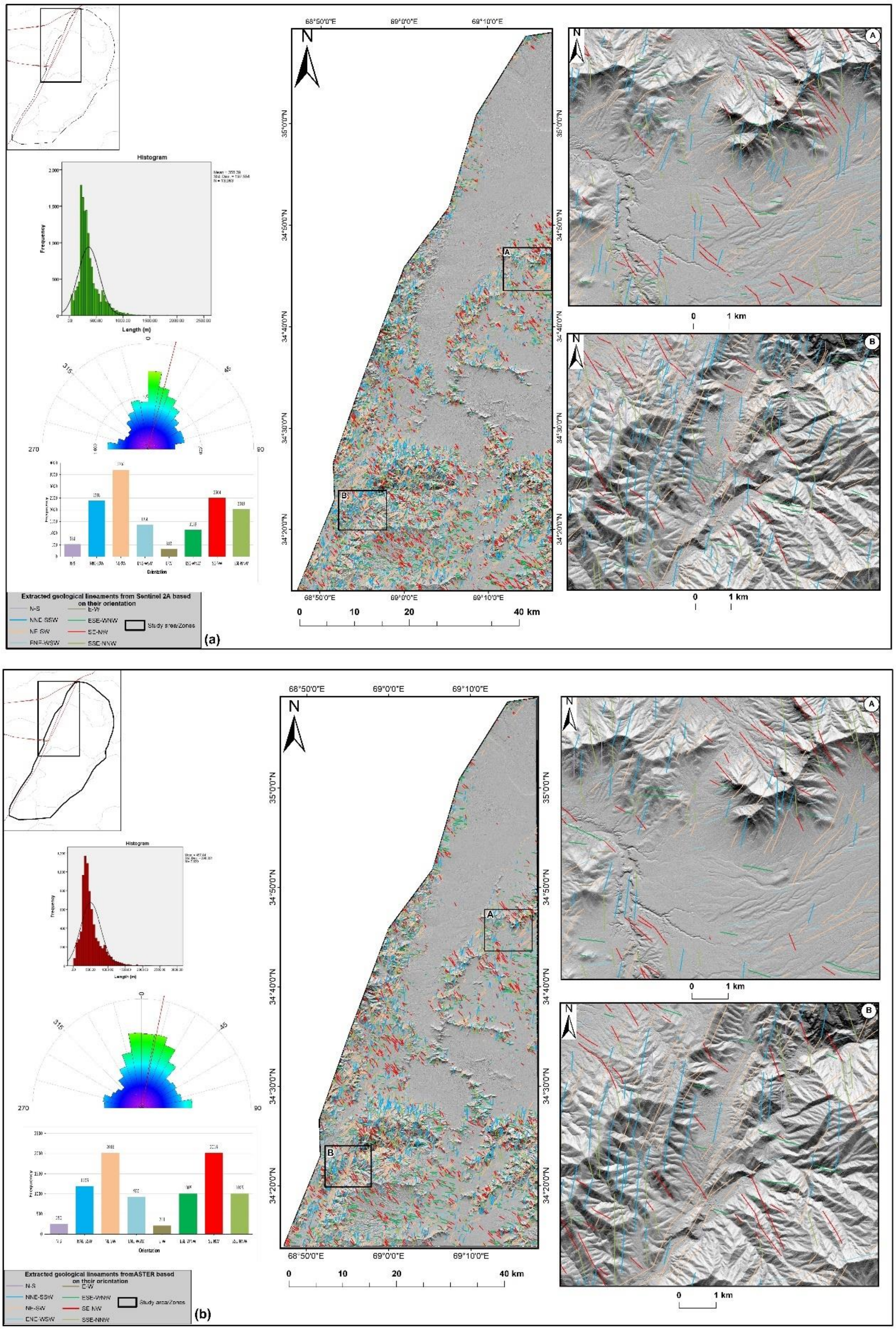

Figure 5.21. *Geospatial distribution of detected lineaments illustrated on shaded relief sourced from a) Sentinel-2A MSI and b) ASTER.*

5.3. Tempo-Spatial Evolution

Compared to the neighboring blocks, the Kabul Block is distinguished by its unique geological units, which range from Precambrian to Quaternary ages. These units include active fault zones and a wide range of solid mineral deposits. The different ages of the geological units in the study area can provide valuable insights into the geological ages of the lineaments that traverse them. However, the accuracy of the extracted lineaments and the scale of the geological map may affect the results. In this research, we used a compiled geological map of Afghanistan with a scale of 1:500,000 to analyze the tempo-spatial evolution of the lineaments. We also attempted to understand the frequency pattern of each age-related lineament (Figure 5.22).

Because the study area is extensive, the temporal evolution and the spatial distribution of lineaments were divided into four separate regions. Figure 5.22 depicts the identification of four primary groupings of lineament ages, which include the Proterozoic, Paleozoic, Mesozoic, and Cenozoic eras. Additionally, there were ten lesser groupings recognized, specifically the Proterozoic, Vendian-Cambrian, Ordovician, Silurian, Carboniferous, Permian, Triassic, Cretaceous, Paleogene, and Quaternary periods. As depicted in Figure 5.22a, within Zone-I, there is an elevated occurrence of extracted lineaments in the eastern and southern areas, primarily within Paleogene formations. In contrast, Proterozoic formations in the central and eastern portions display a lower number of observed lineaments. In our examination of Zone-II, it became evident that the predominant distribution of lineaments occurs within the eastern, southeastern, and southern regions, primarily within the Paleogene and Triassic formations. Conversely, there is a diminished presence of lineaments within the Vendian-Cambrian formations situated in the northwestern part of the zone, as illustrated in Figure 5.22b.

In Zone-III, we noticed a comparable temporal distribution trend, with a notable concentration of lineaments in the central and southern regions within Paleogene and Quaternary formations. In contrast, there were fewer lineaments identified within the Proterozoic formations (Figure 5.22c). Zone-IV exhibits diverse lithological units, including a greater representation of Proterozoic formations. Our examination reveals a concentration of lineaments from both the Cenozoic and Proterozoic periods in the southwestern, southern, and southeastern sections of this zone (Figure 5.22d).

Our thorough examination of the entire Kabul Block demonstrates that the bulk of identified lineaments are clustered within Cenozoic formations, which encompass

Paleogene and Quaternary periods. In contrast, there are relatively fewer lineaments observed within Proterozoic (early and middle Proterozoic, Vendian–Cambrian), Paleozoic (Ordovician, Carboniferous, and Permian), and Mesozoic (Triassic and Cretaceous) formations, showing moderate to low numbers. (Figure 5.22e).

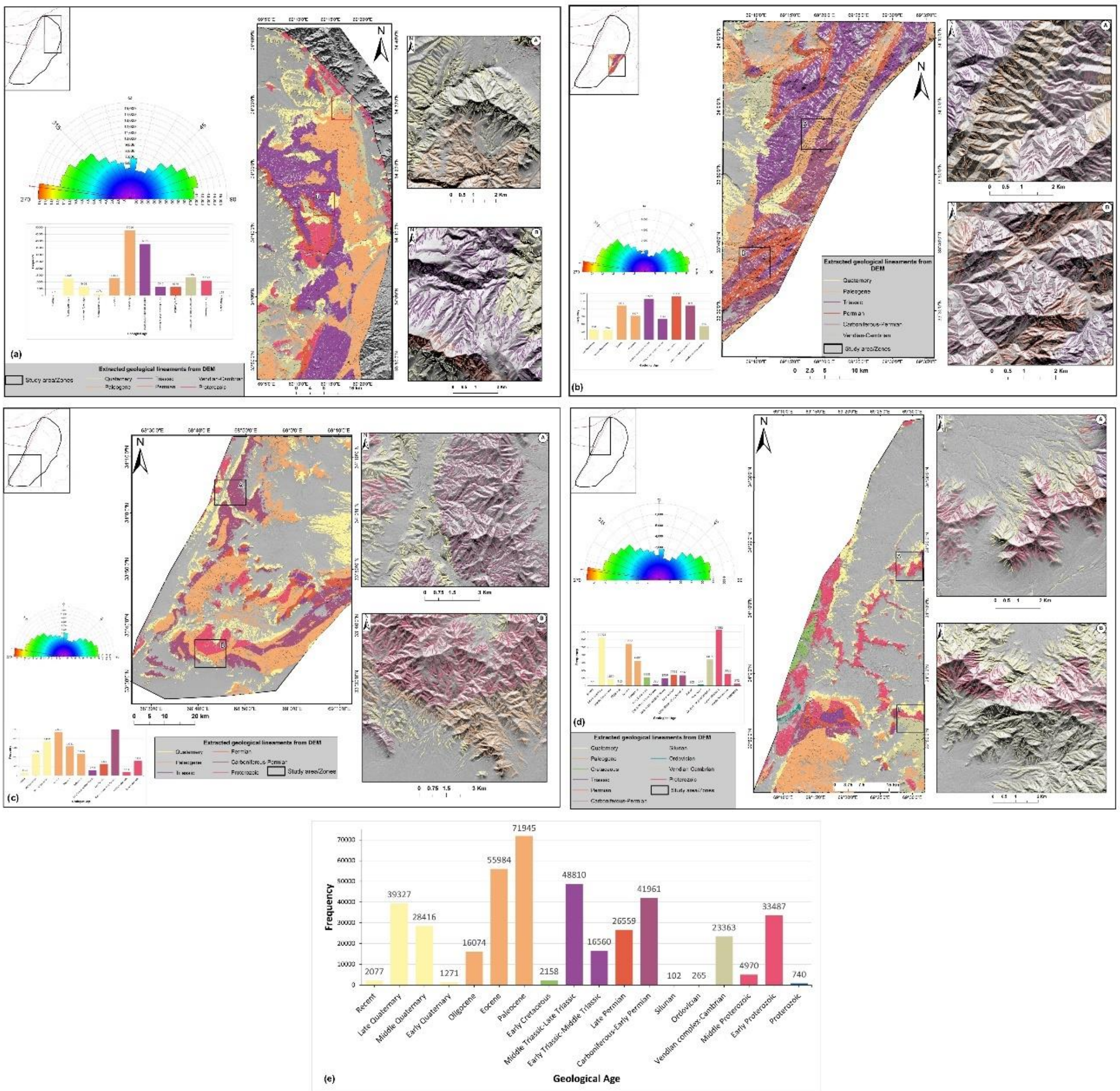

Figure 5.22. *Maps presenting the analysis of lineament trends in different zones, considering both time and space: (a) Zone-I, (b) Zone-II, (c) Zone-III, and (d) Zone-IV. Furthermore, (e) an overall statistical analysis of lineament trends across the entire study area.*

This finding provides important information about the geological evolution of the Kabul Block and has implications for future geological hazards and mineral exploration. The considerable presence of lineaments detected within Cenozoic formations implies that these geological strata might exhibit a heightened vulnerability to geological hazards like earthquakes and landslides. Such hazards could have substantial ramifications for the safety and welfare of the local population. Additionally, the concentration of lineaments in Cenozoic formations can also indicate the presence of solid mineral deposits, which can be of interest for mineral exploration. The relatively limited occurrence of lineaments in Proterozoic, Paleozoic, and Mesozoic formations indicates that these geological formations might offer comparatively lower potential for mineral exploration. Nevertheless, it's worth noting that they may still hold valuable resources.

In summary, our results underscore the significance of grasping the temporal and spatial arrangement of lineaments within the Kabul Block. This knowledge can offer valuable perspectives into the geological history of the area and serve as a foundation for making informed choices concerning geological hazards and the pursuit of mineral resources.

6. DISCUSSION

This research was designed to study the neotectonics of the Kabul Block and surrounding areas. Neotectonics is the study of recent tectonic activity, and the Kabul Block is a region in Afghanistan that is known for its active fault zones. The project used a developed modified approach on a range of geospatial data to gather as much information as possible about the tectonic activity in the region.

The data included high-resolution Google Earth Pro, ESRI base map imagery, shaded relief from DEM 5–30 m, Sentinel-1B GRD & 2A MSI, and ASTER. This data allowed the researcher to closely examine the primary bounding and adjacent fault zones. By doing so, we were able to accurately map and redefine the segments of active fault zones. We also measured stream deflections and offsets along these segments and detected geological lineaments to further refine their analysis.

The results of the study provide a comprehensive understanding of the tectonic activity in the Kabul Block and surrounding areas. We were able to redefine several active fault zones, related segments, neotectonics model, and geological lineaments. The study provides valuable information for future research on the neotectonics of the region.

6.1. Neotectonics

The neotectonics of the Kabul Block are attributed to the surrounding and adjacent active fault zones. These zones play a critical role in shaping the region, causing significant earthquakes, and hosting several hydrothermal alteration zones. Consequently, efforts have been made to accurately detect newly active fault segments and geological lineaments, and to finally present a neotectonics model for the Kabul Block. Novel remote sensing approaches have also been used to redefine the previously active faults. The morphotectonic features present in the study area were interpreted to develop our proposed model. By analyzing the data gathered through our research, we were able to develop a detailed and comprehensive understanding of the tectonic activity in the Kabul Block and surrounding regions. This information could be useful for future studies and help researchers better understand the geological processes in the area.

The location of the Kabul Block, which is bounded by two major fault zones—the Chaman Fault Zone (CFZ) including the Gardiz fault, and the Charikar Fault Zone (CKFZ)—as well as the Sarobi Fault Zone (SFZ), was a key consideration in our research. To gain a comprehensive understanding of the regional tectonic conditions of these faults and examine our hypothesis regarding the tectonic significance of the existing geomorphic expressions, we also took into account two other adjacent fault zones—the Konar Fault Zone (KFZ) and the Herat Fault Zone (HFZ) (as shown in Figures 5.1 and 6.1). By considering all of these fault zones together, we were able to gather a more complete picture of the tectonic activity in the region. We were also able to analyze the geomorphic expressions of the fault zones and gain insights into their tectonic meaning.

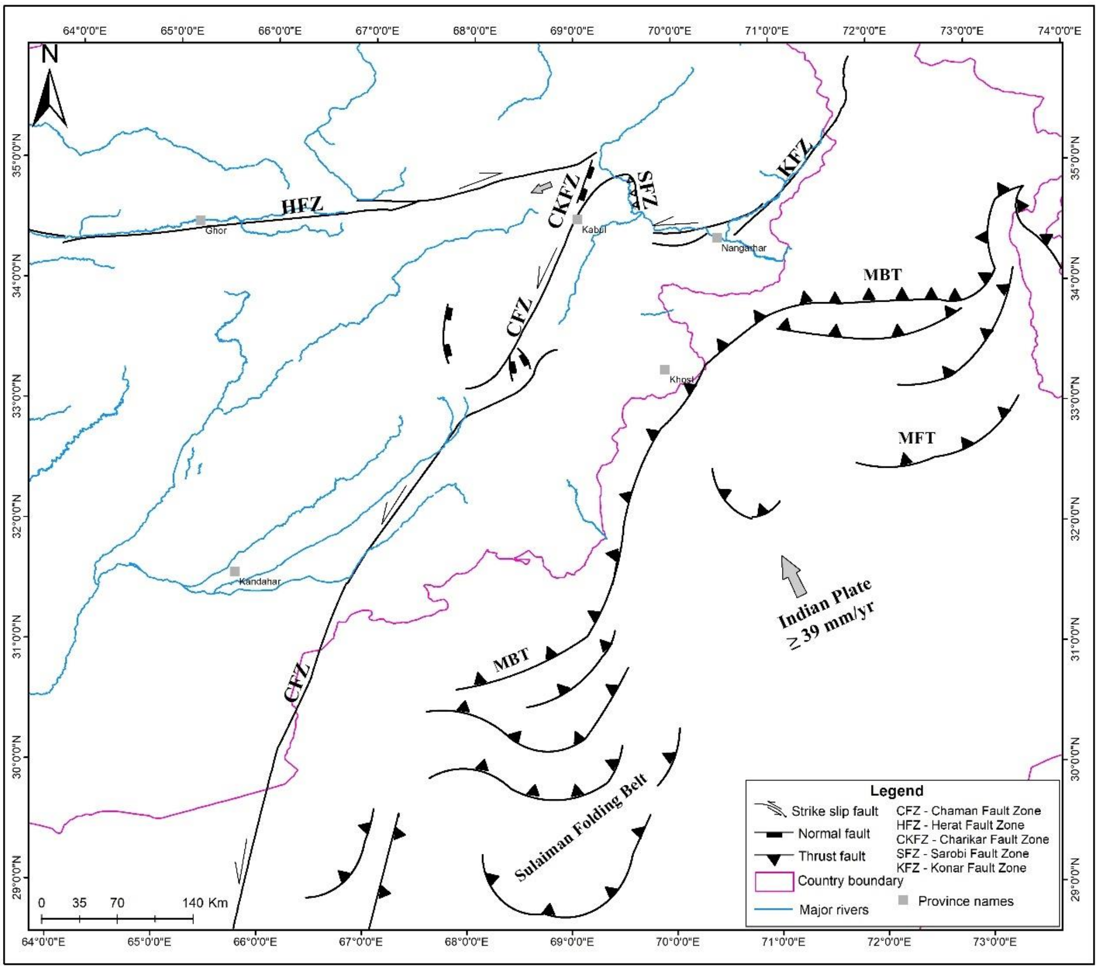

Figure 6.1. *Schematic map showing the bounding and adjacent faults of the Kabul Block, based on our proposed hypothesis. The illustration includes thrust fault lines adapted from Siehl (2017). MFT, Main Frontal Thrust; MBT, Main Boundary Thrust.*

The southern section of the Chaman Fault Zone (CFZ) in the Qarabagh, Giro, Deh Yak, Andar, Waghaz, and Wali Mohammad districts of Ghazni province has experienced a range of geological stresses. These stresses include left-lateral strike-slip motion, extension, and compression, which have contributed to the formation of a secondary fracture system, particularly synthetic fractures. The presence of these fractures in the region is significant and provides valuable insights into the geological processes at work. By studying the impact of the different stress regimes on the area, we can gain a better understanding of the complex geological activity in the region.

In this study, we measured the deflected river channels and compared the results with previous research. Our analysis revealed that we observed more deflected streams than in previous studies. Furthermore, while previous studies only focused on the northern and central sections of the Chaman Fault Zone (CFZ), we made an effort to cover the entire length of the fault zone. The analysis of the Chaman Fault Zone (CFZ) revealed river offsets ranging from 50 meters to 10 kilometers, which control major rivers for up to 35 kilometers. Notably, we observed an increasing trend in deflection from south to north. The fault traces within the areas of interest primarily cut through Eocene and middle Quaternary sediments. These findings suggest that the CFZ has played a significant role in the geological activity of the region, impacting the flow of major rivers and contributing to the development of the region's geology.

As shown in Figure 5.4, the trace of the Chaman Fault Zone (CFZ) declines with a trend of N40°E within the Mir Bacha Kot and Shakar Dara (Şeker Dere) districts. It extends eastward until it reaches the western part of the Koh Band district in Kapisa province, where the river networks intersect with the Sarobi fault trace. In the northwest corner of the Kabul Block, there are several possible normal faults that have developed, such as the Charikar Fault Zone (CKFZ), which was previously referred to as the Paghman Fault and considered a northern section of the CFZ. We propose that the development of these normal faults in the region is due to the fact that the northwest of the Kabul Block (Shomali Plain) is located within an escaping wedge between the left-lateral CFZ and the right-lateral Herat Fault Zone (HFZ) (see Figure 6.1).

The Sarobi Fault Zone (SFZ) is the eastern bounding fault of the Kabul Block. Earlier studies proposed that the fault exhibits left-lateral motion, while others suggested right-lateral motion, but no conclusive evidence was found. In our study, we hypothesize that the SFZ is characterized by thrust-type motion due to its location within a restraining stepover zone between the Chaman and Konar fault zones, both of which exhibit left-lateral strike-slip motion (see Figures 5.2 and 5.9).

Moreover, by examining high-resolution images, we identified and measured multiple right-lateral river channel offsets along the marked SFZ in the two areas of interest, as shown in Figures 5.2 and 5.9 and supplementary data. Our hypothesis is that the SFZ is a thrust fault zone due to its location and the trace of the fault surface on topography. Our measured local AF index, cross-sections, swath profiles perpendicular to the fault zone, and hypocenter locations all support this claim. The effect of thrust fault and uplifting is also evident in the calculated swath profiles, where the maximum and minimum elevation differentials along the fault line demonstrate the uplifting of the hanging wall of the thrust (see Figure 5.12).

By analyzing the topography of the area, we were able to calculate the strike and dip of the SFZ within two sections: the northern section strikes N24°W and dips 27°SW, while the southern section strikes N20°W and dips 23°SW. Utilizing radar and optical data for the automated detection of lineaments proves to be an efficient technique for identifying naturally occurring geological features throughout the Kabul Block. Nonetheless, a review conducted by Ahmadi and Pekkan in 2021 pointed out that relying solely on a single method for extracting geological structure-revealing lineaments might not yield satisfactory results. Hence, it is frequently recommended to employ a hybrid approach that integrates both automated and manual methods.

As emphasized in the pertinent literature, including works by Abdelouhed et al. (2022), Ghosh et al. (2021), and Andongma Wanduku Tende et al. (2022), identifying precise geological lineaments presents a formidable challenge, demanding a robust extraction method and expertise from proficient professionals. In comparison to previous studies, the current work is a comprehensive investigation that aims to identify the capabilities of algorithms and data in demarcating geological lineaments consistent with the field's geology and tectonics. This study aimed to validate geological lineaments using various methodologies. One approach involved an exclusion process to eliminate artificial lineaments, while another involved comparing the findings with existing tectonic and geologic maps. Additionally, manual identification of active fault zone segments was conducted to gain insights into the tectonic conditions associated with these lineaments. These combined efforts enabled a comprehensive interpretation of the tectonic characteristics of the studied lineaments within the Kabul Block. It is important to note that this study's outputs represent the first extensive investigation into the distribution, configuration, and temporal evolution of lineaments within this particular region. In contrast, previous studies conducted by (Peter G. Chirico, 2012; Rustami et al., 2017) employed limited methodologies and validation procedures for extracting lineaments in other parts of Afghanistan.

Although this research offers valuable perspectives on lineament detection, future studies can enhance these insights by incorporating a wider array of data sources and employing supplementary validation methods. Incorporating machine learning algorithms and other artificial intelligence methods holds promise for improving the precision and effectiveness of lineament detection.

In this research, we employed the Riedel shear tectonic model, which incorporates both left and right-lateral components, and adapted it based on the modifications proposed by Wilcox et al. in 1973 to estimate the stress field. This was achieved through an examination of the spatial configuration of the identified lineaments, which was conducted in accordance with the redefined active fault zones. The study's model explored the connection between significant left-lateral fault zones and lineaments in six specific regions of interest, taking into account different fracture types, including Synthetic Fractures (R), Antithetic Fractures (R'), Secondary Synthetic Fractures (P), and Secondary Antithetic Fractures (X).

Considering the predominant orientation of the primary Chaman Fault Zone, which extends in a NE-SW direction, the research findings indicate that lineaments aligned in a NNE-SSW direction corresponded to R-shear fractures, those approximately following an NNW-SSE trend were indicative of right-lateral R'-fractures, and lineaments trending ENE-WSW and WNW-ESE were identified as X and P fractures, respectively (refer to Figure 6.2).

The prevailing stress configuration within the Kabul Block is distinguished by a primary compressive axis (σ1) aligned in a NNW-SSE direction in the western and southwestern areas, while it takes an NE-SW orientation in the northern regions (see Figure 6.2). The primary extensional stress (σ3) predominantly follows an ENE-WSW direction in the western and southwestern areas, while it aligns NW-SE in the northern regions (refer to Figure Riedel). The left-lateral strike-slip faults, which are situated on both sides of the Kabul Block, exert significant influence. The main Chaman Fault zone impacts the western boundary, whereas the eastern boundary, specifically the northeastern section along the Sarobi Fault Zone, falls within a transitional area between the Chaman and Konar Fault zones. Hence, the stress distribution responsible for shaping the Chaman and Konar fault zones experiences a slight rotation in this particular region. This rotation is corroborated by the Reidel shear model, as illustrated in Figure 6.2, where there is alignment between X and R' fractures with the orientation of the Sarobi Fault Zone, and R and P fractures correspond to the primary left-lateral fault zones.

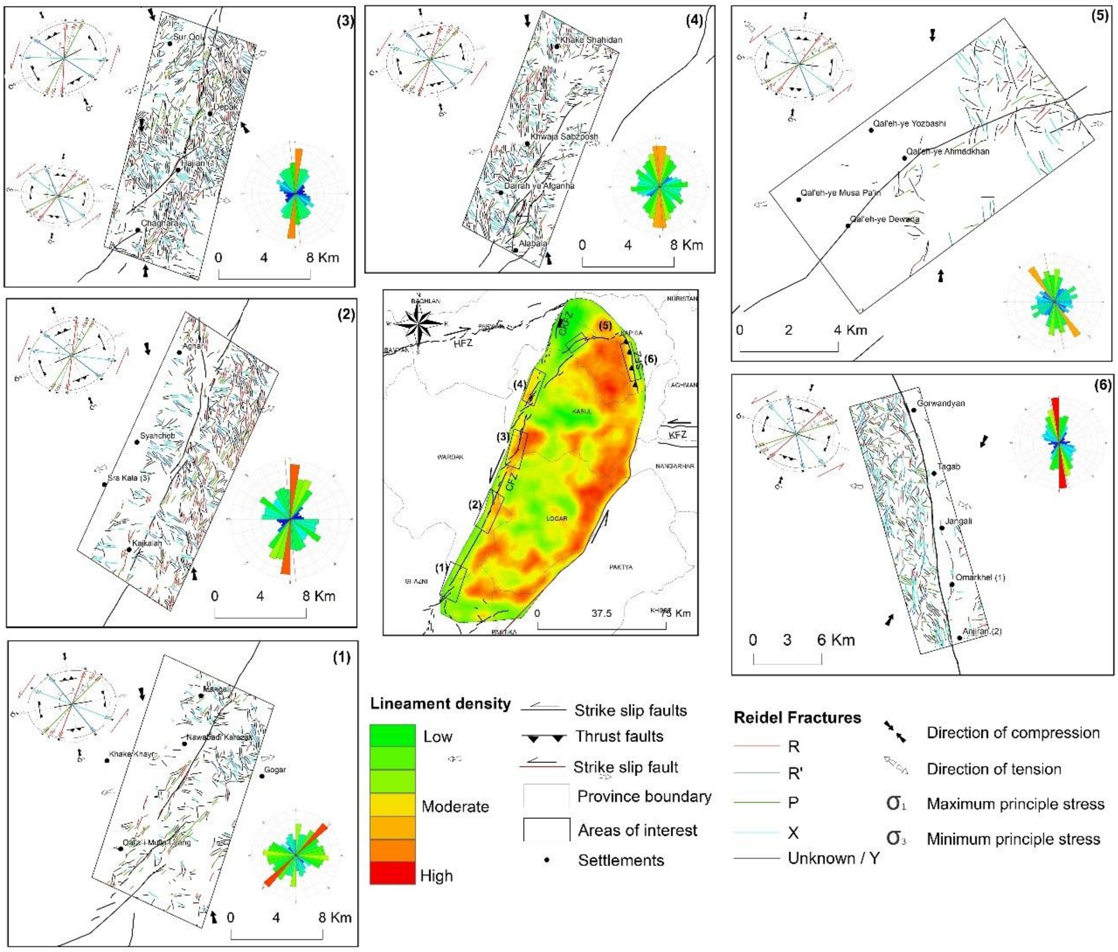

Figure 6.2. *Thematic map demonstrates how the strain ellipse and Riedel shear mechanism model can be applied for the interpretation of various fault types within the Kabul Block. The main synthetic and antithetic Riedel shears are labeled as R and P, respectively. The secondary synthetic and antithetic Riedel shears are labeled as X and R', respectively.*

6.2. Seismic activity

The Kabul Block and its surrounding regions are located in a seismically active region, with a long history of earthquakes. These earthquakes have ranged in magnitude from moderate to large, and have had significant consequences, particularly in urban areas. High-magnitude earthquakes have resulted in substantial casualties and widespread destruction. The Kabul Block and its surrounding regions have a long history of seismic activity, with a number of noteworthy earthquakes striking the area. The most notable earthquakes in the region include the 1505 Chaman earthquake (M = 7.3), the 1892 Kabul earthquake (M = 6.5), and the 1874 Kabul earthquake (M = 7.0). These earthquakes caused widespread devastation and loss of life, and their impact was felt throughout the region. The seismic energy released during these events had a profound impact on the surrounding landscape, and the aftershocks that followed caused significant damage to infrastructure. The affected communities were required to undertake extensive efforts to rebuild and recover.

The Alingar valley northeast of Kabul experienced a significant earthquake on February 19, 1842. The earthquake had a magnitude of 7.5, and it released a significant amount of seismic energy. This energy caused extensive damage and loss of life in the valley. The rugged terrain and the vulnerability of the local infrastructure exacerbated the impact of the earthquake, making the recovery process arduous and challenging. Seismic activity in the northwest of Quetta resulted in a magnitude 5.9 earthquake on March 16, 1978. This earthquake, although of a slightly lower magnitude than other earthquakes in the region, still had a notable impact. It caused destruction and loss of life in the affected area, and the communities in this region had to cope with the aftermath of the earthquake, including the task of rebuilding damaged structures and providing support to the affected population.

A series of earthquakes struck southwest of Khost on June 21, 2022. The earthquakes ranged in magnitude from 5.9 to 6.1, and although they were not as high in magnitude as some of the previously mentioned earthquakes, they still posed a significant threat to the surrounding communities. The shaking and ground motion caused by these earthquakes resulted in localized damage and increased the vulnerability of structures in the affected region.

The Chaman Fault Zone (CFZ) serves as a significant fault boundary delineating the western border of the convergence region between the Eurasian and Indian tectonic plates. The CFZ is known for its strong and shallow seismic activity, and has produced numerous significant and destructive earthquakes. One notable earthquake in the region occurred on July 6, 1505, and had a magnitude of 7.3. This earthquake was located in the western part of Kabul, and is well-documented by Quittmeyer and Jacob (1979). The 1505 earthquake is evidence of the long-standing seismic activity along the CFZ, and highlights the potential for future earthquakes in the region.

Another impactful earthquake occurred on December 20, 1892 ($M_w = 6.5$) near the Afghanistan-Pakistan border, northwest of Quetta. This event, documented by Quittmeyer and Jacob (1979) as well as Lawrence et al. (1992), resulted in a surface rupture spanning 60 kilometers and characterized by a left-lateral slip of 60-75 centimeters. The destructive power of this earthquake left a significant impact on the region, requiring substantial recovery efforts. In the same vicinity, the earthquake on March 16, 1978 (M = 5.9), caused 6 kilometers of ground rupture and reported a left-lateral offset of up to 4 centimeters. This earthquake, documented by Yeats et al. (1979), further illustrates the ongoing seismic activity along the CFZ and the potential for significant ground deformation in the region.

The Chaman Fault Zone (CFZ) is a seismically active area due to its location at the boundary between the Eurasian and Indian plates. The CFZ has a long history of earthquakes, including the 1505 Chaman earthquake (M = 7.3), the 1892 Quetta earthquake (M = 6.5), and the 1978 Quetta earthquake (M = 5.9). These earthquakes serve as important indicators of the region's seismicity and the potential risks associated with future earthquakes.

Understanding the behavior and characteristics of the CFZ is crucial for implementing effective mitigation measures and ensuring the safety and resilience of the communities in the affected areas. This includes developing seismic hazard maps, building codes, and emergency response plans. It is also important to educate the public about the risks of earthquakes and how to prepare for them.

In the Paghman district, situated north of Kabul city, a noteworthy earthquake occurred on October 18, 1874, with a magnitude of 7.0. This specific earthquake has been emphasized by (Boyd et al., 2007). Figure 6.3 provides a comprehensive visualization of all historically and instrumentally significant earthquakes with magnitudes greater than 4.0 in the Chaman Fault Zone (CFZ). Notably, an analysis of instrumentally recorded earthquakes within a 25-kilometer radius of the Gardiz fault, a branch of the CFZ, reveals that most of these earthquakes transpire at shallow depths. Consequently, the potential for causing severe casualties and damage is significantly amplified.

Additionally, the central and northern regions of the CFZ experienced a surface rupture due to a highly destructive earthquake that took place on February 19, 1842, in the Alingar Valley northeast of Kabul, with a magnitude of 7.5. This catastrophic earthquake, depicted in Figure Seismic, had a lasting impact on the area, underscoring the importance of comprehending the dynamics and potential hazards associated with the CFZ.

These observations emphasize the significance of considering both historical and instrumental seismic data in order to obtain a comprehensive understanding of the seismic activity in the region. Such data plays a crucial role in informing hazard assessments, preparedness efforts, and mitigation strategies, thereby ensuring the safety and resilience of communities residing in areas affected by the Chaman Fault Zone (CFZ) and its associated faults.

The study area benefits from the availability of limited fault plane solutions provided by reputable sources like the National Earthquake Information Center (NEIC) and the Global Centroid Moment Tensor Project (GCMTP). These solutions provide valuable insights into the seismic behavior within the region under investigation. Specifically, the analysis of earthquakes occurring prior to 2010, characterized by magnitudes greater than 5, along the central and southern sections of the CFZ, reveals a prevalent left-lateral strike-slip faulting mechanism. This evidence illuminates the kinematic characteristics of fault movements and contributes to our comprehensive understanding of the tectonic processes taking place within the CFZ.

The seismic activity along the Sarobi Fault Zone (SFZ) has been observed to be relatively low. Prevot et al. (1980) conducted an extensive analysis of seismic data obtained from 27 temporary stations, which were operational between 1977 and 1988, covering a period of 28 days. These stations were strategically positioned around Kabul, Charikar, and Jalalabad cities to assess the seismic activities associated with nearby faults. The recorded dataset comprised 341 earthquakes with magnitudes ranging from 1 to 4, with the majority of seismic events occurring in the western part of the SFZ. Based on their findings, the authors concluded that the collected data provided evidence supporting the presence of seismic activity in the region, with most of the recorded earthquake events being associated with the Chaman and Sarobi fault zones.

Based on their comprehensive analysis, Prevot et al. (1980) characterized the Sarobi Fault Zone (SFZ) as a well-defined fault with distinct topographical and seismic characteristics. The fault was determined to exhibit right-lateral motion, supported by the composite fault plane solution derived from the collected data. Additionally, the distribution of earthquake epicenters plotted in Figure 6.3 predominantly clusters along the western margin of the fault, providing further evidence for a west-dipping thrust surface.

In summary, the study conducted by Prevot et al. (1980) yields valuable insights into the seismic behavior of the Sarobi Fault Zone. The observed low seismic activity in the SFZ, coupled with its association with the Chaman and Sarobi fault zones, enhances our understanding of the tectonic processes and seismic hazards within the region.

A wide range of earthquakes, spanning from moderate to high magnitudes, has been reported within the Konar Fault Zone (KFZ), indicating the active nature of this fault zone. To visualize the seismic activity within the KFZ, earthquakes with magnitudes greater than 4 that occurred between 1900 and 2022 have been plotted and are illustrated in Figure 6.3.

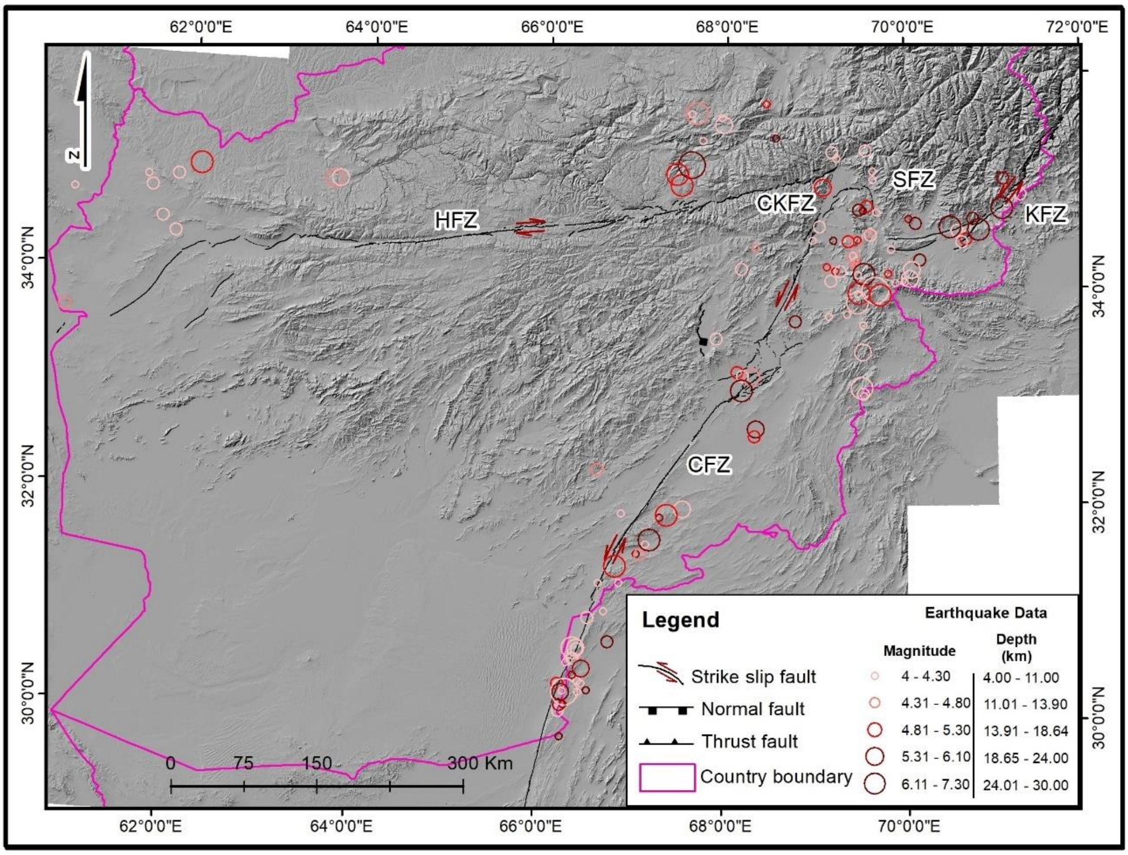

Figure 6.3. *A geographical representation indicating the spatial distribution of earthquakes that have occurred within the fault zones surrounding the Kabul Block. The earthquakes included in the plot have magnitudes exceeding 4 and depths ranging from 4 to 30 kilometers. The earthquake data utilized for this illustration is sourced from the USGS catalog, with references to Boyd et al. (2007) and Dewey (2006). The fault zones represented in the figure are identified by their abbreviations: CFZ (Chaman Fault Zone), CKFZ (Charikar Fault Zone), HFZ (Herat Fault Zone), SFZ (Sarobi Fault Zone), and KFZ (Konar Fault Zone). The time range covered by the earthquake occurrences in the figure spans from 734 to 2022.*

In comparison to other fault zones that bound the Kabul Block and its surroundings, such as the Herat Fault Zone (HFZ), the crustal seismicity within the HFZ is characterized by a lower frequency of occurrence. Analysis of the earthquakes plotted in Figure 6.3 reveals that all earthquakes within the HFZ are of moderate magnitudes and occur at shallow depths.

Based on the earthquake epicenters plotted in Figure 6.3 (with magnitudes equal to or greater than 4 and depths equal to or less than 30 km), it is observed that the Chaman Fault Zone (CFZ), Herat Fault Zone (HFZ), Charikar-Kabul Fault Zone (CKFZ), and Sarobi Fault Zone (SFZ) exhibit shallower seismic activity compared to the Konar Fault Zone (KFZ), as depicted in Figure 6.3.

This analysis highlights the distinct seismic characteristics of each fault zone, with the KFZ displaying a broader range of magnitudes and deeper seismic activity compared to the other fault zones surrounding the Kabul Block. Understanding these seismic characteristics is crucial for conducting comprehensive seismic hazard assessments and developing effective mitigation strategies in the region.

6.3. Validation

To validate the accuracy and reliability of the findings, we conducted a meticulous lineament density analysis across the entire Kabul Block. The goal of this analysis was to determine the spatial distribution and concentration of lineaments within the study area on a per-unit area basis. By quantifying the number of lineaments and their proximity to each other, the lineament density analysis aimed to shed light on the geological features and structural patterns present within the Kabul Block.

We created a classification map using a specialized Geographic Information System (GIS) environment to improve the comprehensibility and provide a visually appealing representation of the lineament density. This GIS-enabled map, referred to as Figure 6.4, was an essential tool for visualizing and interpreting the lineament density patterns observed within the Kabul Block.

The classification map, which was created using GIS technology, depicts the varying degrees of lineament density across the study area. The map uses a range of distinct categories or classes to differentiate between areas of high, moderate, and low lineament concentration. This classification system facilitates a more comprehensive understanding of the spatial distribution of lineaments, allowing researchers and stakeholders to identify any potential patterns, clusters, or trends in the Kabul Block's geological composition.

The scientifically rigorous analysis that led to the creation of the lineament density classification map not only validated the study but also provided a valuable tool for researchers, geologists, and decision-makers. This tool can be used to gain deeper insights into the structural characteristics and geological complexities of the Kabul Block. The use of GIS technology in this context highlights its significance as a powerful tool for spatial analysis. GIS allows for the visualization and interpretation of geospatial data in a meaningful and informative way.

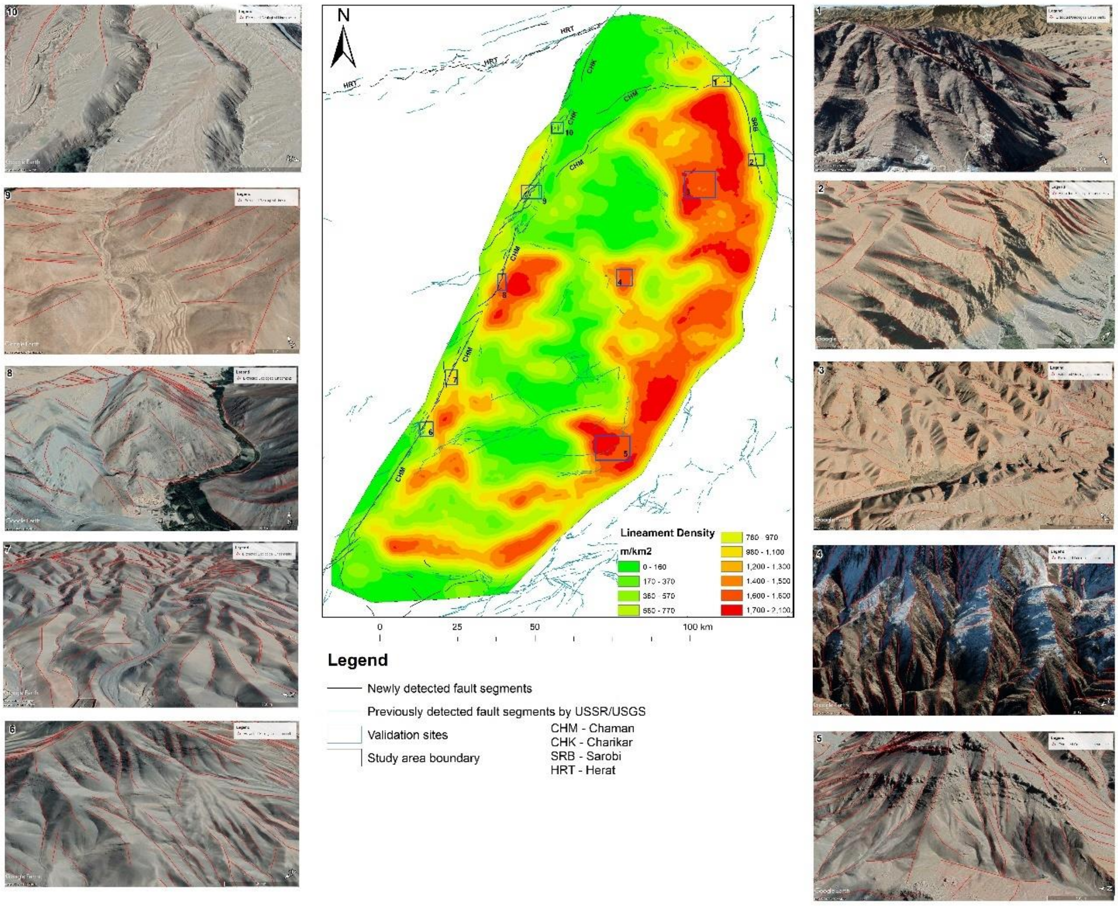

Figure 6.4. *Thematic map displays the dispersion and concentration of lineaments, in addition to segments of active faults. The black fault lines on the map are based on this research, while the light blue fault lines are modified from the studies by Wheeler et al. (2005) and Abdullah et al. (2008).*

Upon careful observation, a significant concentration of lineaments (indicating high density) is notably observed in the northeastern and eastern regions, particularly in Zones I and II. To confirm these results, we carried out a validation procedure by selecting ten random areas from both high and moderate density zones in a meticulous manner. This validation process entailed using high-spatial-resolution 3D imagery sourced from Google Earth Pro.

The results of this verification process, depicted in Figure 6.4, unequivocally demonstrate that the identified lineaments align with prominent features such as ridges, valleys, lithological unit boundaries, and stream channels. This alignment serves as a confirmation of the accurate identification and differentiation of lineaments within the study area. The presence of lineaments in these specific locations further strengthens the notion that they serve as meaningful geological indicators.

When merging the geological map of the Kabul Block with the lineament density map, it becomes evident that the most elevated lineament density values are predominantly linked to igneous rock formations. This suggests a significant correlation between the presence of lineaments and the underlying geology of the region. Furthermore, the gradual color variations observed in the density map, representing the transitions between high, moderate, and low densities, provide insights into the boundaries of lithological units and the presence of an active fault zone.

Overall, the findings derived from this analysis not only validate the accuracy of the lineament detection process but also provide valuable information about the geological characteristics and structural dynamics of the Kabul Block. The integration of remote sensing data, geological maps, and density analysis facilitates a comprehensive understanding of the spatial distribution and geological significance of lineaments within the study area.

7. CONCLUSIONS AND RECOMMENDATIONS

In light of the main objectives of this research, which encompass the determination of active fault zones using automatic and manual remote sensing and GIS approaches in the Kabul Block, along with the proposal of a new tectonic model, a diverse range of methodologies was employed. This involved the analysis of both radar and optical data, leading to the establishment of an integrated approach that facilitated the identification and characterization of active fault zones in the study area.

Through an extensive review of the existing literature on the determination of active faults and geological lineaments, it became evident that no singular method could reliably identify all active fault lines. Therefore, to enhance the accuracy and reliability of fault detection, this research employed a combination of automatic and manual approaches.

The primary focus of the study was twofold. Firstly, it sought to redefine the active fault zones and their associated segments within the Kabul Block and its surrounding regions, specifically the Chaman Fault Zone (CFZ), Sarobi Fault Zone (SFZ), Charikar Fault Zone (CKFZ), Konar Fault Zone (KFZ), and Herat Fault Zone (HFZ). This involved a meticulous examination of high-resolution imagery using manual techniques for active fault detection. By employing this manual approach, a total of 653 fault segments exhibiting various types of motion, including left and right-lateral motions, as well as normal/thrust types, were identified along the Chaman, Sarobi, Charikar, Konar, and Herat fault zones. This detailed delineation of fault segments within the study area contributes significantly to our understanding of the tectonic activity in the Kabul Block.

Secondly, this research aimed to propose a more accurate and suitable tectonic model for the Kabul Block. By combining the results from the fault segment analysis with the available geological and tectonic data, a comprehensive understanding of the tectonic processes and fault interactions in the region was achieved. This improved tectonic model provides valuable insights into the dynamics of the Kabul Block and its surrounding areas, aiding in the assessment of seismic hazards and the development of effective mitigation strategies.

The Chaman Fault Zone (CFZ), positioned as the western perimeter of the Kabul Block, exhibits a left-lateral strike-slip movement and functions as a demarcation line separating the Indian and Eurasian tectonic plates. The displacement observed along the mapped segments of the CFZ ranges from 50m to 10km, providing further evidence of the left-lateral motion of the fault. Moreover, the presence of well-developed regional drag folds and releasing stepover structures supports the interpretation of left-lateral movement along the fault.

While conducting the mapping and characterization task, a novel morphological manifestation of the CFZ was detected in the northern region of the Kabul Block, specifically to the south of Bagram Air Base. In this area, the fault trace bends in an ENE direction, coinciding with observed left-lateral displacement on the Panjsher River.

Moving towards the north and northwest of the CFZ, the Herat Fault Zone (HFZ) becomes prominent as a right-lateral strike-slip fault zone. The HFZ functions as a boundary between the comparably stable Eurasian plate to the north and the extensively altered landscape to the south. Following the characterization of the CFZ and HFZ, an escape wedge is formed between these two fault zones. This wedge is accommodated by the Charikar Normal Fault Zone (CKFZ), which likely plays a role in controlling the development of the Shomali Plain.

To the east of the Kabul Block, the Konar Fault Zone (KFZ) exhibits left-lateral motion, as evidenced by typical river displacement, releasing stepovers, and fault bending. The Sarobi Fault Zone (SFZ) serves as a boundary along the eastern edge of the Kabul Block, separating the left-lateral Konar and Chaman fault zones. This configuration results in the formation of a restraining stepover zone. Through morphotectonic examination and measurement, it was determined that recent uplift has occurred along the SFZ. This uplift provides further evidence of active tectonic processes within the region.

Geospatial analysis of past earthquake epicenters in a GIS environment revealed that the bounding active faults of the Kabul Block are characterized by shallow seismicity, with higher activity observed along the CFZ. This finding suggests that the CFZ is a particularly seismically active fault within the region.

Various radar and optical remote sensing data, such as DEM-5m, Sentinel-1GRD, Sentinel-2MSI, and ASTER, were utilized in combination with different filter and spatial algorithms to identify geological lineaments within the Kabul Block, alongside the active fault segments that were mapped. Through a thorough review of existing literature on automatic lineament detection, we determined the most effective filters for each data type: multi-illumination hill-shade into eight directions for DEM-5m, VV and VH polarization for Sentinel-1GRD, and directional filtering (7×7) into four main directions for Sentinel-2MSI and ASTER data.

To select the most accurate results, we conducted a unification process in a GIS environment and excluded artificial lineaments to focus on naturally occurring geological structures, particularly faults. Differentiating between natural and artificial lineaments solely based on optical data and automatic lineament detection algorithms proved to be a challenging task. Nonetheless, our study tackled this obstacle by integrating radar data and employing a holistic methodology, which encompassed the examination of illumination from various angles.

By manually excluding artifacts and conducting meticulous analysis, we successfully distinguished between geological lineaments and artificial linear structures within the study area. This process enabled us to effectively identify and characterize the geological lineaments present, contributing to a better understanding of the study area's geological features.

In sum, 414,069 lineaments spanning from 10 to 948.31 meters were identified utilizing DEM-5m data, whereas 86,438 lineaments ranging from 16.62 to 2469.91 meters were detected using Sentinel-1GRD data. Moreover, Sentinel-2MSI and ASTER data revealed the presence of 80,243 lineaments, with lengths spanning from 40 to 2436.47 meters, and 42,443 lineaments ranging from 0.46 to 3722.17 meters across the entire Kabul Block. Among the extracted lineaments, those identified through DEM-5m and Sentinel-1GRD data were chosen for additional scrutiny owing to their superior precision. Structural examination unveiled that the notable lineaments derived from DEM-5m consistently displayed NW-SE and NE-SW orientations, akin to the lineaments identified by Sentinel-1GRD and optical data. Additionally, there were less pronounced lineaments observed in the N-S and E-W directions.

The examination of the temporal evolution and spatial distribution of lineaments detected through DEM-5m data revealed that the significant geological features were predominantly located within the youthful sedimentary layers and strata from the Paleogene and Quaternary epochs. In contrast, formations from the Proterozoic, Paleozoic, and Mesozoic eras displayed a lower prevalence of lineaments across the entirety of the Kabul Block.

Density analysis revealed that the identified lineaments were concentrated in a denser arrangement in the eastern and southeastern regions of the Block, influenced by the presence of active regional structures and local fault zones. Through the combination of neotectonics and stress analysis of the geological lineaments alongside the identification of active fault lines, it was established that the primary compressive stress direction extends in a NNW-SSW orientation within the western regions of the Kabul Block. This direction shifts to NE-SW in the northern and southeastern portions.

The strong alignment observed between the geological lineaments detected by the automatic algorithms and the manually identified active fault zones and their associated segments highlights the robustness and accuracy of the established methodology. This alignment provides compelling evidence that automatic lineament detection techniques can effectively map geological structures in various geographic settings, including the complex terrain of the Kabul Block. The reliability and effectiveness of these techniques open up new possibilities for utilizing remote sensing and GIS in geosciences, offering valuable tools for geologists, geophysicists, and researchers working in similar regions.

By combining manual and automatic detection approaches, this study has made significant contributions to our scientific understanding of the geology, neotectonics, and seismicity of the Kabul Block and its surrounding regions. The detailed analysis of active fault zones, geological lineaments, and neotectonic studies has provided unprecedented insights into the geological processes shaping the region. These findings have the potential to inform future research endeavors and guide decision-making processes related to land use planning, hazard assessment, and resource exploration.

Moreover, the integrated results of active fault zones and geological lineaments offer substantial value in the exploration of mineral deposits within the Kabul Block. The identification and characterization of these geological structures provide crucial information for assessing the potential for mineral resources and understanding the geological controls on their distribution. This knowledge can facilitate targeted exploration efforts, optimize resource utilization, and contribute to the economic development of the region.

However, to further enhance our understanding of the complex geological dynamics in the Kabul Block, it is strongly recommended to undertake detailed fieldwork and geophysical surveys with a particular focus on areas exhibiting a high concentration of active fault lines and geological lineaments. The implementation of a seismic reflection approach in these regions can provide invaluable insights into the subsurface structures, deformation patterns, and fault architecture. Such investigations will not only advance our understanding of the region's geological evolution but also contribute to mineral exploration, seismic hazard assessment, infrastructure planning, and disaster mitigation strategies.

REFERENCES

Abdelouhed, F., Ahmed, A., Abdellah, A., & Mohammed, I. (2021). Lineament mapping in the Ikniouen area (Eastern Anti-Atlas, Morocco) using Landsat-8 Oli and SRTM data. *Remote Sensing Applications: Society and Environment*, *23*. https://doi.org/10.1016/j.rsase.2021.100606

Abdullah, S. H., Chmyriov, V. M., & Dronov., V. I. (2008). Geology and Mineral Resources of Afghanistan, 2 Volumes. In *British Geological Survey- Occasional Publication No. 15. (Reprint of the 1980 English translation of the 1977 Russian publication)*. British Geological Survey.

Abrams, M. J., Blusson, A., Carrere, V., Nguyen, P. T., & Rabu, Y. (1985). IMAGE PROCESSING APPLICATIONS FOR GEOLOGIC MAPPING. *IBM Journal of Research and Development*, *29*(2), 177–187. https://doi.org/10.1147/rd.292.0177

Adiri, Z., El Harti, A., Jellouli, A., Lhissou, R., Maacha, L., Azmi, M., Zouhair, M., & Bachaoui, E. M. (2017). Comparison of Landsat-8, ASTER and Sentinel 1 satellite remote sensing data in automatic lineaments extraction: A case study of Sidi Flah-Bouskour inlier, Moroccan Anti Atlas. *Advances in Space Research*, *60*(11), 2355–2367. https://doi.org/10.1016/j.asr.2017.09.006

Ahmadi, H., & Kalkan, K. (2021). Mapping of Ophiolitic Complex in Logar and Surrounding Areas (SE Afghanistan) With ASTER Data. *Journal of the Indian Society of Remote Sensing*. https://doi.org/10.1007/s12524-021-01319-4

Ahmadi, H., Kaya, O., Babadagi, E., Savas, T., & Pekkan, E. (2021). GIS – based groundwater potentiality mapping using AHP and FR models in central Antalya, Turkey. *Environ. Sci*, 8741. https://doi.org/10.3390/iecg2020-08741

Ahmadi, H., & Pekkan, E. (2021). Fault-Based Geological Lineaments Extraction Using Remote Sensing and GIS—A Review. *Geosciences*, *11*(5), 183. https://doi.org/10.3390/geosciences11050183

Ahmadi, H., Pekkan, E., & Seyitoğlu, G. (2022). Neotectonics of Kabul Block (SE Afghanistan) and surroundings: A new approach based on remote sensing data. *Tectonophysics*, *Under reiv*.

Ahmadi, H., & Uygucgil, H. (2021). Targeting iron prospective within the Kabul Block (SE Afghanistan) via hydrothermal alteration mapping using remote sensing techniques. *Arabian Journal of Geosciences*, *14*(3). https://doi.org/10.1007/s12517-020-06430-3

Akanji, A. O., Sanuade, O. A., Osinowo, O. O., & Okafor, O. (2020). Interpretation of high resolution aeromagnetic data for hydrocarbon exploration in Bornu Basin, Northeastern, Nigeria. *Annals of Geophysics*, *63*(2), 1–15. https://doi.org/10.4401/AG-8064

Akram, M. S., Mirza, K., Zeeshan, M., & Ali, I. (2019). Correlation of Tectonics with Geologic Lineaments Interpreted from Remote Sensing Data for Kandiah Valley, Khyber-Pakhtunkhwa, Pakistan. *Journal of the Geological Society of India*, *93*(5), 607–613. https://doi.org/10.1007/s12594-019-1224-7

Ali, A., & Pour, A. (2014). Lithological mapping and hydrothermal alteration using Landsat 8 data: a case study in ariab mining district, red sea hills, Sudan. *International Journal of Basic and Applied Sciences*, *3*(3). https://doi.org/10.14419/ijbas.v3i3.2821

Ambraseys, N., & Bilham, R. (2003). Earthquakes in Afghanistan. *Seismological Research Letters*, *74*(2), 107–123. https://pubs.geoscienceworld.org/ssa/srl/article/74/2/107/142840

Aslam, B., & Naseer, F. (2020). A statistical analysis of the spatial existence of earthquakes in Balochistan: clusters of seismicity. *Environmental Earth Sciences*, *79*(1). https://doi.org/10.1007/s12665-019-8790-2

Awoyemi, M. O., Falade, S. C., Arogundade, A. B., Hammed, O. S., Ajama, O. D., Falade, A. H., Adebiyi, L. S., Dopamu, K. O., & Alejolowo, E. A. (2022). Magnetically inferred regional heat flow and geological structures in parts of Chad Basin, Nigeria and their implications for geothermal and hydrocarbon prospects. *Journal of Petroleum Science and Engineering*, *213*, 110388. https://doi.org/10.1016/j.petrol.2022.110388

Ayoobi, A. W., Ahmadi, H., Inceoglu, M., & Pekkan, E. (2021). Seasonal impacts of buildings' energy consumption on the variation and spatial distribution of air pollutant over Kabul City: application of Sentinel—5P TROPOMI products. *Air Quality, Atmosphere and Health*. https://doi.org/10.1007/s11869-021-01085-9

Ayten KOÇ. (2005). *REMOTE SENSING STUDY OF SÜRGÜ FAULT ZONE (MALATYA, TURKEY)*. Middle East Technical University, M.Sc. Thesis.

Azman, A. I., Talib, J. A., & Sokiman, M. S. (2020). The Integration of Remote Sensing Data for Lineament Mapping in the Semanggol Formation, Northwest Peninsular Malaysia. *IOP Conference Series: Earth and Environmental Science, 540*(1). https://doi.org/10.1088/1755-1315/540/1/012026

Barkah, A., & Daud, Y. (2021). Identification of Structural Geologyat the Tangkuban Parahu Geothermal Area, West Java Based on Remote Sensing and Gravity Data. *AIP Conference Proceedings*, *2320*(1), 040006. https://doi.org/10.1063/5.0038809

Barnhart, W. D. (2017). Fault creep rates of the Chaman fault (Afghanistan and Pakistan) inferred from InSAR. *Journal of Geophysical Research: Solid Earth*, *122*(1), 372–386. https://doi.org/10.1002/2016JB013656

Benaafi, M., Hariri, M., Abdullatif, O., Makkawi, M., & Al-Shaibani, A. (2017). Analysis of lineaments within the Wajid Group, SW Saudi Arabia, and their tectonic significance. *Arabian Journal of Geosciences*, *10*(5). https://doi.org/10.1007/s12517-017-2860-0

Benham, A. J., Kováč, P., Petterson, M. G., Rojkovic, I., Styles, M. T., Gunn, A. G., Mckervey, J. A., & Wasy, A. (2009). Chromite and PGE in the logar ophiolite complex, Afghanistan. *Transactions of the Institutions of Mining and Metallurgy,* *Section B: Applied Earth Science*, *118*(2), 45–58. https://doi.org/10.1179/174327509X434957

Beun, N., Border, P., & Carbonnel, J. (1979). Premi�res donn�es quantitative relatives au coulissage du d�crochement de Chaman (Afghanistan du sud-est). *C. R. Acad. Sci. Paris*, *288*, 931–934. https://pascal-francis.inist.fr/vibad/index.php?action=getRecordDetail&idt=PASCALGEODEBRGM7920342222

Bohannon, R. G. (2010). Geologic and Topographic Maps of the Kabul North 30 ’ × 60 ’ Quadrangle, Afghanistan. *U.S. Geological Survey Scientific Investigations Map 3120*, *188*, 34. https://pubs.er.usgs.gov/publication/sim3120

Boyd, O. S., Mueller, C. S., & Rukstales, K. S. (2007). Preliminary Earthquake Hazard Map of Afghanistan. *U.S. Geological Survey (U.S.) Open-File Report*, *2007-1137*, 1–25. http://www.usgs.gov/pubprod

Burdick, R. G., & Speirer, R. A. (1980). Development of a method to detect geologic faults and other linear features from Landsat images. Report of investigations 1980 (Wyoming). *Google Book*. https://books.google.com/books?hl=en&lr=&id=bK_MGIQdFUEC&oi=fnd&pg=PA1&dq=Development+of+a+method+to+detect+geologic+faults+and+other+linear+features+from+Landsat+images&ots=bDXB8Tt-sD&sig=DqvJ5v0AJ7E-V3PZw9JjwGe17BA

Caltech/JPL. (2004). *SWIR - ASTER User Advisory*. SWIR - ASTER User Advisory. https://asterweb.jpl.nasa.gov/swir-alert.asp

Campbell, J. B. (1996). Introduction to remote sensing. In *Taylor and Francis Ltd., London*.

Chaabouni, R., Bouaziz, S., Peresson, H., & Wolfgang, J. (2012). Lineament analysis of South Jenein Area (Southern Tunisia) using remote sensing data and geographic information system. *Egyptian Journal of Remote Sensing and Space Science*, *15*(2), 197–206. https://doi.org/10.1016/j.ejrs.2012.11.001

Copernicus. (2022a). *ESA - Data products*. Copernicus. https://www.esa.int/Applications/Observing_the_Earth/Copernicus/Sentinel-1/Data_products

Copernicus. (2022b). *Sentinel-1 - Overview - Sentinel Online - Sentinel Online*. Copernicus. https://sentinels.copernicus.eu/web/sentinel/missions/sentinel-1/overview

Davis, L. S. (1975). A survey of edge detection techniques. *Computer Graphics and Image Processing*, *4*(3), 248–270. https://doi.org/10.1016/0146-664x(75)90012-x

Elliott, J. R., Biggs, J., Parsons, B., & Wright, T. J. (2008). InSAR slip rate determination on the Altyn Tagh Fault, northern Tibet, in the presence of topographically correlated atmospheric delays. *Geophysical Research Letters*, *35*(12). https://doi.org/10.1029/2008GL033659

Epuh, E. E., Okolie, C. J., Daramola, O. E., Ogunlade, F. S., Oyatayo, F. J., Akinnusi, S. A., & Emmanuel, E. O. I. (2020). An integrated lineament extraction from satellite imagery and gravity anomaly maps for groundwater exploration in the Gongola Basin. *Remote Sensing Applications: Society and Environment*, *20*, 100346. https://doi.org/10.1016/j.rsase.2020.100346

Farah, A., Algouti, A., Algouti, A., El Badaoui, K., Errami, M., & Ifkirne, M. (2021). Lithological mapping and automatic lineament extraction using Aster and Gdem data in the Imini-Ounilla-Asfalou district, South High Atlas of Marrakech, Morocco. *E3S Web of Conferences*, *240*. https://doi.org/10.1051/e3sconf/202124004002

Farahbakhsh, E., Chandra, R., Olierook, H. K. H., Scalzo, R., Clark, C., Reddy, S. M., & Müller, R. D. (2020). Computer vision-based framework for extracting tectonic lineaments from optical remote sensing data. *International Journal of Remote Sensing*, *41*(5), 1760–1787. https://doi.org/10.1080/01431161.2019.1674462

Farrand, W. R. (2006). Isobase. In *Geomorphology* (pp. 576–577). Springer, Berlin, Heidelberg. https://doi.org/10.1007/3-540-31060-6_196

Faryad, S. W., Collett, S., Finger, F., Sergeev, S. A., Čopjaková, R., & Siman, P. (2016). The Kabul Block (Afghanistan), a segment of the Columbia Supercontinent, with a Neoproterozoic metamorphic overprint. *Gondwana Research*, *34*, 221–240. https://doi.org/10.1016/j.gr.2015.02.019

Filosofov, V. P. (1960). Brief guide to morphometric methods in search of tectonic structures, Saratov. *Saratov Univ. Publ. House.*

Fischer Jochen. (1971). *Zur Geologie des Kohe Safi bei Kabul (Afghanistan)*.

Furuya, M., & Satyabala, S. P. (2008). Slow earthquake in Afghanistan detected by InSAR. *Geophysical Research Letters*, *35*(6). https://doi.org/10.1029/2007GL033049

Gabriel, A. K., Richard M. Goldstein, & Howard A. Zebker. (1990). Method for detecting surface motions and mapping small terrestrial or planetary surface deformations with synthetic aperture radar. *U.S. Patent*. https://patents.google.com/patent/US4975704A/en

Gloaguen, R., Marpu, P. R., & Niemeyer, I. (2007). Automatic extraction of faults and fractal analysis from remote sensing data. *Nonlinear Processes in Geophysics*, *14*(2), 131–138. https://doi.org/10.5194/npg-14-131-2007

Griesbach, C. L. (1893). Notes on the earthquake in Baluchistan on the 20th December 1892. *Records of the Geological Survey of India*, *26*(2), 57–61. https://scholar.google.com/scholar?hl=en&as_sdt=0%2C5&q=Notes+on+the+earthquake+in+Baluchistan+on+the+20th+December+1892&btnG=

Grohmann, C. H., Riccomini, C., & Chamani, M. A. C. (2011). Regional scale analysis of landform configuration with base-level (isobase) maps. *Hydrology and Earth System Sciences*, *15*(5), 1493–1504. https://doi.org/10.5194/hess-15-1493-2011

Guha, A., & Vinod Kumar, K. (2016). New ASTER derived thermal indices to delineate mineralogy of different granitoids of an Archaean Craton and analysis of their potentials with reference to Ninomiya's indices for delineating quartz and mafic minerals of granitoids-An analysis in Dharwar Cr. *Ore Geology Reviews*, *74*, 76–87. https://doi.org/10.1016/j.oregeorev.2015.10.033

Han, L., Liu, Z., Ning, Y., & Zhao, Z. (2018). Extraction and analysis of geological lineaments combining a DEM and remote sensing images from the northern Baoji loess area. *Advances in Space Research*, *62*(9), 2480–2493. https://doi.org/10.1016/j.asr.2018.07.030

Hancock, P. L. (1994). Continental deformation. *Choice Reviews Online*, *32*(01), 32-0317-32–0317. https://doi.org/10.5860/choice.32-0317

Hobbs, W. H. (1904). Lineaments of the Atlantic Border region. *Bulletin of the Geological Society of America*, *15*, 483–506. https://doi.org/10.1130/GSAB-15-483

Hung, L., Batelaan, O., & Smedt, D. F. (2005). Lineament extraction and analysis, comparison of LANDSAT ETM and ASTER imagery. Case study: Suoimuoi tropical karst catchment, Vietnam. *In Proceedings-SPIE The International Society for Optical Engineering (Vol. 5983, P. 59830t)*. https://doi.org/10.1117/12.627699

Jaiswara, N. K., Kotluri, S. K., Pandey, P., & Pandey, A. K. (2020). MATLAB functions for extracting hypsometry, stream-length gradient index, steepness index, chi gradient of channel and swath profiles from digital elevation model (DEM) and other spatial data for landscape characterisation. *Applied Computing and Geosciences*, *7*, 100033. https://doi.org/10.1016/j.acags.2020.100033

Jay, C. N., Flesch, L. M., & Bendick, R. O. (2017). Kinematics and dynamics of the Pamir, Central Asia: Quantifying surface deformation and force balance in an intracontinental subduction zone. *Journal of Geophysical Research: Solid Earth*, *122*(6), 4741–4762. https://doi.org/10.1002/2017JB014177

Jensen, J. R. (2015). Introductory digital image processing: a remote sensing perspective. Second edition. In *Introductory digital image processing: a remote sensing perspective. Second edition* (4th Editio).

Joel, P. K., Louise-Clotilde, O. A. M., Evariste, N., Nfor, N., Malquaire, K. P. R., & Philippe, N. N. (2022). Identification of Geothermal Reservoirs in South Cameroon from a Combined Landsat 8 and AMT Data. *International Journal of Geophysics*, *2022*. https://doi.org/10.1155/2022/1324766

Joshi, A. K. (1989). Automatic detection of lineaments from Landsat data. *Digest - International Geoscience and Remote Sensing Symposium (IGARSS)*, *1*, 85–88. https://doi.org/10.1109/igarss.1989.567160

Karapetov, S., Sorokin, Y., Sytov, Y., Report, V. C.-U., Afghan, U., & 1981, U. (1981). *Geological structure of Kabul town region (Report of Logar and Helmand prospecting-mapping group in 1979–1981).*

Keller, E. A., & Pinter, N. (1996). *Active tectonics*. Upper Saddle River, NJ: Prentice Hall.

Khalifa, A. (2018). *Morphotectonic analysis of the east Anatolian fault zone (e. Turkey) using remote sensing techniques*. Istanbul Technical University.

Khan, I. H., & Clyde, W. C. (2013). Lower paleogene tectonostratigraphy of Balochistan: Evidence for time-transgressive late paleocene-early eocene uplift. *Geosciences (Switzerland)*, *3*(3), 466–501. https://doi.org/10.3390/geosciences3030466

Khan, M. J., Ali, M., Xu, M., & Khan, M. (2020). Seismicity analysis of selected faults in Makran Southern Pakistan. *Acta Geophysica*, *68*(4), 965–978. https://doi.org/10.1007/s11600-020-00447-8

Koike, K., Nagano, S., & Ohmi, M. (1995). Lineament analysis of satellite images using a Segment Tracing Algorithm (STA). *Computers and Geosciences*, *21*(9), 1091–1104. https://doi.org/10.1016/0098-3004(95)00042-7

Kowalik, W., & Gold, D. (1974). *The use of Landsat-1 imagery in mapping lineaments in Pennsylvania*. http://archives.datapages.com/data/uga/data/091/091001/236_ugs0910236.htm

Lahai, Y. A., Anderson, K. F. E., Jalloh, Y., Rogers, I., & Kamara, M. (2021). A comparative geological, tectonic and geomorphological assessment of the Charlotte, Regent and Madina landslides, Western area, Sierra Leone. *Geoenvironmental Disasters*, *8*(1), 1–17. https://doi.org/10.1186/s40677-021-00187-x

Lawrence, R., Khan, S. H., & Nakata, T. (1992). Chaman Fault, Pakistan-Afghanistan. *Ann. Tectonicae*, 196–223. https://pascal-francis.inist.fr/vibad/index.php?action=getRecordDetail&idt=6475690

Lee, T. H., & Moon, W. M. (2002). Lineament extraction from Landsat TM, JERS-1 SAR, and DEM for geological applications. *International Geoscience and Remote Sensing Symposium (IGARSS)*, *6*, 3276–3278. https://doi.org/10.1109/igarss.2002.1027154

Leven, E. J. (1997). Permian stratigraphy and fusulinida of Afghanistan with their paleogeographic and paleotectonic implications. *Special Paper of the Geological Society of America*. https://doi.org/10.1130/0-8137-2316-7.1

Mahmood, S. A., & Gloaguen, R. (2012). Appraisal of active tectonics in Hindu Kush: Insights from DEM derived geomorphic indices and drainage analysis. *Geoscience Frontiers*, *3*(4), 407–428. https://doi.org/10.1016/j.gsf.2011.12.002

Maleki, M., Niroomand, S., Farahbakhsh, E., Modabberi, S., & Tajeddin, H. A. (2021). Hydrothermal alteration and structural mapping of the Qolqoleh-Kasnazan shear zone in Iran using remote sensing data. *Arabian Journal of Geosciences*, *14*(16). https://doi.org/10.1007/s12517-021-07920-8

Mallick, J. (2021). Municipal solid waste landfill site selection based on fuzzy-ahp and geoinformation techniques in ASIR region Saudi Arabia. *Sustainability*

(Switzerland), *13*(3), 1–33. https://doi.org/10.3390/su13031538

Mallick, J., Singh, R. K., AlAwadh, M. A., Islam, S., Khan, R. A., & Qureshi, M. N. (2018). GIS-based landslide susceptibility evaluation using fuzzy-AHP multi-criteria decision-making techniques in the Abha Watershed, Saudi Arabia. *Environmental Earth Sciences*, *77*(7), 1–25. https://doi.org/10.1007/s12665-018-7451-1

Marghany, M., & Hashim, M. (2010). Lineament mapping using multispectral remote sensing satellite data. *International Journal of Physical Sciences*, *5*(10), 1501–1507. http://www.academicjournals.org/IJPS

Mashkoor, R., Ahmadi, H., Rahmani, A. B., & Pekkan, E. (2022). Detecting Li-Bearing Pegmatites Using Geospatial Technology: The Case of SW Konar Province, Eastern Afghanistan. *Geocarto International*, 1–19. https://doi.org/10.1080/10106049.2022.2086633

Masoud, A. A., & Koike, K. (2011). Auto-detection and integration of tectonically significant lineaments from SRTM DEM and remotely-sensed geophysical data. *ISPRS Journal of Photogrammetry and Remote Sensing*, *66*(6), 818–832. https://doi.org/10.1016/j.isprsjprs.2011.08.003

Masoud, A., & Koike, K. (2017). Applicability of computer-aided comprehensive tool (LINDA: LINeament Detection and Analysis) and shaded digital elevation model for characterizing and interpreting morphotectonic features from lineaments. *Computers and Geosciences*, *106*, 89–100. https://doi.org/10.1016/j.cageo.2017.06.006

Mavrantza, O., & Argialas, D. P. (2003). Implementation and evaluation of spatial filtering and edge detection techniques for lineament mapping: case study - Alevrada, Central Greece. *Remote Sensing for Environmental Monitoring, GIS Applications, and Geology II*, *4886*, 417. https://doi.org/10.1117/12.463275

McMahon, A. H. (1897). The Southern Borderlands of Afghanistan. *The Geographical Journal*. https://doi.org/10.2307/1774479

Merritts, D., & Vincent, K. R. (1989). Geomorphic response of coastal streams to low, intermediate, and high rates of uplift, Mendocino triple junction region, northern California. *Geological Society of America Bulletin*, *101*(11), 1373–1388. https://doi.org/10.1130/0016-7606(1989)101<1373:GROCST>2.3.CO;2

Mohadjer, S., Bendick, R., Ischuk, A., Kuzikov, S., Kostuk, A., Saydullaev, U., Lodi, S., Kakar, D. M., Wasy, A., Khan, M. A., Molnar, P., Bilham, R., & Zubovich, A. V. (2010). Partitioning of India-Eurasia convergence in the Pamir-Hindu Kush from GPS measurements. *Geophysical Research Letters*, *37*(4). https://doi.org/10.1029/2009GL041737

Msaddek, M. H., Moumni, Y., Chenini, I., & Dlala, M. (2019). Applicability of Developed Algorithm for Semi-automated Extraction and Morphotectonic Interpretation of Lineaments Using Remotely Sensed Data, Southwestern Tunisia. *Remote Sensing in Earth Systems Sciences*, *2*(4), 292–307.

https://doi.org/10.1007/s41976-019-00028-4

Ngoroyemoto, T. F. K. (2021). Evaluating the Implications of Lineaments on Petroleum Fields: South Sumatra, Indonesia. *Journal of Applied Geology*, *6*(2), 77. https://doi.org/10.22146/jag.58161

O'leary, D. W., Friedman, J. D., & Pohn, H. A. (1976). Lineament, linear, lineation: Some proposed new standards for old terms: Discussion. In *Bulletin of the Geological Society of America* (Vol. 89, Issue 1, pp. 1463–1469). https://doi.org/10.1130/0016-7606(1978)89<159a:LLLSPN>2.0.CO;2

Othman, A. A., Al-Maamar, A. F., Al-Manmi, D. A. M. A., Liesenberg, V., Hasan, S. E., Obaid, A. K., & Al-Quraishi, A. M. F. (2020). GIS-Based modeling for selection of dam sites in the Kurdistan Region, Iraq. *ISPRS International Journal of Geo-Information*, *9*(4), 244. https://doi.org/10.3390/ijgi9040244

Pérez-Peña, J. V., Al-Awabdeh, M., Azañón, J. M., Galve, J. P., Booth-Rea, G., & Notti, D. (2017). SwathProfiler and NProfiler: Two new ArcGIS Add-ins for the automatic extraction of swath and normalized river profiles. *Computers and Geosciences*, *104*, 135–150. https://doi.org/10.1016/j.cageo.2016.08.008

Perfetto, S., Wilder, J., & Walther, D. B. (2020). Effects of spatial frequency filtering choices on the perception of filtered images. *Vision (Switzerland)*, *4*(2). https://doi.org/10.3390/vision4020029

Peter G. Chirico, and B. E. H. S. G. P. S. S. K. (2012). Summaries of Important Areas for Mineral Investment and Production Opportunities of Nonfuel Minerals in Afghanistan. *Economic Geology*, *107*(7), 1515–1517. https://doi.org/10.2113/econgeo.107.7.1515-b

Podwysocki, M., Moik, J., & Shoup, W. (1975). Quantification of Geological Lineaments by Manual and Machine Processing Technique. *NASA Earth Resources Survey Symposium, Houston, Texas*, 885–903. https://books.google.com/books?hl=en&lr=&id=SY1WAAAAMAAJ&oi=fnd&pg=PA885&dq=Quantification+of+geologic+lineaments+by+manual+and+machine+processing+techniques&ots=0hjDYzDuEP&sig=X8VY4-ufGl3F_M31ZtuzdSnOPAM

Pour, A. B., & Hashim, M. (2015). Structural mapping using PALSAR data in the Central Gold Belt, Peninsular Malaysia. *Ore Geology Reviews*, *64*(1), 13–22. https://doi.org/10.1016/j.oregeorev.2014.06.011

Powell, J. W. (1875). *Exploration of the Colorado River of the West and its Tributaries*.

Pratt, W. (1991). *Digital image processing*. Elsevier.

Pratt, W. K. (2014). *Digital Image Processing* (4th Editio). Boca Raton: CRC Press.

Prevot, R., Hatzfeld, D., Roecker, S. W., & Molnar, P. (1980). Shallow earthquakes and active tectonics in eastern Afghanistan. *Journal of Geophysical Research*, *85*(B3), 1347–1357. https://doi.org/10.1029/JB085iB03p01347

Quittmeyer, R. C., & Jacob, K. H. (1979). Historical and modern seismicity of Pakistan, Afghanistan, northwestern India, and southeastern Iran. *Bulletin of the Seismological Society of America*, *69*(3), 773–823. https://pubs.geoscienceworld.org/ssa/bssa/article/69/3/773/117903

Rahnama, M., & Gloaguen, R. (2014). TecLines: A matlab-based toolbox for tectonic lineament analysis from satellite images and DEMs, part 1: Line segment detection and extraction. *Remote Sensing*, *6*(7), 5938–5958. https://doi.org/10.3390/rs6075938

Rawat, A., Banerjee, S., & Sundriyal, Y. (2021). Geomorphological and statistical assessment of tilt-Block tectonics in the garhwal synform: Implications for the active tectonics, garhwal lesser Himalaya, India. *Geosciences (Switzerland), 11*(8), 345. https://doi.org/10.3390/geosciences11080345

Revel Sella A. (2002). A model for recent plate velocities from space geodesy/GF... - Google Scholar. *Journal of Geophysical Research*, *107*. https://scholar.google.com/scholar?hl=en&as_sdt=0%2C5&q=A+model+for+recent+plate+velocities+from+space+geodesy%2FGF+Sella%2C+TH+Dixon%2C+A.+Mao&btnG=

Richards, J. A. (2013). Remote sensing digital image analysis: An introduction. In *Remote Sensing Digital Image Analysis: An Introduction* (Vol. 9783642300). https://doi.org/10.1007/978-3-642-30062-2

Rosenfeld, A. (1970). A Nonlinear Edge Detection Technique. *Proceedings of the IEEE, 58*(5), 814–816. https://doi.org/10.1109/PROC.1970.7756

Ruleman, C. a., Crone, a. J., Machette, M. N., Haller, K. M., & Rukstales, K. S. (2007). Map and Database of Probable and Possible Quaternary Faults in Afghanistan. *USGS Afghanistan Project Product No. 150, Open-File Report 2007-1103*.

Rustami, S., Saadi, N. M., Aboud, E., Yonezu, K., & Watanabe, K. (2017). Investigating Structural and Tectonic Evolution of Central Afghanistan Using Remote Sensing and Gravity Data. *Journal of Geology & Geophysics*, *06*(06). https://doi.org/10.4172/2381-8719.1000313

Sadiq, S., Muhammad, U., & Fuchs, M. (2022). Investigation of landslides with natural lineaments derived from integrated manual and automatic techniques applied on geospatial data. *Natural Hazards*, *110*(3), 2141–2162. https://doi.org/10.1007/s11069-021-05028-6

Saha, S. K. (2022). Remote Sensing and Geographic Information System Applications in Hydrocarbon Exploration: A Review. *Journal of the Indian Society of Remote Sensing*, 1–19. https://doi.org/10.1007/s12524-022-01540-9

Salvi, S. (1995). Analysis and interpretation of Landsat synthetic stereo pair for the detection of active fault zones in the Abruzzi region (Central Italy). *Remote Sensing of Environment, 53*(3), 153–163. https://doi.org/10.1016/0034-4257(94)00039-P

SARP, G. (2005). *LINEAMENT ANALYSIS FROM SATELLITE IMAGES, NORTH-*

WEST OF ANKARA. Middle East Technical University, M.Sc. Thesis.

Sborshchikov, I. M., Savostin, L. A., & Zonenshain, L. P. (1981). Present plate tectonics between Turkey and Tibet. *Tectonophysics*, *79*(1–2). https://doi.org/10.1016/0040-1951(81)90232-8

Scheiber, T., Fredin, O., Viola, G., Jarna, A., Gasser, D., & Łapinska-Viola, R. (2015). Manual extraction of bedrock lineaments from high-resolution LiDAR data: methodological bias and human perception . *Taylor & Francis*, *137*(4), 362–372. https://doi.org/10.1080/11035897.2015.1085434

Schreiber, A., Weippert, D., Wittekindt, H. P., & Wolfart, R. (1972). GEOLOGY AND PETROLEUM POTENTIALS OF CENTRAL AND SOUTH AFGHANISTAN. In *American Association of Petroleum Geologists Bulletin* (Vol. 56, Issue 8, pp. 1494–1519). https://doi.org/10.1306/819a40f6-16c5-11d7-8645000102c1865d

Seyitoğlu, G., Toori, M., Esat, K., & Kaypak, B. (2019). Tectonic significance of the thrust parallel- normal faulting in the northern Makran accretionary wedge of Iran and Pakistan. *72 Nd Geological Congress of Turkey Proceedings and Abstract Book*, 967–972.

Shah, S. T., Özacar, A. A., & Gülerce, Z. (2021). Fault-based probabilistic seismic hazard assessment of the eastern Makran subduction and the Chaman transform fault, Pakistan: Emphasis on the source characterization of megathrust. *Journal of Asian Earth Sciences*, *205*. https://doi.org/10.1016/j.jseaes.2020.104604

Shahzad, F., & Gloaguen, R. (2011). TecDEM: A MATLAB based toolbox for tectonic geomorphology, Part 2: Surface dynamics and basin analysis. *Computers and Geosciences*, *37*(2), 261–271. https://doi.org/10.1016/j.cageo.2010.06.009

Shareq, A. (1981). Geological observations and geophysical investigations carried out in Afghanistan over the period of 1972–1979. *Wiley Online Library*, 75–86. https://agupubs.onlinelibrary.wiley.com/doi/abs/10.1029/GD003p0075

Sheikhrahimi, A., Pour, A. B., Pradhan, B., & Zoheir, B. (2019). Mapping hydrothermal alteration zones and lineaments associated with orogenic gold mineralization using ASTER data: A case study from the Sanandaj-Sirjan Zone, Iran. *Advances in Space Research*, *63*(10), 3315–3332. https://doi.org/10.1016/j.asr.2019.01.035

Shirazi, A., Hezarkhani, A., & Pour, A. B. (2022). Fusion of Lineament Factor (LF) Map Analysis and Multifractal Technique for Massive Sulfide Copper Exploration: The Sahlabad Area, East Iran. *Minerals*, *12*(5), 549. https://doi.org/10.3390/MIN12050549

Shnizai, Z. (2020). Mapping of active and presumed active faults in Afghanistan by interpretation of 1-arcsecond SRTM anaglyph images. *Journal of Seismology*. https://doi.org/10.1007/s10950-020-09933-4

Shnizai, Z., Matsushi, Y., & Tsutsumi, H. (2020). Late Pleistocene slip rate of the Chaman fault based on 10Be exposure dating of offset geomorphic surfaces near Kabul, Afghanistan. *Tectonophysics*. https://doi.org/10.1016/j.tecto.2020.228593

Shroder, J. F., Eqrar, N., Waizy, H., Ahmadi, H., & Weihs, B. J. (2021). Review of the Geology of Afghanistan and its water resources. *International Geology Review*, 1–23. https://doi.org/10.1080/00206814.2021.1904297

Siehl, A. (2017). Structural setting and evolution of the Afghan orogenic segment - A review. In *Geological Society Special Publication* (Vol. 427, Issue 1, pp. 57–88). https://doi.org/10.1144/SP427.8

Sigtryggsdóttir, F. G., & Snæbjörnsson, J. T. (2019). Geological challenges and geohazard monitoring of a mega engineering hydropower project in Iceland. *Engineering Geology*, *259*. https://doi.org/10.1016/j.enggeo.2019.105152

Slama, T., Deffontaines, B., & Turki, M. M. (2015). Morphotectonic and Morphodynamic investigations revealed by isobase surfaces analysis and derived differential mapping using GIS, Teboursouk area, northern Tunisia. *Earth Science Informatics*, *8*(4), 759–773. https://doi.org/10.1007/s12145-015-0208-4

Soto-Pinto, C., Arellano-Baeza, A., & Sánchez, G. (2013). A new code for automatic detection and analysis of the lineament patterns for geophysical and geological purposes (ADALGEO). *Computers and Geosciences*. https://doi.org/10.1016/j.cageo.2013.03.019

Strahler, A. N. (1957). Quantitative analysis of watershed geomorphology. *Eos, Transactions American Geophysical Union*, *38*(6), 913–920. https://doi.org/10.1029/TR038i006p00913

Suzen, M. L., & Toprak, V. (1998). Filtering of satellite images in geological lineament analyses: An application to a fault zone in Central Turkey. *International Journal of Remote Sensing*, *19*(6), 1101–1114. https://doi.org/10.1080/014311698215621

Szeliga, W., Bilham, R., Kakar, D. M., & Lodi, S. H. (2012). Interseismic strain accumulation along the western boundary of the Indian subcontinent. *Journal of Geophysical Research: Solid Earth*, *117*(8). https://doi.org/10.1029/2011JB008822

Tagnon, B. O., Assoma, V. T., Mangoua, J. M. O., Douagui, A. G., Kouamé, F. K., & Savané, I. (2020). Contribution of SAR/RADARSAT-1 and ASAR/ENVISAT images to geological structural mapping and assessment of lineaments density in Divo-Oume area (Côte d'Ivoire). In *Egyptian Journal of Remote Sensing and Space Science* (Vol. 23, Issue 2, pp. 231–241). Elsevier. https://doi.org/10.1016/j.ejrs.2018.12.001

Tapponnier, P., Mattauer, M., Proust, F., & Cassaigneau, C. (1981). Mesozoic ophiolites, sutures, and arge-scale tectonic movements in Afghanistan. *Earth and Planetary Science Letters*. https://doi.org/10.1016/0012-821X(81)90189-8

Telbisz, T., Kovács, G., Székely, B., & Szabó, J. (2013). Topographic swath profile analysis: A generalization and sensitivity evaluation of a digital terrain analysis tool. *Zeitschrift Fur Geomorphologie*, *57*(4), 485–513. https://doi.org/10.1127/0372-8854/2013/0110

Tende, Andongma W., Aminu, M. D., Amuda, A. K., Gajere, J. N., Usman, H., &

Shinkafi, F. (2021). A spatial reconnaissance survey for gold exploration in a schist belt. *Heliyon*, *7*(11), e08406. https://doi.org/10.1016/j.heliyon.2021.e08406

Tende, Andongma Wanduku, Mustapha, T., Fru, M. I. N., Gajere, J. N., & Aminu, M. D. (2022). Hybrid extraction of tectonic lineaments from digital elevation model. *Applied Geomatics*, *14*(2), 163–180. https://doi.org/10.1007/s12518-022-00422-6

Treloar, P. J., & Izatt, C. N. (1993). Tectonics of the Himalayan collision between the Indian Plate and the Afghan Block: A synthesis. *Geological Society Special Publication*. https://doi.org/10.1144/GSL.SP.1993.074.01.06

Trifonov, V. G. (1978). Late Quaternary tectonic movements of western and central Asia. *Bulletin of the Geological Society of America*, *89*(7), 1059–1072. https://doi.org/10.1130/0016-7606(1978)89<1059:LQTMOW>2.0.CO;2

Ul-Hadi, S., Khan, S. D., Owen, L. A., Khan, A. S., Hedrick, K. A., & Caffee, M. W. (2013). Slip-rates along the Chaman fault: Implication for transient strain accumulation and strain partitioning along the western Indian plate margin. *Tectonophysics*, *608*, 389–400. https://doi.org/10.1016/j.tecto.2013.09.009

USGS. (2021). *LP DAAC - ASTER Overview*. https://lpdaac.usgs.gov/data/get-started-data/collection-overview/missions/aster-overview/

van der Werff, H., & van der Meer, F. (2016). Sentinel-2A MSI and Landsat 8 OLI provide data continuity for geological remote sensing. *Remote Sensing*, *8*(11). https://doi.org/10.3390/rs8110883

Viveen, W., Baby, P., & Hurtado-Enríquez, C. (2021). Assessing the accuracy of combined DEM-based lineament mapping and the normalised SL-index as a tool for active fault mapping. *Tectonophysics*, *813*, 228942. https://doi.org/10.1016/j.tecto.2021.228942

Wang, J., & Howarth, P. J. (1990). Use of the Hough Transform in Automated Lineament Detection. *IEEE Transactions on Geoscience and Remote Sensing*, *28*(4), 561–567. https://doi.org/10.1109/TGRS.1990.572949

Wellman, H. W. (1966). Active wrench faults of Iran, Afghanistan and Pakistan. *Geologische Rundschau*, *55*(3), 716–735. https://doi.org/10.1007/BF02029650

Wells, S. G., Bullard, T. F., Menges, C. M., Drake, P. G., Karas, P. A., Kelson, K. I., Ritter, J. B., & Wesling, J. R. (1988). Regional variations in tectonic geomorphology along a segmented convergent plate boundary pacific coast of Costa Rica. *Geomorphology*, *1*(3), 239–265. https://doi.org/10.1016/0169-555X(88)90016-5

Wheeler, B. L., Bufe, C. G., & Johnson, M. L. (2005). Seismotectonic Map of Afghanistan, with Annotated Bibliography. *U.S. Geological Survey (U.S.) Open-File Report*. http://www.usgs.gov/pubprod

wilcox, R. E., Harding, T. P., & Seely, D. R. (1973). BASIC WRENCH TECTONICS. *American Association of Petroleum Geologists Bulletin*, *57*(1), 74–96. https://doi.org/10.1306/819a424a-16c5-11d7-8645000102c1865d

Wobus, C. W., Whipple, K. X., & Hodges, K. V. (2006). Neotectonics of the central Nepalese Himalaya: Constraints from geomorphology, detrital40Ar/39Ar thermochronology, and thermal modeling. *Tectonics*, *25*(4). https://doi.org/10.1029/2005TC001935

Yamusa, I. B., Yamusa, Y. B., Danbatta, U. A., & Najime, T. (2018). Geological and structural analysis using remote sensing for lineament and lithological mapping. *IOP Conference Series: Earth and Environmental Science*, *169*(1), 12082. https://doi.org/10.1088/1755-1315/169/1/012082

Yeats, R. S., Lawrence, R. D., Jamil-Ud-Din, S., & Khan, S. H. (1979). Surface effects of the 16 March 1978 earthquake, Pakistan-Afghanistan border. *Geodynamics of Pakistan*, *97331*(March 1978), 359–361.

Yousufi, A., Ahmadi, H., Bekbotayeva, A., Arshamov, Y., Baisalova, A., Omarova, G., & Pekkan, E. (2023). Integration of Remote Sensing and Field Data in Ophiolite Investigations: A Case Study of Logar Ophiolite Complex, SE Afghanistan. *Minerals*, *13*(2). https://doi.org/10.3390/min13020234

Zlatopolsky, A. A. (1992). Program LESSA (Lineament Extraction and Stripe Statistical Analysis) automated linear image features analysis-experimental results. *Computers and Geosciences*, *18*(9), 1121–1126. https://doi.org/10.1016/0098-3004(92)90036-Q

APPENDIX

Appendix 1

Chaman fault zone (CFZ)

We mapped several morphotectonic expressions, including channel offsets, along the southern and central sections of the CFZ. As shown in Figure A.1.1, four areas were identified with dominant left-lateral stream channel displacement in the southern and central regions of the CFZ, and two areas were identified in the northern extension. From south to central, the first highlighted area is in the central parts of the Shinkay district of Zabul province (i.e., Segments Chm-31c-d; Figure A.1.1A). As depicted, the stream channels are cut by the fault trace and have been displaced to the left. The second highlighted area is located in the western Shinkay district of Zabul province, where the extracted fault trace is between the Eocene and Late Quaternary sediments along the segments Chm-30d-e. Two stream deflections of 105 m and 1300 m are observed in this area, respectively (Figure A.1.1B).

The third offset area is in central and western Ghazni City, where middle Quaternary sediments cover the area. Left-lateral offsets of channel streams are observed on the left side of the main faults, where synthetic shear fractures have developed. The offsets range from 80 to 350 m (i.e., Segments Chm-11b and 12a; Figure A.1.1C). The fourth highlighted area is in the Azadkhayl village of the Sayed Abad district of Wardak province, where a straight fault scarp is present in the middle of Quaternary sediments along the segment Chm-10f. Shnizai (2020) also reported a continuous fault scarp in piedmont alluvium at the mountain fronts in this area. Left-lateral stream offsets of 108 to 177 m are observed on satellite imagery (Figure A.1.1D).

Using high-spatial-resolution DEM and natural-color composite imagery, we mapped the left-lateral displacement of stream channels and deposits within the northern extension of the CFZ. We identified two areas of interest with clear displacement, as shown in Figure A.1.1. These areas are located in the Shakardara and Paghman districts. We measured two river channel left-lateral movements of 517 to 623 m, and possible lithology left-lateral displacement with smaller offsets of 120 to 150 m within the segments Chm-3e and 3f (Figure A.1.1E). The CFZ trace declines to the NE and ENE from the SW of Bagram Air Base. In this area, several left stream deflections are observed, such as 585 m and 857 m in the Qaleh-ye-Shahi village in the Qara Bagh district (i.e., segments Chm-2b-c), and 490 m in the Qaleh-ye-Ahmadkhan village in the Bagram district (i.e., segment Chm-2b). (Figure A.1.1F).

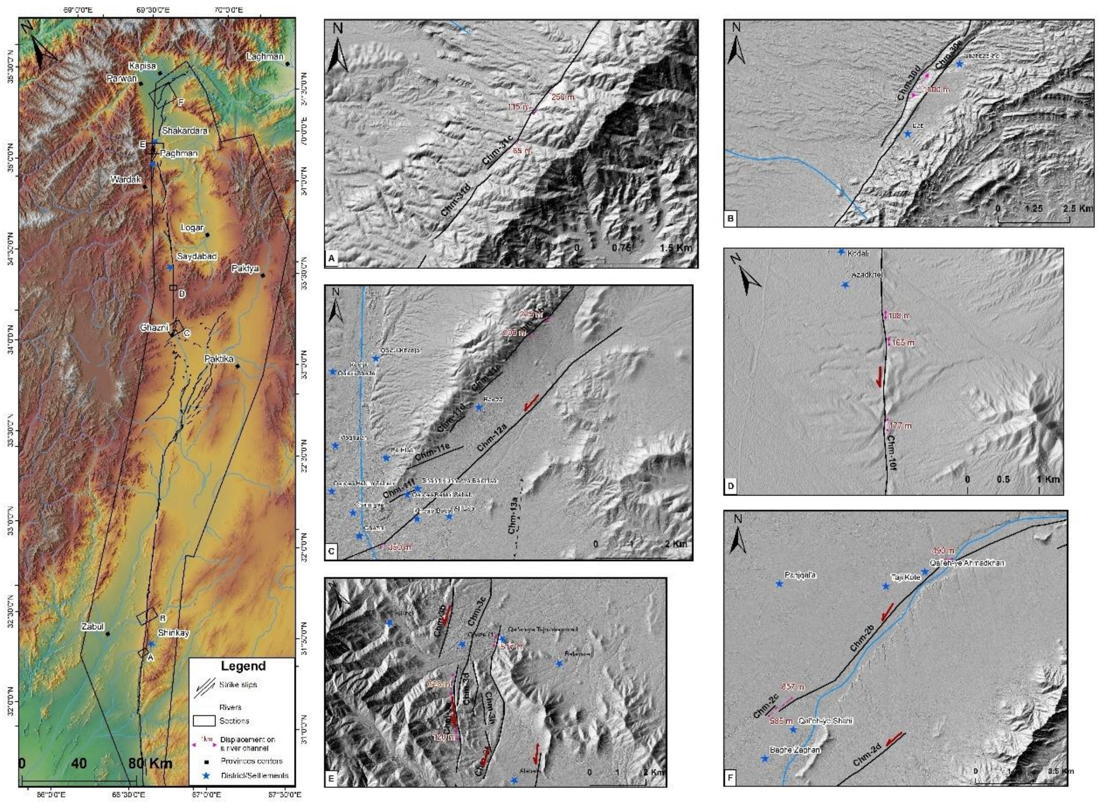

Figure A.1.1. *Color-shaded relief and hillshade maps generated from a high-resolution 5m DEM showing topographical features and measured areas with offsets. (A) Offset measurements over the Shinkay district of Zabul. (B) Stream offset measurements within the same deposits. (C) Stream offset over the central and western Ghazni province. (D) Stream offset within the Azadkhayl village of the Sayed Abad district, where the fault trace cut through the Quaternary sediments. (E) Displaced streams indicate possible lithology displacement over the Paghman district. (F) Stream offset observed within the last highlighted area associated with NE and ENE extension of CFZ.*

Appendix 2

Herat fault zone (HFZ)

The effects of right-lateral strike-slip are also considered along the HFZ within the valleys, rivers, and local drainages (Figure A.2.1). During the segmentation of the HFZ, we defined and measured right-lateral channel deflections and stream bending, and clustered them into four areas of interest. The first area of interest is located in the center of Lal Wa Sarjangal district of Ghor province, where the HFZ crosses.

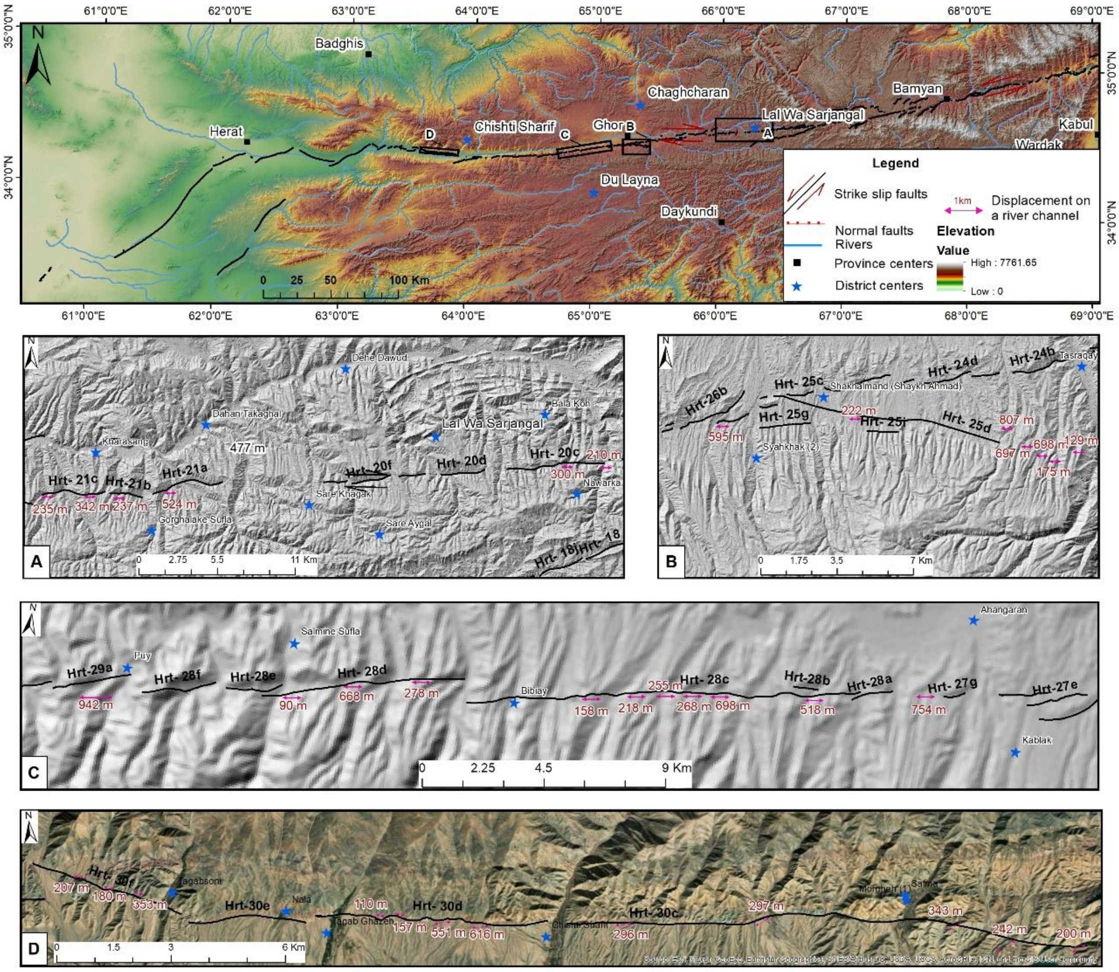

Figure A.2.1. *Right displacement measured lines of the streams overlaid on the shaded-relief map along the Herat Fault Zone (HFZ). (A) Offset measurements over the central Lal Wa Sarjangal district of Ghor. (B) Stream offset measurements within the southern Chaghcheran district of Ghor. (C) Stream offset over the northwestern part of the Du Layna district of the same province. (D) Stream offsets and bending observed in the northwestern region of Chasti Sharif in Herat province.*

The streams are displaced differently, ranging from 221 to 524 m along the segments Hrt-20c and 21a-c (Figure A.2.1A). As shown in Figure A.2.1B,C, typical stream displacement with different lengths representing right-lateral offset is observed in the southern Cheghcheran and NW Du Layna districts of Ghor province. Our measurements in these areas show displacements between 50 and 942 m (i.e., segments Hrt-25d, 26a, 27g, 28b-d, 29a). In the last area of interest, in the NW of Chishti Sharif district of Herat province, typical right-lateral displacement and stream bending are observed, as depicted in Figure A.2.1B. We measured this displacement ranging from 29 to 340 m along the segment Hrt-30c-f.

Appendix 3

Sarobi fault zone (SFZ)

Our remote sensing observations show limited offset displacement along the Sarobi Fault Zone. We measured very few sets of right-lateral displacement of stream channels along the mountain fronts over the southern and northern sections of the SFZ (Figure A.3.1).

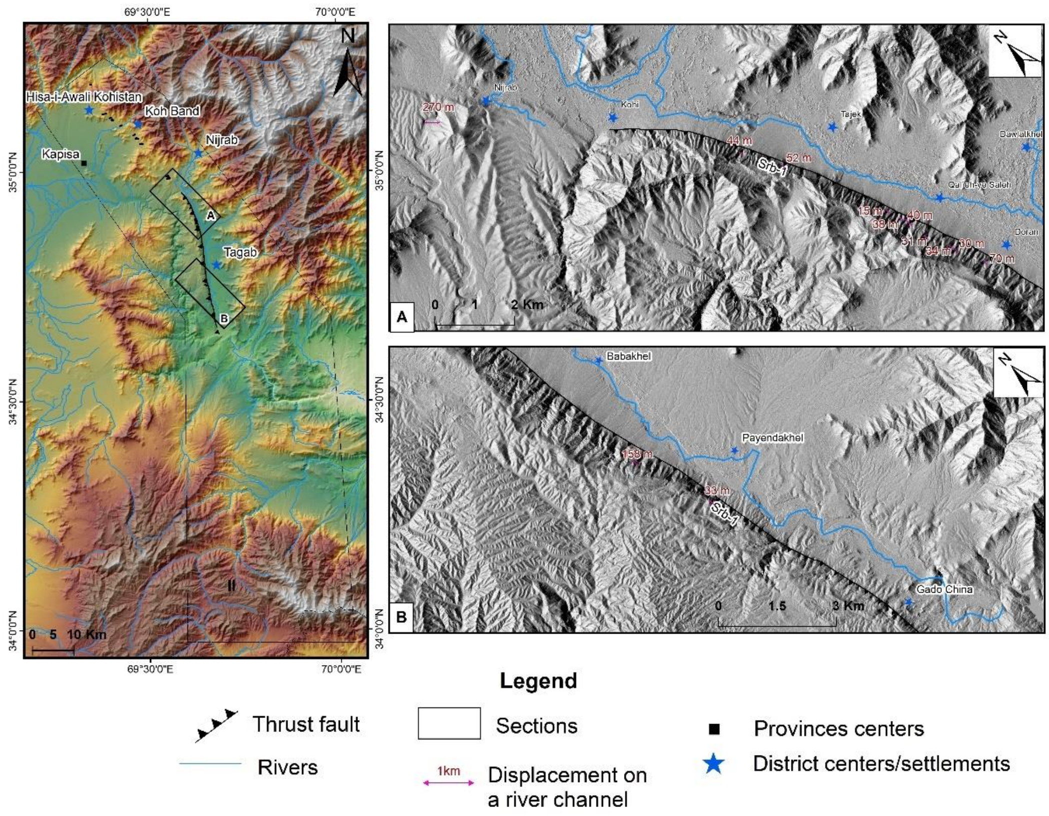

Figure A.3.1. *Thematic illustration depicting the location of the Sarobi fault and the measured right-lateral stream displacement. (A) Displaced river channels ranging from 15 to 270m along the alluvial fans. (B) River channels exhibiting right-lateral displacement with similar geometry to the previous area of interest, ranging from 33 to 158m.*

Using the DEM imagery with 5 m spatial resolution and complementary data from Google Earth images as base maps, we were able to measure some stream offsets in two areas over the section of the SFZ, as depicted in Figure A.3.1. The first area of interest is in the northern Tagab and western Nijrab districts of Kapisa province. The deflected streams are mostly directed from NE to SE along the fault, as illustrated in Figure A.3.1A. The fault scarp cuts through the Proterozoic and Quaternary formations, which distinguishes it from other highlighted areas. We mapped right-lateral stream offsets ranging from 15 to 270 m. The second area of interest is situated within the western Tagab district of Kapisa province, where the Proterozoic formations cover the measured area. We measured right-lateral displacement of streams in mountain fronts ranging from 33 to 158 m (Figure A.3.1B).

Appendix 4

Konar fault zone (KFZ)

We also considered left-lateral stream displacement along the KFZ, which we measured in seven areas of interest (Figure A.4.1). The first area of interest is located in the southeast part of the Qarghayi district of Laghman province, where the Kabul River has been displaced left-laterally by about 6.4 km along the segment Knr-11c (Figure A.4.1A). The second area of interest is located in the Bela and Gerdi Kac settlements between the Behsud and Kama districts of Nangarhar province, where an 8.5 km left-lateral displacement was measured on the Konar River (segment Knr-10o) (Figure A.4.1B).

We mapped a left displacement of about 195 m in the third area of interest, which is located in the west of Sarkani district of Konar province, near the segment between Knr-10g and Knr-10i (Figure A.4.1C). The fourth highlighted area is located in the southeast of Shaygal wa Shital district of Konar province, where we measured a left displacement of 75 to 195 m on the Konar River, associated with the segments Knr-9g and Knr-9h (Figure A.4.1D). As depicted in Figure 4E-S, the fifth area of interest is located in the center of Bar Konar district, around the Aremkhan Kalay settlement. We observed three different left displacements of 150 m, 670 m, and 850 m on the local drainage system, along the segments Knr-9c and Knr-9d.

The sixth and seventh areas of interest are situated outside the territory of Afghanistan (Figure A.4.1F and Figure A.4.1G). To the east of the Nari district, we measured left displacements of 750 m and 1 km on the local drainages (i.e., segments Knr-7f and Knr-7h) (Figure A.4.1F). Following the mapped segmentation along the KFZ outside of the Afghanistan boundary, reaching the Chitral region, we mapped the last area of interest, which contains several channels with left displacements ranging from 51 to 518 m (i.e., segments Knr-1a, Knr-1d, Knr-2b-c, Knr-4a-b, and Knr-4f) (Figure A.4.1G). All the displaced streams along the KFZ occur within the recent and Quaternary deposits, which can express the younger activity of the fault zone.

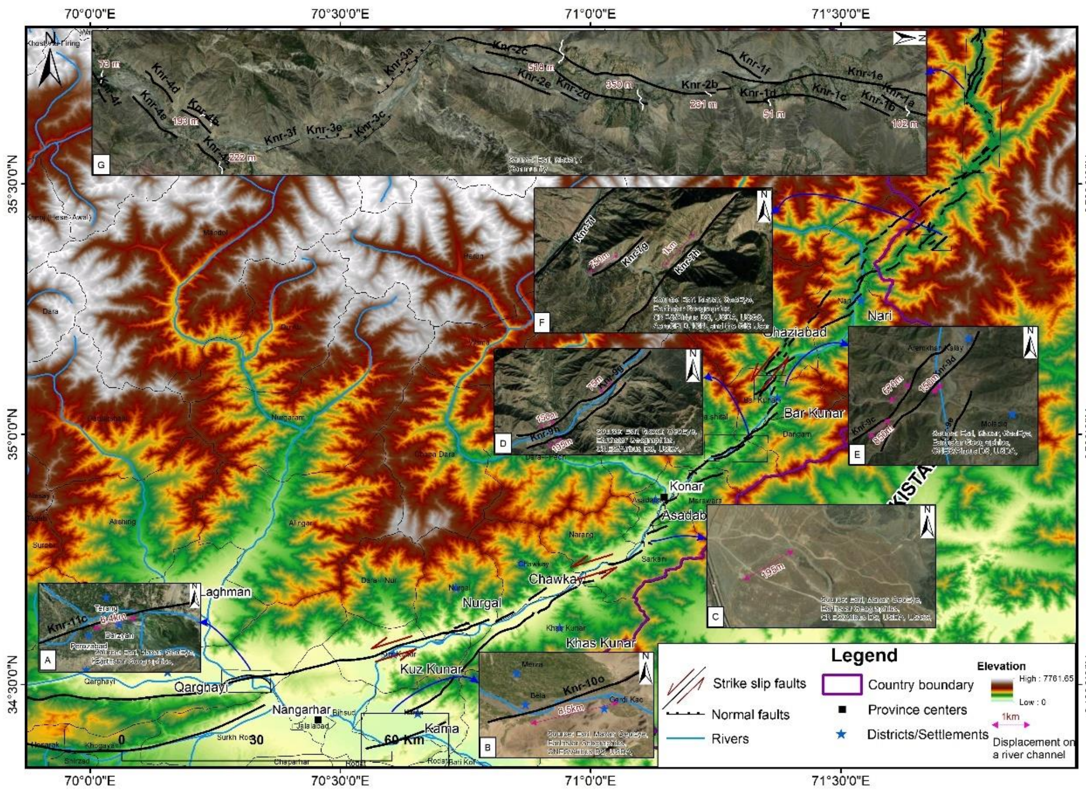

Figure A.4.1. *Thematic illustration depicting the left-lateral displacement of streams along the Konar Fault Zone (KFZ). (A&B) Streams within the southern Qarghayi and Kama districts. (C) Streams located to the west of the Sarkani district. (D) Streams within the Shaygal wa Shital district. (E) Streams in the center of the Bar Konar district. (F) Streams located eastward of the Nari district, outside the Afghanistan border. (G) Streams located outside of Afghanistan within the Chitral region, Pakistan.*

Appendix 6

The script for downloading Sentinel 1 GRD data with VH polarization:

```
var bo = table;
Map.centerObject(bo);
Map.addLayer(bo);

var sentinel = ee.ImageCollection("COPERNICUS/S1_GRD")
.filterBounds(bo)
.filterDate('2021-07-20','2021-07-30')
.median()
.clip(bo);
print(sentinel)

var VH = sentinel.select('VH');



print(VH)
Map.addLayer(VH);

Export.image.toDrive({
  image : VH,
  description : 'SENTINEL_1_VH_KBL',
  scale : 20,
  region : bo
  });
```

The script for downloading Sentinel 1 GRD data with VH polarization:

```
var bo = table;
Map.centerObject(bo);
Map.addLayer(bo);

var sentinel = ee.ImageCollection("COPERNICUS/S1_GRD")
```

```
.filterBounds(bo)
.filterDate('2021-07-20','2021-07-30')
.median()
.clip(bo);
print(sentinel)

var VV = sentinel.select('VV');



print(VV)
Map.addLayer(VV);

Export.image.toDrive({
  image : VV,
  description : 'SENTINEL_1_VV_KBL',
  scale : 20,
  region : bo
  });
```

Appendix 7

The script for downloading the Edge-SWIR bands of Sentinel-2MSI with surface reflectance.

```
Var bo = table;
Map.centerObject(bo);
Map.addLayer(bo);

var sentinel = ee.ImageCollection("COPERNICUS/S2_SR")
.filterBounds(bo)
.filterDate('2021-07-24','2021-07-30')
.median()
.clip(bo);
print(sentinel)

var bands = sentinel.select('B5','B6','B7','B8A','B11','B12');


print(bands)
Map.addLayer(bands);

Export.image.toDrive({
  image : bands,
  description : 'SENTINEL_Edge_SWIR_KBL',
  scale : 30,
  region : bo
  });
```

Appendix 8

The script for downloading the selected bands of ASTER data.

```
var bo = table;
Map.centerObject(bo);
Map.addLayer(bo);

var aster = ee.ImageCollection('ASTER/AST_L1T_003')
.filterBounds(bo)
.filterDate('2007-07-01','2007-07-30')
.median()
.clip(bo);
print(aster)

var vnir = aster.select('B01','B02','B3N');
print(vnir)

var swir = aster.select('B04','B05','B06','B07','B08','B09');

print(swir)

var stack = ee.Image.cat([vnir,swir]);

print(stack)
Map.addLayer(stack);

Export.image.toDrive({
  image : stack,
  description : 'ASTER_KBL',
  scale : 30,
  region : bo
  });
```

Appendix 9

To define degrees (0-360º):

Pre-Logic Script Code:

```
def azimuth(Shape):
  degBearing = math.degrees(math.atan2((Shape.lastPoint.X - Shape.firstPoint.X),(Shape.lastPoint.Y - Shape.firstPoint.Y)))
  if (degBearing < 0):
     degBearing += 360.0
  return degBearing
```

Field (Type Double) =

```
azimuth( !Shape! )
```

To normalize the azimuth (0-180º):

Pre-Logic Script Code:

```
def Nazimuth(Azimuth):
  if (Azimuth > 180):
    return (Azimuth - 180)
  else:
    return (Azimuth)
```

Field (Type Double) =

```
Nazimuth( !Azimuth! )
```

To define the four azimuthal directions:

Pre-Logic Script Code:

```
def quad(var):
    if (var >= 0) & (var <= 5):
        return "N-S"
    if (var >= 175) & (var <= 180):
        return "N-S"
```

```
        elif (var > 5) & (var <= 85):
            return "NE-SW"
        elif (var > 85) & (var <= 95):
            return "E-W"
        else:
            return "NW-SE"
```

Field (Type Text) =

```
quad( !Nazimuth! )
```

To define the eight azimuthal directions:

Pre-Logic Script Code:

```
def azim(var):
        if (var < 1):
            return "N-S"
        if (var >= 180):
            return "N-S"
        elif (var >= 1) & (var <= 22.5):
            return "NNE-SSW"
        elif (var > 22.5) & (var <= 67.5):
            return "NE-SW"
        elif (var > 67.5) & (var < 89):
            return "ENE-WSW"
        elif (var >= 89) & (var <= 91):
            return "E-W"
        elif (var > 91) & (var <= 112.5):
            return "WNW-ESE"
        elif (var > 112.5) & (var <= 157.5):
            return "NW-SE"
        else:
            return "NNW-SSE"
```

Field (Type Text) =

```
quad( !Nazimuth!
```

CURRICULUM VITAE

ORCID ID: 0000-0002-8995-0234

Name Surname : Hemayatullah AHMADI

Foreign Language : English, Russian, and Turkish

Education Background:

- 2019-2023, (Ph.D.) Eskişehir Technical University, Institute of Graduate Programs, Department of Remote Sensing and Geographic Information Systems, Türkiye
- 2014-2016, (M.Sc.) Satbayev University, Institute of Geology and Oil & Gas Engineering, Department of Geological Engineering and Exploration of Mines, Kazakhstan
- 2007-2012, (B.Sc.) Kabul Polytechnic University, Faculty of Geology and Mines, Department of Geological Engineering and Exploration of Mines, Afghanistan

Professional Background

- 2016-2023, Assistant Professor, Kabul Polytechnic University, Department of Geological Engineering and Exploration of Mines
- 2013-2016, Faculty Member/Lecture Assistant, Kabul Polytechnic University, Department of Geological Engineering and Exploration of Mines
- 2012-2013, Teaching Assistant, Kabul Polytechnic University, Department of Geological Engineering and Exploration of Mines

Publications:

- **Ahmadi, H**., Hussaini, M.R., Yousufi, A., Bekbotayeva, A., Baisalova, A., Amralinova, B., Mataibayeva, I., Rahmani, A.B., Pekkan, E., Sahak, N. (2023). Geospatial Insights into Ophiolitic Complexes in the Cimmerian Realm of the Afghan Central Block (Middle Afghanistan). *Minerals*, 13(11), 1453. https://doi.org/10.3390/min13111453
- **Ahmadi, H.,** Pekkan, E., & Seyitoğlu, G. (2023). Automatic lineaments detection using radar and optical data with an emphasis on geologic and tectonic implications: a case study of Kabul Block, Southeast Afghanistan. *Geocarto International*, 38(1), 1-71. https://doi.org/10.1080/10106049.2023.2231400

- **Ahmadi, H.,** Sahak, A. S., Ayoobi, A. W., Pekkan, E., Inceoğlu, M., & Karsli, F. (2023). Application of GIS-Based AHP Model for the Impact Assessment of COVID-19 Lockdown on Environment Quality: The Case of Kabul City, Afghanistan. Journal of the Indian Society of Remote Sensing, 51(3), 439-452. https://doi.org/10.1007/s12524-022-01633-5
- Yousufi, A., **Ahmadi, H.,** Bekbotayeva, A., Arshamov, Y., Baisalova, A., Omarova, G., & Pekkan, E. (2023). Integration of Remote Sensing and Field Data in Ophiolite Investigations: A Case Study of Logar Ophiolite Complex, SE Afghanistan. *Minerals*, 13(2), 234. https://doi.org/10.3390/min13020234
- Mashkoor, R., **Ahmadi, H.,** Rahmani, A. B., & Pekkan, E. (2022). Detecting Li-bearing pegmatites using geospatial technology: the case of SW Konar Province, Eastern Afghanistan. *Geocarto International*, 37(26), 14105-14126. https://doi.org/10.1080/10106049.2022.2086633
- Shroder, J. F., Eqrar, N., Waizy, H., **Ahmadi, H.,** & Weihs, B. J. (2022). Review of the Geology of Afghanistan and its water resources. *International Geology Review*, 64(7), 1009-1031. https://doi.org/10.1080/00206814.2021.1904297
- Ayoobi, A. W., **Ahmadi, H.,** Inceoglu, M., & Pekkan, E. (2022). Seasonal impacts of buildings' energy consumption on the variation and spatial distribution of air pollutant over Kabul City: application of Sentinel—5P TROPOMI products. *Air Quality, Atmosphere & Health*, 15(1), 73-83. https://doi.org/10.1007/s11869-021-01085-9
- **Ahmadi, H.,** & Kalkan, K. (2021). Mapping of ophiolitic complex in logar and surrounding areas (SE Afghanistan) with ASTER data. *Journal of the Indian Society of Remote Sensing*, 49(6), 1271-1284. https://doi.org/10.1007/s12524-021-01319-4
- **Ahmadi, H**., & Pekkan, E. (2021). Fault-based geological lineaments extraction using remote sensing and GIS—a review. *Geosciences*, 11(5), 183. https://doi.org/10.3390/geosciences11050183
- **Ahmadi, H**., & Uygucgil, H. (2021). Targeting iron prospective within the Kabul Block (SE Afghanistan) via hydrothermal alteration mapping using remote sensing techniques. *Arabian Journal of Geosciences*, 14(3), 183. https://doi.org/10.1007/s12517-020-06430-3

- Arif, N. M., **Ahmadi, H.,** & Arian, H. (2021). The importance of index fossils in the determination of the geologic age of strata: a case of Band-e-Amir of Bamiyan province, Central Afghanistan. *Геология и охрана недр,* (2), 61-76. https://www.elibrary.ru/item.asp?id=46360651
- **Ahmadi, H.,** Kaya, O. A., Babadagi, E., Savas, T., & Pekkan, E. (2020). GIS-based groundwater potentiality mapping using AHP and FR models in central antalya, Turkey. *Environmental Sciences Proceedings*, 5(1), 11. https://doi.org/10.3390/IECG2020-08741
- **Ahmadi, H.,** Yousufi, A., & Mosazai, A. M. (2020). Mineralogical Composition and Physical–Mechanical Properties of Dasht-E-Taatrang Zar Sand Deposits (Afghanistan). *Environmental Sciences Proceedings*, 4(1). https://doi.org/10.3390/IECG2020-08832
- Sadat, S. A., & **Ahmadi, H.** (2019). The relation of geological structure with mining method and environmental assessment in Aynak copper deposit (Afghanistan*). Геология и охрана недр*, (4), 20-26. https://www.elibrary.ru/item.asp?id=41514433
- Yousufi, A., Bekbotayeva, A., Muszynski, A., **Ahmadi, H.**, & Baibatsha, A. (2019). Distribution of ultramafic complexes in Afghanistan. *International Multidisciplinary Scientific GeoConference*: SGEM, 19(1.1), 163-170. DOI: 10.5593/sgem2019/1.1/S01.020
- **Ahmadi, H**., & Rahmani, A. B. (2018). Study on the mineral anomalies of Muqur-Chaman fault and its comparison with Harirud (Herat) fault (Afghanistan) using geophysical and remote sensing (Aster-Hymap) data. *Геология и охрана недр*, (1), 28-38. https://www.elibrary.ru/item.asp?id=35123999
- Zaryab, A., Jafari, I., Amini, M. A., & **Ahmadi, H**. (2018). Triggering factor evaluation of Argo landslide using limit equilibrium slope stability analysis. *Геология и охрана недр*, (4), 71-77. https://www.elibrary.ru/item.asp?id=36665543
- Mosazai, A. M., Yousufi, A., & **Ahmadi, H**. (2017). The geological characteristics and economical importance of pegmatite belt of Afghanistan. *Геология и охрана недр*, (4), 26-33. https://www.elibrary.ru/item.asp?id=32327602

Conferences:

- 2021, The 73rd Geological Congress of Turkey – Oral Presentation, Virtual
- 2021, Geologists' Association, Student Symposium, UK – Poster Presentation, Virtual
- 2020, The 3rd International Electronic Conference on Geosciences - Oral Presentation, Virtual
- 2018, The 36th National and 3rd International Geosciences Congress - Oral Presentation, Tehran, Iran
- 2017, The International Scientific – Practical Conference (Minerageny of Kazakhstan) – Oral Presentation, Institute of Geological Sciences, Almaty, Kazakhstan
- 2017, The 6th International Hindu Kush Geoscience Conference – Oral Presentation, Kabul Polytechnic University, Kabul, Afghanistan
- 2016, AMEA: Mining Education Meets Mining Business: A Multilateral Exchange Afghanistan-Iran-Germany-China, Germany
- 2016, The 4th International Mine & Industries Congress & 6th Iranian Mining Engineering Conference – Oral Presentation, Tehran, Iran

Reviewer:

- Remote Sensing Applications: Society and Environment (Elsevier)
- Geocarto International (Taylor and Francis)
- International Journal of Digital Earth (Taylor and Francis)
- GeoJournal (Springer)
- Heliyon (Elsevier)
- Advances in Space Research (Elsevier)
- Geo-Spatial Information Science (Taylor and Francis)
- International Journal of Engineering and Geosciences
- Mersin Photogrammetry Journal
- Turkish Journal of Geographic Information Systems
- Turkish Journal of Geosciences
- International Journal of Earth Sciences Knowledge and Applications
- Petroleum Science and Technology

Awards:

- 2018, Ph.D., YTB Scholarship, Türkiye
- 2013, M.Sc., Kazakhstan Government Scholarship, Kazakhstan

Professional Union/Association/Organization Memberships:

- 2020 – Present, International Society for Photogrammetry and Remote Sensing: Worldwide, Maryland, NL
- 2017 – Present, Organizing committee of the International Hindu Kush Geosciences Conference, Afghanistan
- 2016-2018, Quality Assurance and Accreditation Committee of Kabul Polytechnic University at the faculty level, Afghanistan
- 2016-2018, Professional Development Center (PDC) at Kabul Polytechnic University, Afghanistan